Mechanistic Study of Cell Death Induction by O^6-Methylating Agents, Focusing on the Role of Homologous Recombination as a Molecular Target for Sensitization of Tumor Cells to Chemotherapeutic Alkylating Agents

Dissertation
zur Erlangung des Grades
„Doktor der Naturwissenschaften“

am Fachbereich Biologie
der Johannes Gutenberg-Universität Mainz

vorgelegt von
Steve Quirós Barrantes

Geb. am 14.01.1980 in San José, Costa Rica

Mainz, 2012

Dekan:

1. Berichterstatter:

2. Berichterstatter:

Tag der Prüfung: 12.06.2012

A mi familia

Table of Contents

1. Introduction

1.1. DNA damage repair

In contrast to other cellular macromolecules in an organism, DNA, the carrier of the genetic information, can not be replaced. Therefore, efficient removal or repair of DNA lesions caused by endogenous or exogenous sources is essential for genomic stability and the proper function and survival of cells. Multiple DNA repair pathways that provide this protective function have evolved in organisms. Its relevance is clearly evident, as deficiencies in DNA repair mechanisms in multicellular organisms is often associated either with lethality during early embryonic development or with severe diseases and cancer predisposition.

The principal DNA repair systems are described in the next Sections. Unless otherwise stated, the following descriptions are limited to human repair pathways. As discussed below, this study centers on the mechanism of cell death trigger by S_N1-methylating agents (described in Section 1.3). Some repair pathways (namely Direct damage reversal (Section 1.1.1), DNA mismatch repair (Section 1.1.2), Base excision repair (Section 1.1.3) and Homologous recombination (Section 1.1.5) are of prominent importance both for the mechanism of toxicity and the repair of lesions caused by these agents. Therefore, these repair systems will be discussed in more detail.

1.1.1. Direct damage reversal

Direct damage reversal refers to single enzyme mechanisms able to correct DNA lesions without performing incisions in the DNA backbone or removal of DNA bases. Given their enzymatic nature, these repair mechanisms are error free, with a very narrow substrate range (Eker *et al.*, 2009).

1.1.1.1. Dioxygenases

The nuclear alpha-ketoglutarate-dependent dioxygenases alkB homolog 2 and 3 [ALKBH2 and ALKBH3] directly demethylate N1-methyladenine [N1MeA] and N3-methylcytosine [N3MeC] lesions from ssDNA (ALKBH3), RNA (ALKBH3) and dsDNA (ALKBH2) (see Section 1.3.2 for description of these lesions) (Sedgwick *et al.*, 2007; Eker *et al.*, 2009).

The Fe^{2+}-dependent oxydative demethylation involves hydroxylation of the methyl group using 2-ketoglutarate and O_2, which restores the original base and releases formaldehyde (Sedgwick *et al.*, 2007; Eker *et al.*, 2009).

1.1.1.2. O^6-methylguanine-DNA methyltransferase

O^6-methylguanine-DNA methyltransferase [MGMT] is a protein capable of performing a single-step irreversible stoichiometric transfer reaction of an alkyl group from the oxygen substituent in the 6th position of guanine in DNA to a cysteine residue in its catalytic pocket. The reaction thus restores the modified base to a guanine and results in inactivation of MGMT. After this "suicide reaction", inactivated MGMT is ubiquitinated and subjected to proteasomal degradation (Lindahl *et al.*, 1982; Srivenugopal *et al.*, 1996; Xu-Welliver & Pegg, 2002; Kaina *et al.*, 2007). Besides the repair of O^6-alkylguanine, MGMT can also repair the minor lesion O^4-methylthymine (Sassanfar *et al.*, 1991), which is induced at much lower level than alkylations at O^6-guanine (<1% vs 7-8% for S_N1-alkylating agents) (Beranek, 1990).

The biological significance of the O^6-methylguanine [O^6MeG] lesion and its repair by MGMT is of cardinal significance for this work. A detailed description of the toxic cellular responses triggered by this lesion is provided in Section 1.3.4.

1.1.2. DNA mismatch repair

DNA mismatch repair [MMR] is responsible for the repair of mismatches generated during DNA replication that escaped the proofreading activity of DNA polymerase, and mismatches generated by base modifications. These include potentially promutagenic base substitution mismatches and insertion-deletion loops. The system works by excision of a lesion-containing track of the newly synthesized DNA-strand followed by gap filling using the parent strand as a template. Inactivation of MMR causes a strong mutator phenotype, with mutation rates of up to 1 000-fold greater than in MMR proficient cells. MMR inactivation is associated with hereditary and sporadic human cancers, particularly Hereditary Nonpolyposis Colorectal Cancer (HNPCC) and other sporadic colon cancers (Li, 2008; Hsieh & Yamane, 2008; Kunz *et al.*, 2009; Martin *et al.*, 2010).

During the repair of post-replicative mismatches, the heterodimeric ATPases MutSα (MSH2 and MSH6) and MutSβ (MSH2 and MSH3) are responsible for mismatch recognition. MutSα participates in the recognition of base substitution mismatches and small (1 or 2 nucleotides) mismatched loops, while MutSβ does so for small and longer (10 nucleotides) loops. Upon recognition of the mismatch, MutS recruits MutLα (MLH1 and PMS2) to the site of damage. While MutLβ (MLH1 and PMS1) plays a minor role in MMR, no function for MutLγ (MLH1 and MLH3) has been ascribed. Different

models have been proposed to explain the series of events following initial mismatch recognition. In the stationary model, MutS-induced bending of the DNA molecule brings together both the mismatch site and a site allowing for new and parent strand discrimination, in a process dependent on the ATPase activity of MutS. In the translocation model, ATP binding reduces the affinity of the recognition complex with the mismatch, and subsequent ATP hydrolysis facilitates translocation of the complex along the DNA molecule, with DNA being threaded through the complex in a loop forming process that continues until a strand discrimination site is found for excision initiation.

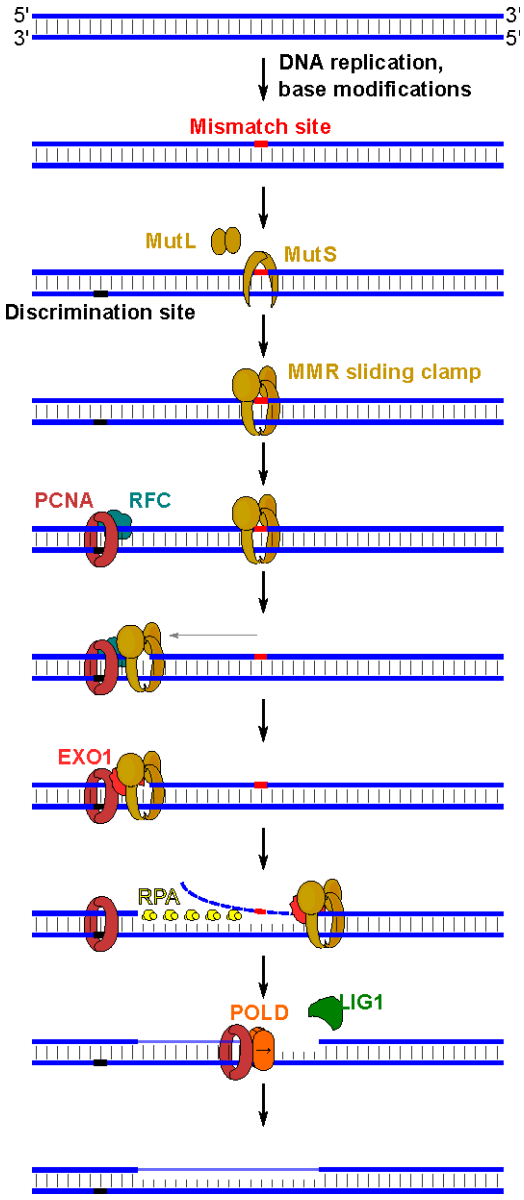

Figure 1. Simplified overview of the main players and steps of the sliding clamp model of DNA mismatch repair. See text in Section 1.1.2 for details. Modified from Li (2008), Hsieh & Yamane (2008), Kunz *et al*. (2009) and Martin *et al*. (2010).

The most widely accepted model is the molecular switch or sliding clamp model (Fig. 1) which states that the mismatch binding by MutS triggers a conformational change allowing for ADP to ATP exchange, which reduces the affinity for the mismatch and induces a second conformational change of the complex to form a ternary complex with MutL (in the form of a sliding clamp) which slides to the discrimination site. Gaps between the Okazaki fragments on the lagging strand seem to provide the discrimination signal for MMR, while the corresponding signal for the leading strand still needs to be identified. Proliferating cell nuclear antigen [PCNA] and Replication factor C protein complex [RFC] are required at the discrimination site for excision activation. Guided by MutS and MutL, Exonuclease 1 [EXO1], a 5' to 3' exonuclease, carries out 5' and 3' nick directed excision towards and beyond the mismatch site, a process terminated by MutL. 3' nick directed excision additionally depends on the PCNA and RFC activated endonuclease activity of PMS2 (component of MutLα), which incises 5' from the mismatch site, allowing for EXO1 activity. Following excision by EXO1, DNA polymerase delta [POLD] takes over DNA re-synthesis, while DNA ligase 1 [LIG1] completes nick ligation. Other proteins also participate at different stages of MMR, including Replication protein A [RPA] in the excision and re-synthesis steps and PCNA during the recruitment and binding of the recognition complex and the excision and re-synthesis steps (Li, 2008; Hsieh & Yamane, 2008; Kunz *et al.*, 2009; Martin *et al.*, 2010).

1.1.3. Base excision repair

Base excision repair [BER] is responsible for the repair of a variety of abnormal or modified bases, including those arising from alkylation, deamination and oxidative damage. The repair pathway works by excision of the damaged base and its replacement with the correct one using the undamaged strand as a template. The process might or might not involve re-synthesis mediated displacement and elimination of a oligonucleotides stretch. BER is also involved in the repair of DNA single-strand breaks [SSBs] using the same machinery employed for single base repair (Baute & Depicker, 2008; Hegde *et al.*, 2008; Zharkov, 2008; Horton *et al.*, 2008; Robertson *et al.*, 2009).

BER (Fig. 2) is initiated by recognition and excision of the damaged base by a DNA glycosylase. Eleven DNA glycosylases have been identified in humans, classified in four structural superfamilies, namely Helix-Hairpin-Helix superfamily (including MBD4, NTHL1, MUTYH and OGG1), Helix-Two turn-Helix superfamily (comprising NEIL1, NEIL2 and NEIL3), UDG superfamily (with UNG, TDG and SMUG1 as their representatives) and AAG superfamily (represented by MPG). Cleavage of the N-glycosidic bond of the damaged base by the DNA glycosylase generates an apurinic-apyrimidinic site [abasic site, AP site], a toxic intermediate (upon replication AP sites can

generate mutations or DNA double-strand breaks), which is a substrate for an DNA-AP endonuclease [APE].

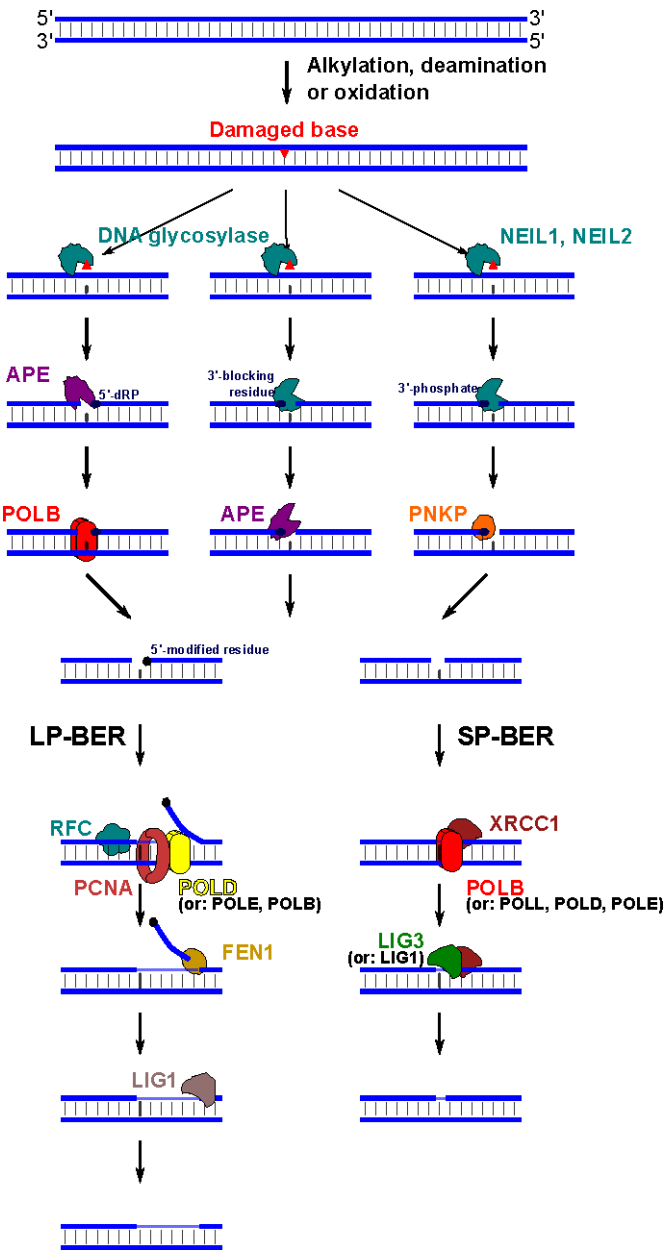

Figure 2. Pathways for Base excision repair. See text in Section 1.1.3 for details. Modified from Baute & Depicker (2008), Hegde *et al*. (2008), Zharkov (2008) and Robertson *et al*. (2009).

AP endonuclease 1 and 2 [APEX1 and APEX2] cleave the phosphodiester bond immediately 5' to the AP site to generate 3'-OH and 5'-deoxyribose phosphate [5'-dRP]. Alternatively, the intrinsic DNA AP lyase activity of some DNA glycosylases can cut 3' to the AP site, generating a 5'-phosphate and a 3'-blocking residue, commonly in the form of an unsaturated aldehyde. The trimming of non canonical DNA ends require the removal of the 5'-dRP by the lyase activity of DNA polymerase beta [POLB]

and removal of the 3'-blocking lesion by the 3'-diesterase activity of APE. Polynucleotide kinase 3'-phosphatase [PNKP] can also perform an APE-independent sub-pathway, involving 3'-phosphate removal after NEIL1 or NEIL2 glycosylase processing. Additionally, other proteins like Tyrosyl-DNA phosphodiesterase 1 [TDP1] and ERCC1-XPF have also been reported to have end cleaning properties. Once a 3'-OH is available, the DNA polymerase activity of POLB (or alternatively DNA polymerase lambda [POLL], delta [POLD] or epsilon [POLE]) fills the 1 nucleotide gap. Selection among two possible BER pathways depends in great part on the type of DNA ends generated after processing of the AP site. In the presence of 5'-dRP, processing of this structure by POLB is followed immediately by nick sealing by DNA ligase 3 [LIG3]/XRCC1 or alternatively LIG1, in a process referred to as short-patch or single nucleotide BER [SP-BER]. If the 5'-end can not be processed, as would occur in the case of further oxidation of the aldehyde group in deoxyribose, the long-patch BER [LP-BER] pathway take place. In a PCNA- and RFC-dependent process, replicative POLD or POLE, or alternatively POLB, perform strand synthesis with displacement of the original DNA strand containing the altered 5'-terminal moiety. Flap structure-specific endonuclease 1 [FEN1] catalyze the removal of the 4 to 6 nucleotides flap generated by the polymerase, and replicative LIG1 seals the nick. Additional to the 5'-terminus, local concentration of BER proteins, protein-protein interactions, relative ATP concentration and the replicative status of the cells have been suggested to determine the choice between SP-BER and LP-BER pathways (Baute & Depicker, 2008; Hegde *et al.*, 2008; Zharkov, 2008; Robertson *et al.*, 2009).

BER also participate in SSBs repair. In this case, SSBs are initially recognized by Poly (ADP-ribose) polymerase 1 [PARP1], which then recruits XRCC1, a scaffold protein that facilitate recruitment of further factors required for ends trimming and subsequent BER, making use of the pathways described above (Baute & Depicker, 2008; Horton *et al.*, 2008).

1.1.4. Nucleotide excision repair

Nucleotide excision repair [NER] is a versatile repair system where many structurally unrelated DNA lesions can be recognized based on the distortion they cause in the DNA structure. These lesions include bulky DNA adducts, intra- and inter-strand cross-links, cyclobutane pyrimidine dimers, pyrimidine-pyrimidone photoproducts and oxidized bases difficult to excise by BER, like cyclopurines. This repair system works by removal of a short nucleotide track containing the lesion followed by gap filling using the complementary strand as a template. Mutations in genes involved in NER have been linked to several genetic disorders, including Xeroderma pigmentosum, Cockayne syndrome, Cerebro-occulofacio-skeletal syndrome, Ultraviolet light [UV]-sensitive syndrome and

Trichothiodystropy, a series of hereditary disorders that depending on the specific protein deficiency might or might not manifest with different degrees of sun hyper sensitivity, high skin cancer incidence, neurological abnormalities, dwarfism and reduced life expectancy (Leibeling *et al.*, 2006; Shuck *et al.*, 2008; Nouspikel, 2009).

Two pathways of NER have been described: transcription coupled NER [TC-NER] and global genomic NER [GG-NER]. TC-NER is a specialized NER pathway that operates in the transcribed strands of actively expressed genes, while GG-NER does so both in transcribed and untranscribed strands of actively or inactively expressed genes (Shuck *et al.*, 2008; Nouspikel, 2009). TC-NER and GG-NER share most of the NER machinery, but they differentiate in their mode of damage recognition. In TC-NER, the arrest of transcribing RNA polymerase when it encounters a lesion acts as a sensor of DNA damage (Goosen, 2010). Stabilization of CSB interaction with the arrested polymerase is required for chromatin remodeling, lesion assessment and recruitment of NER factors (Fousteri & Mullenders, 2008; Tornaletti, 2009). For GG-NER the heterotrimeric complex XPC/RAD23B/Centrin-2 [CETN2] fulfill the initial distortion recognition function (Goosen, 2010). Additionally, the high affinity for DNA damage to the DNA damage-binding heterodimeric complex [DDB1 and DDB2] is required during GG-NER for efficient recruitment of XPC to lesions that do not induce a strong distortion in the DNA structure, like in the case of cyclobutane pyrimidine dimers (Nouspikel, 2009).

Initial damage recognition is followed by recruitment of TFIIH, a multimeric complex containing, among other proteins, XPB and XPD. These two DNA helicases, containing opposite polarity, have a damage verification function. In the presence of chemically modified DNA they open a bubble by denaturing the DNA duplex around the lesion. This open bubble generates short stretches of ssDNA, which is stabilized by binding of XPA and RPA. During GG-NER, this process displaces the XPC complex, while in the TC-NER the RNA polymerase remains at the site of damage. XPG and the ERCC1-XPF heterodimer are responsible for 3' and 5' incision, respectively, of the bubble structure. Excision of a 25 to 30 nucleotide fragment is followed by gap filling by POLD in association with PCNA and RFC, and nick sealing by LIG3 together with XRCC1. POLE and LIG1 may also contribute to gap filling and nick sealing in replicating cells to a small amount. Other proteins, additional activities of those protein described above and post-translational modifications are also involved in NER, adding additional layers of damage verification and repair regulation (Shuck *et al.*, 2008; Nouspikel, 2009; Goosen, 2010). Remarkably, in conjunction with CSB, CSA is required for XPA binding protein 2 [XAB2], High mobility group nucleosome binding domain 1 [HMGN1] and Transcription elongation factor A [TCEA1] recruitment during TC-NER. XAB2 associates with XPA and the stalled RNA polymerase and seems to function as a scaffold protein. HMGN1 is required for

chromatin remodeling and TCEA1 for restart of transcription upon lesion removal (Fousteri & Mullenders, 2008; Tornaletti, 2009).

NER also participates in the repair of DNA inter-strand cross-links, together with components of other pathways like Homologous recombination, the Fanconi anemia network, DNA mismatch repair, and Translesion DNA synthesis (Wood, 2010).

1.1.5. Homologous recombination

Homologous recombination [HR] is a high fidelity DNA double-strand break [DSB] repair system that relies on the use of the homologous DNA strand as a template to achieve error-free repair. In addition to DSB repair, HR also participates in inter-strand cross-links repair, recovery of stalled or broken replication forks and telomere maintenance. Additionally, meiotic HR plays a role in the generation of genetic variability and proper chromosomal segregation. HR is essential in maintaining genome stability and in tumor suppression. Mono-allelic mutations in either Breast cancer type 1 or 2 susceptibility protein [BRCA1 or BRCA2] genes predispose affected women to breast and ovarian cancer, and mutations in *BRCA2* predispose men to breast, pancreas and prostate cancer. Inherited bi-allelic mutations in *BRCA2* (*a.k.a.* FANCD1) can cause the cancer-prone condition Fanconi anemia, a disorder characterized by congenital defects and progressive bone marrow failure. Similar phenotypes are also observed in loss of function mutations of BRCA1 interacting protein C-terminal helicase 1 [BRIP1, *a.k.a.* FANCJ] or Partner and localizer of BRCA2 [PALB2, *a.k.a.* FANCN] (Li & Heyer, 2008; San Filippo *et al.*, 2008; Moynahan & Jasin, 2010).

HR (Fig. 3) is initiated by recognition of DSB by MRN, a protein complex composed of MRE11, RAD50 and Nibrin [NBN]. Following damage recognition, the complex is responsible for recruitment and activation of the serine-protein kinase Ataxia telangiectasia mutated [ATM], and participate in DSB 5'-end resection to generate 3'-ssDNA overhangs, which subsequently leads to activation of the serine/threonine-protein kinase Ataxia telangiectasia and Rad3 related [ATR]. 5'-end resection relies on the combined action of MRN and CTBP-interacting protein [CtIP], in complex with BRCA1. The cellular concentration and the Cyclin-dependent kinase 1 [CDK1]-dependent phosphorylation status of CtIP determine in part the dominance of end resection during late S-phase and G_2-phase of the cell cycle. Initial end resection by the MRN/CtIP/BRCA1 complex is further extended by EXO1 and Bloom syndrome protein [BLM]. Generated ssDNA are protected by RPA, which additionally prevents the formation of ssDNA secondary structure (Takeda *et al.*, 2007; Pardo *et al.*, 2009; Lamarche *et al.*, 2010).

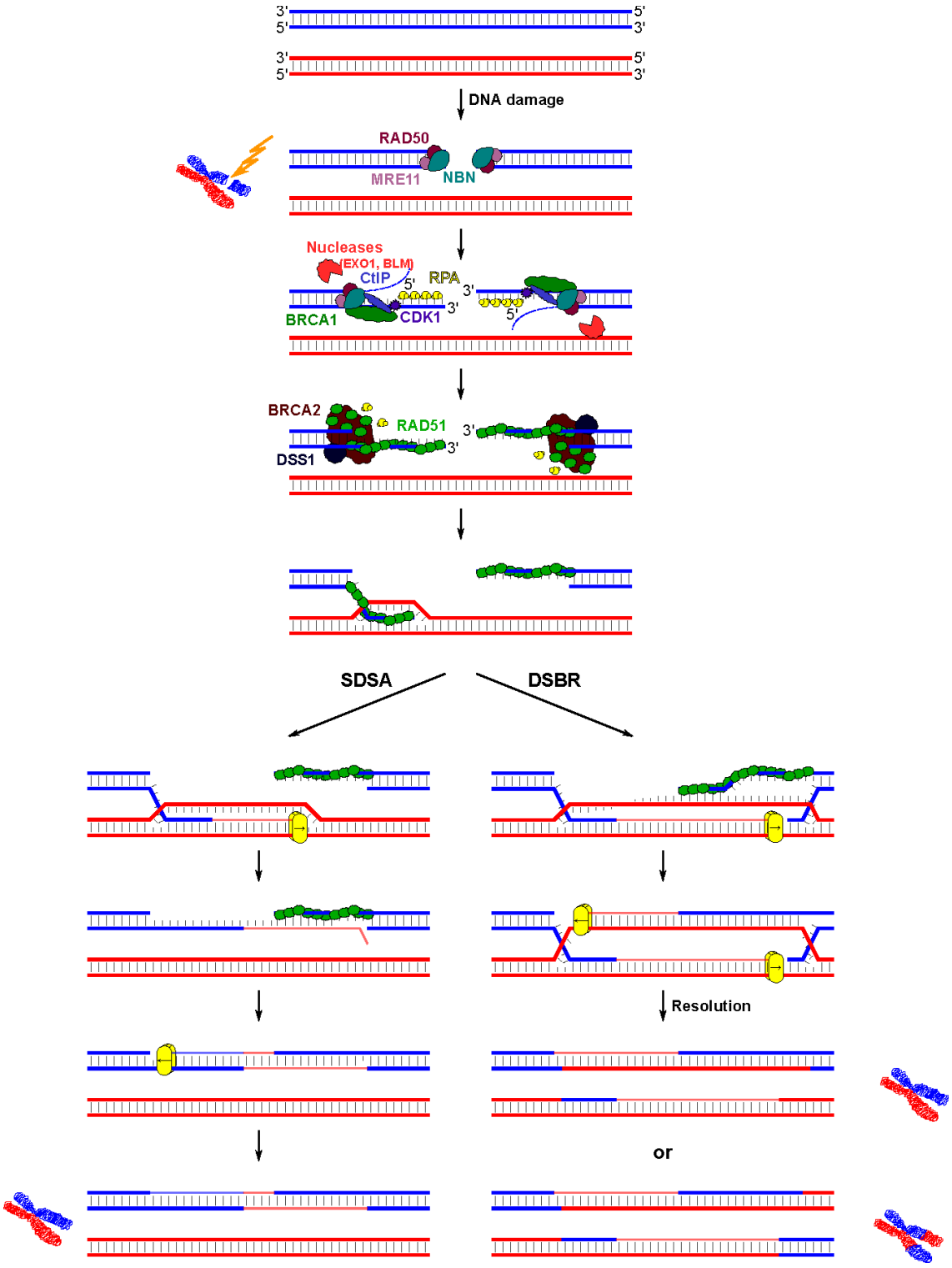

Figure 3. Simplified overview of the main players and steps of the Double strand break repair (DSBR) and Synthesis-dependent strand annealing (SDSA) pathways of Homologous recombination. See text in Section 1.1.5 for details. Modified from Li & Heyer (2008), San Filippo *et al*. (2008), Pardo *et al*. (2009) and Svendsen & Harper (2010).

The scaffold protein BRCA2 specifically recognizes dsDNA with ssDNA tails and stimulates RPA

displacement from ssDNA by RAD51, thereby promoting the formation of RAD51-ssDNA nucleoprotein filaments (presynaptic filaments). BRCA2 facilitates the formation of these presynaptic filaments by the combined action of six of its eight BRC repeats, bound by monomeric RAD51, and its carboxyl-terminus RAD51 binding domain, bound by oligomeric RAD51. Additionally, BRCA2 directly interacts with DSS1, which seems to regulated DNA binding, and with PALB2, which likely has a role in the intranuclear localization and accumulation of BRCA2. In addition to BRCA2 and its interacting proteins, presynaptic filament formation also depends on the RAD51 paralogs RAD51B, RAD51C, RAD51D, XRCC2 and XRCC3 (San Filippo *et al.*, 2008; Pardo *et al.*, 2009; Jensen *et al.*, 2010; Zou, 2010).

RAD51-coated 3'-ssDNA tails generated by DNA end resection perform the central reaction of the HR pathway, namely homology search and strand invasion. Invasion of the homologous DNA displaces a DNA strand forming a Displacement loop [D-loop] intermediate, and provides a 3'-end to prime DNA synthesis within the D-loop (Li & Heyer, 2008; San Filippo *et al.*, 2008; Pardo *et al.*, 2009). From this point on, three HR pathways have been described. In the Double strand break repair [DSBR] pathway (Fig. 3, right), initial DNA synthesis is followed by either an invasion event or an end capture of the second resected 3'-ssDNA tail to the extended D-loop, resulting in the formation of a double Holliday junction. Migration of the two Holliday junctions towards each other by a helicase (BLM) followed by dissolution of the hemicatenane structures by DNA topoisomerase 3-alpha [TOP3A] results in non-crossover events, while resolution by endonucleases (Flap endonuclease GEN homolog 1[GEN1] or Structure-specific endonucleases SLX1-SLX4 [SLX1 and SLX4]) results in crossover or non-crossover events. Double Holliday junction processing has the potential to create genomic rearrangements. In the synthesis-dependent strand annealing [SDSA] pathway (Fig. 3, left), migration of the D-loop caused by DNA synthesis eventually displaces the newly extended invading strand, which re-anneals with the second resected 3'-ssDNA tail. Only non-crossover products are formed by this pathway. In the Break-induced replication [BIR] pathway (Fig. 4), the presynaptic filament forms a replication fork with the homologous DNA sequence, resulting in copy of information from the homologous sequence and loss of that information (loss-of-heterozygosity) distal to the break site (Li & Heyer, 2008; San Filippo *et al.*, 2008; Pardo *et al.*, 2009; Svendsen & Harper, 2010). Other proteins participate during HR. For example, RAD54 is a motor protein involved in strand exchange and Holliday junction branch migration and resolution (Mazin *et al.*, 2010).

HR is a highly regulated pathway. Both the cell cycle control and the DNA damage response [DDR] participate in the control of the pathway, and a series of HR proteins are subject to post-translational modification (e.g. BLM, BRCA1, BRCA2, CtIP, EXO1, RAD51), contributing to the regulation of protein-protein interactions during HR. The formation or dissociation of some intermediates such as

the presynaptic filaments, D-loop and double Holliday junctions are important reversible control points of the pathway, with motor proteins playing a important anti-recombinogenic role. Irreversible 5'-end resection and endonucleolytic processing of junction intermediates are, on the other hand, considered key commitment steps in the pathway (Heyer *et al.*, 2010).

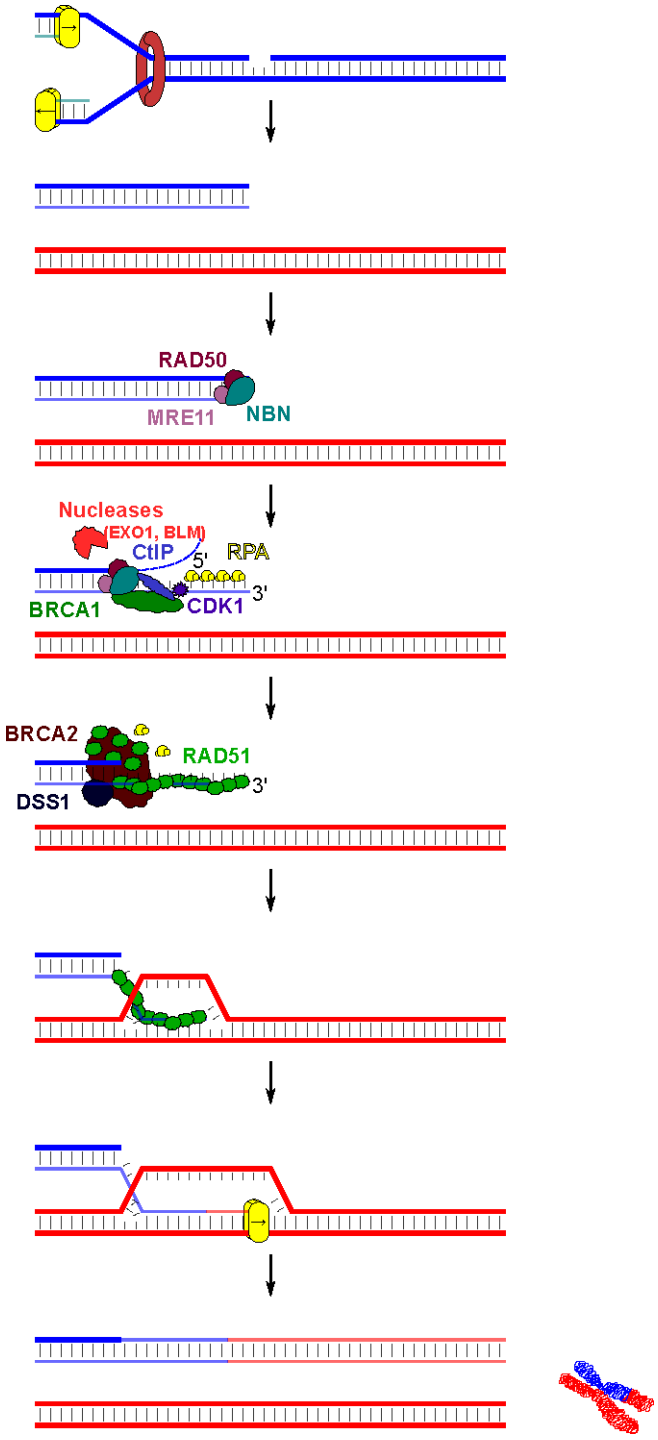

Figure 4. Simplified overview of the main players and steps of Break-induced replication (BIR) pathway of Homologous recombination. See text in Section 1.1.5 for details. Modified from Li & Heyer (2008) and Pardo *et al*. (2009).

1.1.6. Single-strand annealing

Single-strand annealing [SSA] is an error-prone DSB repair pathway that relies on the use of sequence homology at both ends of the break. Although it is related to HR, it is a RAD51-independent pathway (Li & Heyer, 2008; San Filippo *et al.*, 2008; Pardo *et al.*, 2009).

Like HR, repair is started by end resection (Fig. 5), but this is followed by annealing of the resected ends to each other at regions of direct repeats flanking the DSB. Protruding ends are then trimmered by nucleases and gaps or nicks are filled by DNA synthesis and ligation by the replication machinery. The pathway is error-prone, as it results in deletion of one of the two homologous repeats and the sequence among them (Li & Heyer, 2008; San Filippo *et al.*, 2008; Pardo *et al.*, 2009).

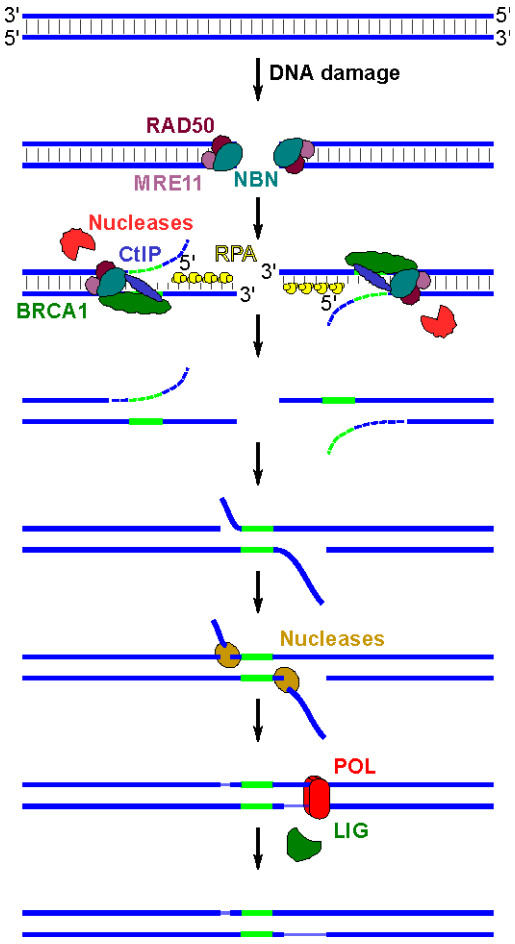

Figure 5. Simplified overview of the main players and steps of Single-strand annealing. See text in Section 1.1.6 for details. Modified from Li & Heyer (2008), San Filippo *et al.* (2008) and Pardo *et al.* (2009).

1.1.7. Non-homologous end joining

Non-homologous end joining [NHEJ] is an error-prone repair system that function by re-joining two ends of a DNA double-strand break. Besides repair of accidental DSB, NHEJ also participate during V(D)J Recombination and Class Switch Recombination, both indispensable processes during development and maturation of the adaptive immune system. Deficiencies in NHEJ are rare in humans (e.g. Radiosensitive-severe Combined Immunodeficiency (SCID) by Artemis null mutation, and immunodeficiency syndromes by LIG4 or XLF mutations) and are characterized by radiation sensitivity, immunodeficiency, increase leukaemogenesis, developmental delay, chromosome instability and microcephaly (de Villartay *et al.*, 2003; Buck *et al.*, 2006; Weterings & Chen, 2008; Lieber, 2010).

DNA-PKcs dependent NHEJ [D-NHEJ] (Fig. 6) is initiated by binding of the Ku70/Ku80 heterodimer to the ends of a DSB. Once bound to the break ends, Ku functions as a platform for other recruited NHEJ proteins. Recruited DNA-dependent protein kinase catalytic subunit [DNA-PKcs] is activated by autophosphorylation. Activated DNA-PKcs interacts with and activates proteins required for DNA end processing, polymerization and ligation. DNA-PKcs interacts with Artemis, forming a complex with endonuclease activity able to process different types of DNA ends. Other proteins, including PNKP (kinase and phosphatase activity) and Aprataxin [APTX] can also participate in end processing. Polymerization can be performed by Ku/DNA recruited DNA polymerase mu [POLM] (which can perform template-dependent, template-independent and discontinuous template synthesis) and lambda [POLL] (which also has lyase activity). The DNA-PKcs/Ku/DNA complex (i.e. DNA-PK holoenzyme) bridges the two DNA ends by direct interaction between two DNA-PKcs subunits, each bound to a DNA end. Tethered ends are then joined by the Ligase 4 [LIG4]/XRCC4/XRCC4-like factor [XLF] complex, with XRCC4 acting as a mediator for interaction with Ku/DNA. Additional proteins also participate in the process (Weterings & Chen, 2008; Mahaney *et al.*, 2009; Lieber, 2010; Mladenov & Iliakis, 2011).

Backup NHEJ [B-NHEJ] is an error prone repair pathway that operates with slower kinetics and comes into play only when D-NHEJ is defective. PARP1 seems to play a role in the recognition of DSB, doing so with a much lower affinity for DNA ends than Ku. The MRN complex, and more specifically MRE11, has been implicated in this pathway, suggesting a DNA end processing step. LIG3, in complex with XRCC1 and regulated by PARP1, performs the ligation reaction in the absence of LIG4 (Mladenov & Iliakis, 2011).

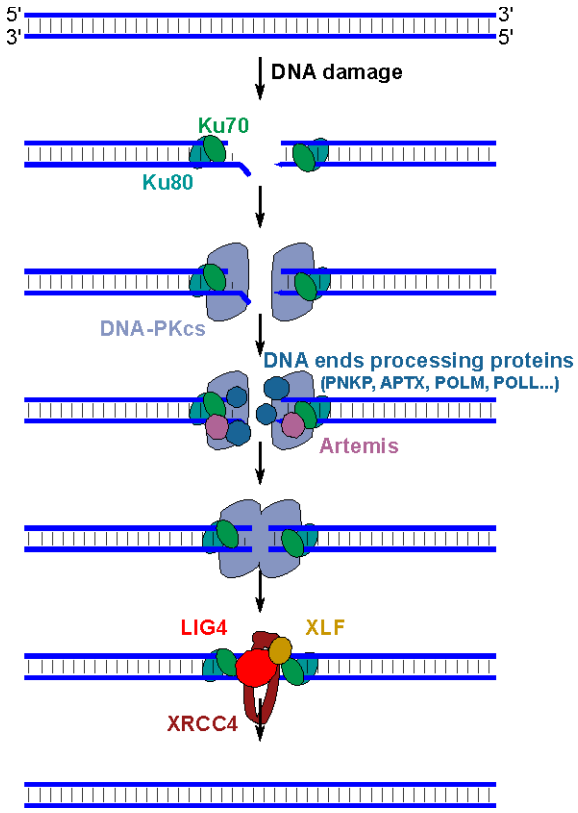

Figure 6. Simplified overview of the main players and steps of the DNA-PKcs dependent-Non-homologous end joining. See text in Section 1.1.7 for details. Modified from Weterings & Chen (2008), Mahaney *et al*. (2009), Lieber (2010) and Mladenov & Iliakis (2011).

1.1.8. Translesion DNA synthesis

Translesion DNA synthesis [TLS] refers to DNA nucleotide incorporation opposite a site of DNA damage. Although TLS can be essentially performed by replicative polymerases (POLA, POLE and POLD), most DNA lesions block their progression as a result of their restrictive active sites. In order to bypass the lesion, a switch to low stringency error-prone polymerases is performed. In this process, largely activated by ubiquitination of PCNA, the replicative polymerase is switched with a TLS polymerase (Lehmann *et al.*, 2007; Andersen *et al.*, 2008).

TLS polymerases include the Y-family DNA polymerases eta [POLH], iota [POLI], kappa [POLK] and REV1, and the B-family polymerase REV3L (catalytic subunit of DNA polymerase zeta [POLZ]). These polymerases are characterized by lower stringency, poorer processivity and lower fidelity than replicative polymerases, the last in part due to incorrect base pairing and/or lack of a 3'-5' proofreading exonuclease activity. POLH is mainly involved in synthesis past cyclobutane thymine dimers, and its deficiency leads to a Xeroderma pigmentosum phenotype. With a very low processivity and very high

error rate, POLI tends to incorporate G opposite T, and is not capable of synthesis extension. POLI seems to play a role in bypassing UV-induced DNA lesions. POLK performs synthesis opposite benzo[a]pyrene-guanine and other adducts on N^2guanine. REV1 is a deoxycytidyl transferase that always inserts a C opposite from lesions, and has a role in recruiting other TLS polymerases. B-family REV3L does not bypass modified bases, but it can extend from misincorporated bases (Lehmann *et al.*, 2007; McCulloch & Kunkel, 2008; Gan *et al.*, 2008).

1.2. Cell death

According to the Nomenclature Committee on Cell Death 2009, a cell is considered dead when it meets one of the following criteria:
"1: the cell has lost the integrity of its plasma membrane, as defined by the incorporation of vital dyes (e.g., PI) *in vitro*
2: the cell, including its nucleus, has undergone complete fragmentation into discrete bodies (which are frequently referred to as 'apoptotic bodies')
3: its corpse (or its fragments) has been engulfed by an adjacent cell *in vivo*" (Kroemer *et al.*, 2009).

Several modalities of programed cell death have been described based on morphological and biochemical classifications. The principal forms of cell death, namely apoptosis, autophagic cell death and necrosis (Kroemer *et al.*, 2009; Galluzzi *et al.*, 2012) are described below, together with other related cellular processes. As discussed below (see Section 1.3), apoptosis constitute the principal form of cell death triggered after treatment with clinically relevant doses of S_N1-alkylating agents (the object of investigation in this study). Consequently, the following description will focus on apoptosis, and will only briefly address the other principal forms of cell death. Other cell death modalities (i.e. anoikis, cornification, entosis, netosis, parthanatos, pyroptosis) (Kroemer *et al.*, 2009; Yuan & Kroemer, 2010; Galluzzi *et al.*, 2012) are omitted from this discussion.

1.2.1. Apoptosis

Apoptosis defines a type of cell death originally (Kerr *et al.*, 1972) described on the basis of specific morphological features, including rounding-up of the cell, retraction of pseudopodes, reduction of cellular and nuclear volume, nuclear fragmentation, minor modifications of cytoplasmic organelles,

plasma membrane blebbing and *in vivo* engulfment by resident phagocytes. This form of cell death has been commonly associated with the activation of proapoptotic Apoptosis regulator BCL2 [BCL2] family proteins, activation of Caspases [CASP], dissipation of the Mitochondrial transmembrane potential [$\Delta\psi_m$], Mitochondrial outer membrane permeabilization [MOMP], oligonucleosomal DNA fragmentation, exposure of phosphatidylserine on the outer cell membrane and plasma membrane rupture (Kroemer *et al.*, 2009; Hotchkiss *et al.*, 2009).

Apoptosis can be divided in extrinsic apoptosis (activated either by death receptors or by dependence receptors) and intrinsic apoptosis (with a caspase-dependent and a caspase-independent component) (Galluzzi *et al.*, 2012).

Extrinsic apoptosis is initiated by extracellular signals sensed and propagated by transmembrane receptors (e.g. FAS, TNFR1, TRAILR1, netrin receptors). It uses one of the following pathways:
a) ligand-induced death receptor signaling, leading to Death-inducing signaling complex [DISC] formation, activation of CASP8 (or CASP10), followed by CASP3, CASP6 and CASP7 activation.
b) ligand-induced death receptor signaling, leading to DISC formation, activation of CASP8, proteolytic cleavage of BH3 interacting domain death agonist [BID] to form Truncated BID [tBID], MOMP, apoptosome assembly, activation of CASP9, and CASP3, CASP6 and CASP7 activation. Other events related to MOMP (described below for intrinsic apoptosis) are also activated.
c) ligand deprivation-induced dependence receptor signaling, leading to activation of CASP9 (either directly or MOMP-dependent), followed by CASP3, CASP6 and CASP7 activation (Galluzzi *et al.*, 2012).

Intrinsic apoptosis is initiated by intracellular stress (e.g. oxidative stress, DNA damage, unfolded protein accumulation), and is mediated by irreversible MOMP by BCL2-associated X protein [BAX] and BCL2-antagonist/killer 1 [BAK1]. It is associated with the dissipation of the mitochondrial transmembrane potential, release of mitochondrial intermembrane space proteins (e.g. Cytochrome c [CYTC], Apoptosis-inducing factor [AIF], Endonuclease G [ENDOG], DIABLO, serine protease HTRA2 [HTRA2]) into the cytosol and inhibition of the respiratory chain. Release of CYTC, together with Apoptotic peptidase activating factor 1 [APAF1] and dATP triggers assembly of the apoptosome, with activation of CASP9, followed by CASP3, CASP6 and CASP7 activation. AIF and ENDOG participate in caspase-independent DNA fragmentation, while DIABLO and HTRA2 contribute to caspase activation by interfering with inhibitors of apoptosis (Hotchkiss *et al.*, 2009; Galluzzi *et al.*, 2012).

1.2.2. Autophagy

Autophagy is a pro-survival cellular process by which non essential, redundant, or damaged organelles and macromolecules are recycled, thereby generating ATP necessary for cell viability. Cell death with autophagy (not necessarily by autophagy, as this is in most cases rather a survival mechanism) has been defined as a type of cell death characterized by massive vacuolization of the cytoplasm, accumulation of double-membraned autophagic vacuoles, lack of chromatin condensation, and little or no uptake by phagocytic cells, *in vivo*. The dissociation of Beclin-1 [BECN1] from BCL2/Apoptosis regulator Bcl-XL [BCLXL], its dependency on *ATG* gene products, the LC3-I to LC3-II conversion and Sequestosome 1 [SQSTM1] degradation characterize this process (Kroemer *et al.*, 2009; Hotchkiss *et al.*, 2009).

Cell death mediated by autophagy (i.e. autophagic cell death) is defined as that exhibiting general markers of autophagy (described in the paragraph above) and that can be suppressed by the chemical or genetic inhibition of the autophagic pathway (Galluzzi *et al.*, 2012).

1.2.3. Necrosis

Necrosis is a form of cell death presenting cytoplasmic swelling, rupture of the plasma membrane, swelling of cytoplasmic organelles and moderate chromatin condensation. Regulated necrotic cell death can be accompanied by activation of calpains, activation of cathepsins, drop in ATP levels, High mobility group box 1 [HMGB1] release, Receptor-interacting protein 1 [RIP1] phosphorylation, RIP1 ubiquitination, Reactive oxygen species [ROS] overgeneration and a specific PARP1 cleavage pattern. Activation of distinct signaling modules defines different forms of regulated necrosis (Kroemer *et al.*, 2009; Hotchkiss *et al.*, 2009; Galluzzi *et al.*, 2012).

1.2.3.1. Necroptosis

Necroptosis (receptor-interacting protein 1 kinase activity-dependent necrotic cell death) refers to a specific case of regulated necrosis trigger by TNFR1 signaling, which is dependent on the kinase activity of RIP1 in complex with RIP3. This pathway mediates cell death mainly upon pathological conditions, can occur in the immune system, and can be involved in the response against viral infections. An involvement of ROS and/or mitochondria has been hypothesized as mediators of necroptosis execution (Yuan & Kroemer, 2010; Galluzzi *et al.*, 2012).

1.2.4. Other related terminology

1.2.4.1. Mitotic Catastrophe

Mitotic catastrophe is not considered to be a cell death pathway. It is an oncosuppressive mechanism that is initiated during M-phase following perturbation of the mitotic apparatus. Mitotic catastrophe is accompanied, to some degree, by mitotic arrest and eventually triggers cell death (apoptosis or necrosis) or senescence (Galluzzi *et al.*, 2012).

1.2.4.2. Senescence

Cellular senescence refers to a cellular response mechanism that generally occurs in response to potential oncogenic stimuli. Cellular senescence is not considered a form of cell death (Kroemer *et al.*, 2009; Campisi, 2011; Rodier & Campisi, 2011; Galluzzi *et al.*, 2012). It is characterized by an irreversible growth arrest that occurs in the presence of sustained DDR signaling originating from nuclear foci termed DNA segments with chromatin alterations reinforcing senescence. Senescent cells generally increase in size and are characterized by expression of senescence-associated β-galactosidase 1 [GLB1]. Many senescent cells also express the cyclin-dependent kinase inhibitor 2A [CDKN2A] (Campisi, 2011; Rodier & Campisi, 2011).

1.3. Alkylating agents

1.3.1. Generalities, distribution and use

Alkylating agents are substances with the ability of attach alkyl groups (C_nH_{2n+1}) to a substrate. Humans are continually exposed to alkylating agents from several endogenous and exogenous sources. Remarkable sources of endogenous alkylation include the intracellular methyl group donor S-adenosyl-methionine, responsible for ubiquitous low grade non-enzymatic methylation of the DNA (Rydberg & Lindahl, 1982), and alkylating nitroso compounds generated in the gastrointestinal tract by nitrosation of dietary precursors (Shephard & Lutz, 1989). Alkylating agents are also widely distributed in the environment, present in food and in tobacco smoke (Christmann & Kaina, 2011). Among them, atmospheric organohalogen compounds such as chloromethane, bromomethane and iodomethane account for the principal environmental alkylating agents. These compounds are

generated not only industrially but also by marine and terrestrial living organisms and by natural abiogenic processes (Gribble, 2003). Tobacco smoke related alkylating agents include the carcinogenic tobacco-specific N-nitrosamines 4-(methylnitrosamino)-1-(3-pyridyl)-1-butanone, 4-(Methylnitrosamino)-1-(3-pyridyl)-1-butanol and N'-nitrosonornicotine and other nitroso compounds like N-nitrosodimethylamine (IARC, 2007).

Alkylating agents have been in use for several decades as chemotherapeutic anticancer drugs. Initially used in chemical warfare, observations of the toxic effects of sulfur mustards (mustard gas) in exposed individuals gave rise to the use of alkylating agents for combating cancer. Since pioneering work in the 1940's (Goodman *et al.*, 1946) where the nitrogen mustard mustine hydrochloride was used in the treatment of leukemia, alkylating agents have been established as some of the most widely used anticancer drugs (Scott, 1970; Hurley, 2002; Ralhan & Kaur, 2007).

According to The Anatomical Therapeutic Chemical Classification System by the World Health Organization Collaborating Centre for Drug Statistics Methodology, chemotherapeutic antineoplastic alkylating agents are classified in six groups (http://www.whocc.no/atc_ddd_index/?code=L01A. Retrieved in December 2011):

1. Nitrogen mustard analogues: cyclophosphamide, chlorambucil, melphalan, chlormethine, ifosfamide, trofosfamide, prednimustine, bendamustine.
2. Alkyl sulfonates: busulfan, treosulfan, mannosulfan.
3. Ethylene imines: thiotepa, triaziquone, carboquone.
4. Nitrosoureas: carmustine, lomustine, semustine, streptozotocin, fotemustine, nimustine, ranimustine.
5. Epoxides: etoglucid.
6. Other alkylating agents: mitobronitol, pipobroman, **temozolomide**, dacarbazine.

There is a broad clinical spectrum of use for these agents. For example, the methylating agent streptozotocin is prescribed for treatment of metastatic cancer of the pancreatic islet cells, procarbazine for treatment of Hodgkin's lymphoma and malignant gliomas, dacarbazine in cases of metastatic melanoma, Hodgkin's lymphoma and sarcoma, and temozolomide for combating malignant gliomas and melanomas. The chloroethylating agents nimustine, carmustine and lomustine are used in the treatment of malignant gliomas, other Central nervous system [CNS] malignancies, melanoma, multiple myeloma and Hodgkin's and non-Hodgkin lymphomas, while fotemustine is used in the treatment of metastasising melanoma (Kaina *et al.*, 2010).

1.3.2. Profile of DNA adduct formation

Alkylating agents react with biological macromolecules via unimolecular (S_N1) or bimolecular (S_N2) nucleophilic substitution. S_N1-alkylating agents follow first-order kinetics, with the formation of an alkyl-diazonium cation being the rate-determining step of the reaction. Once formed, the electrophilic cation reacts rapidly with nucleophilic centers in the cell forming a covalent bond between the macromolecules and the adduct. Conversely, S_N2-alkylating agents follow second-order kinetics, where the rate-determining step involves a transition state between the electrophile and the nucleophile, which results in the formation of an alkylated macromolecule and release of a leaving group (Beranek, 1990; Wyatt & Pittman, 2006).

Thirteen base adducts can be formed in double-stranded DNA upon alkylation, namely N1-, N3-, N^6- and N7-alkyladenine, O^2- and N3-alkylcytosine, N1-, N3-, O^6- and N7-alkylguanine, and O^2-, N3- and O^4-alkylthymidine (Beranek, 1990; Kaina *et al.*, 2007).

Following treatment with S_N1-methylating agents, N7-methylguanine [N7MeG] and N3-methyladenine [N3MeA] account for most of the methyl-adducts (roughly 70-80% and 10%, respectively). O^6-methylguanine [O^6MeG] accounts for 7-8% of the total methylation, the remaining adducts making up no more than 5% of the total methylation. The adduct formation profile for S_N2-methylating agents is also dominated by N7MeG and N3MeG. The main difference between S_N1- and S_N2-methylating agents is the formation of O^6MeG, as S_N2-methylating agents produces only about 0.3% of this adduct (Beranek, 1990). This difference in reactivity towards the O^6 position of guanine causes the differences in biological response of cells treated with S_N1- or S_N2-methylating agents.

1.3.3. Repair pathways involved in dealing with S_N1-alkylating agent-induced DNA damage

Below its repair saturation level, the N-methylation adducts N3MeG, N7MeG and N3MeA, as well as other methyl adducts, are repaired rapidly and efficiently via base excision repair (Baute & Depicker, 2008) (BER, described in Section 1.1.3). N3MeA, but not the guanine-methylated adducts, is a replication blocking lesion (Larson *et al.*, 1985) which contribute to chromosomal damage and toxicity triggered by alkylating agents (Engelward *et al.*, 1996).

The covalent modifications N1MeA and N3MeC are repaired by a direct reversal mechanism catalyzed by ALKBH2 and ALKBH3 (described in Section 1.1.1.1) (Duncan *et al.*, 2002; Sedgwick *et*

al., 2007). Accordingly, ALKBH2 mediated removal of N1MeA have been shown to protect against alkylation-induced toxicity (Ringvoll *et al.*, 2006).

On the other hand, the pre-toxic O^6-alkyl adducts, by far the most toxic lesion induced by clinically relevant doses of S_N1-methylating agents, are directly repaired by the repair protein O^6-methylguanine-DNA methyltransferase (MGMT, described in Section 1.1.1.2). Consequently, MGMT expression is a major determinant of resistance to this group of agents (Kaina *et al.*, 2007). O^6-ethyl adducts, but not O^6-methyl adducts, can also be repaired by nucleotide excision repair (Bronstein *et al.*, 1992a; Bronstein *et al.*, 1992b) (NER, described in Section 1.1.4). O^6-chloroethylguanine [O^6ClEtG] undergoes an intramolecular rearrangement to form the intermediate N1-O^6-ethanoguanine, followed by the formation of the N1-guanine-N3-cytosine inter-strand cross-link (Tong *et al.*, 1982; Fischhaber *et al.*, 1999). MGMT can correct the original O^6ClEtG lesion (Kaina *et al.*, 1991), while inter-strand cross-links are repaired by components of NER, Homologous recombination and Translesion DNA synthesis (Muniandy *et al.*, 2010). (NER, HR and TLS, described in Sections 1.1.4, 1.1.5 and 1.1.8).

BER is functional in most tissues and no repair-deficient disorders have been described to date in humans. Although its functionality is limited in some cellular precursors (Briegert *et al.*, 2007; Briegert & Kaina, 2007) (a fact with potential implications in the side effects upon clinical use of these agents), treatment of cancer and most differentiated tissues with clinically relevant doses of chemotherapeutic S_N1-alkylating agents produces levels of N-alkylation below the saturation level of this repair system, thereby blocking most of the potential toxic effects caused by these lesions. Contrary to BER, there is considerable inter-individual and tissue specific variability in MGMT expression, this variability being even higher in tumor tissue (Christmann *et al.*, 2011). As a consequence, upon treatment with clinically relevant doses of S_N1-alkylating agents, O^6-alkylguanine is the principal pre-toxic lesion.

Two major groups of S_N1-alkylating agents are currently being used in chemotherapy, namely O^6-methylating and O^6-chloroethylating agents. The present work will focus on the mechanism of toxicity induced by clinically relevant doses of O^6-methylating agents. Consequently, further descriptions of models will apply mainly to O^6MeG-triggered end points. Relevant information on O^6-chloroethylating agents will be pertinently provided.

1.3.4. O^6MeG-triggered biological effects

O^6MeG is a pre-mutagenic, pre-carcinogenic, pre-recombinogenic, pre-clastogenic and pre-cytotoxic

lesion (Kaina *et al.*, 2007). O^6MeG is considered a pre-toxic and -genotoxic lesion, as it has to be processed in order to elicit its detrimental effects.

1.3.4.1. O^6MeG-induced mutagenesis and carcinogenesis

Fairly well understood for several decades (Loveless, 1969), mutagenicity induced by S_N1-methylating agents can be explained on the basis of the mispairing properties of O^6MeG. Methylation of the O^6 position of guanine leads to changes in the bond distances and angles around the six-membered ring of guanine. As a result, the most energetically favorable conformation adopted by the modified base blocks sites required for proper Watson-Crick base pairing (Parthasarathy & Fridey, 1986). Upon replication of DNA, O^6MeG mispairs with thymine. This mispairing is competitive with the incorporation of cytosine, with about one mispair for every three modified bases when synthesis occurs in an isostoichiometric deoxynucleoside 5'-triphosphate pool (Abbott & Saffhill, 1979). If not repaired by MGMT nor recognized by mismatch repair (MMR, described in Section 1.1.2), the O^6MeG/T mispairing causes a G-C to A-T transition mutation upon a further round of DNA replication (Coulondre & Miller, 1977; Eadie *et al.*, 1984). Consistent with the central role of O^6MeG in mutagenicity triggered by S_N1-methylating agents, induction of an unique O^6MeG site is sufficient to produce a pattern of mutagenesis identical to that found after S_N1-methylation (Loechler *et al.*, 1984). Additionally, mutagenicity induced by these agents can be abrogated upon expression of the repair enzyme MGMT (Fox *et al.*, 1987; Fox & Margison, 1988; Kaina *et al.*, 1991). From a clinical point of view it is important to note that not all mutations are lethal, some mutant cells may even have a growth advantage, and therefore become more resistance to treatment.

As for mutagenesis, O^6MeG has been implicated as the principal carcinogenic lesion induced by S_N1-methylating agents. Persistence of this adduct in brain tissue has been associated with tumor formation in rats (Margison & Kleihues, 1975), and low MGMT expression levels have been proposed to be a predisposing factor to S_N1-methylation-induced carcinogenesis in human brain (Silber *et al.*, 1996). Consistent with these observations, transgenic expression of MGMT protected mice from developing thymic lymphomas after S_N1-methylating treatment (Dumenco *et al.*, 1993). MGMT expression has also been shown to protect against skin tumor initiation (Becker *et al.*, 1996; Becker *et al.*, 1997) and promotion (Becker *et al.*, 2003) by S_N1-alkylating agents in mice two-stage carcinogenesis models. Mutagenesis plays a prominent role in carcinogenesis, as O^6MeG-triggered G-C to A-T point mutations in the *Hras* oncogene is responsible for oncogene activation and initiation of mammary carcinogenesis in rats after treatment with S_N1-methylating agents (Zarbl *et al.*, 1985). Mutation on the *Hras* oncogene has also been involved in skin tumor initiation (Becker *et al.*, 1997) by S_N1-alkylating agents. Besides its carcinogenic role through mutagenicity, other events triggered by

S_N1-methylating agents may contribute to cancer generation, such as DSB and chromosomal breaks, which contribute to an increased genomic instability in treated cells. Additionally, a role for BER depended repair of N-methylation lesions have also recently been implicated in the defense against colon cancer formation caused by S_N1-methylating agents (Wirtz *et al.*, 2010).

1.3.4.2. O^6MeG-induced clastogenesis and recombination

MGMT confers strong protection against Sister chromatid exchanges [SCE] and Chromosomal aberrations [CA] induction by S_N1-alkylating agents, pointing out O^6MeG as the principal primary pre-clastogenic and pre-recombinogenic lesion. Evidence suggests a need for processing of the lesion in order to accomplish its recombinogenic and clastogenic potential (Kaina *et al.*, 1991; Preuss *et al.*, 1996). MMR is required for this processing, as cell lines defective in MMR are refractory to CA production after S_N1-alkylating damage, at the expense of increased mutation rates (Goldmacher *et al.*, 1986; Galloway *et al.*, 1995).

Following treatment with S_N1-alkylating agents, SCE and CA are induced at high level at late times. This late induction can be attributed to O^6MeG, as MGMT expression abolishes them. At early times, recombination events and aberrations occur only when treatment is performed with high dose of these agents, e.g. doses that saturate the repair capacity of BER. These early events are refractory to suppression by MGMT, indicating its independence from the O^6MeG adduct. In this case, the high level of AP sites generated by enzyme-catalyzed or spontaneous hydrolysis of N-alkylated bases exceeds the repair capacity of the cell. Additionally, overlapping BER repair patches may occur leading to the formation of DSB, and thus trigger recombinogenic and clastogenic events (Kaina & Aurich, 1985; Coquerelle *et al.*, 1995; Kaina *et al.*, 1997).

1.3.4.3. O^6MeG-induced cell death

Exploited mainly in cancer chemotherapy, cell death constitute an clinically desirable biological effect induced by S_N1-alkylating agents. Despite being in use for decades, the mechanism (or mechanisms) leading to cellular death after treatment with this group of agents is not yet completely understood, and disagreement in the scientific community has not been appeased. Some features surrounding toxicity triggered by S_N1-methylating agents are nevertheless widely accepted (namely dependence on DNA replication and MMR (Kaina *et al.*, 2007)), as described below.

Although it is not the only signal for cell death generated by S_N1-alkylating agents, O^6MeG constitute the principal primary pre-toxic adduct after treatment with a clinically relevant dose of these agents

(Day *et al.*, 1980; Kaina *et al.*, 1991). Toxicity triggered by these agents is executed via apoptosis, and MGMT expression inversely correlates with S_N1-alkylating agent-induced apoptosis (Kaina *et al.*, 1997; Tominaga *et al.*, 1997; Meikrantz *et al.*, 1998). O^6MeG-triggered apoptosis is dependent on DNA replication, as non-proliferating cells show no induction of apoptosis following S_N1-methylating treatment, while they did engaged in cell death after ionizing radiation (Roos *et al.*, 2004).

Several lines of evidence have been provided consistent with the participation of MMR in toxicity triggered by S_N1-alkylating agents. Alkylation tolerant cell lines isolated by multiple treatment with increasing doses of alkylating agents showed high resistance to killing by S_N1-alkylating agents. Treatment with these agents also induced much more mutations in these cell lines. Although these cell lines tolerate alkylation, no effect on the repair of these lesions was observed (Goldmacher *et al.*, 1986). These tolerant cell lines were found to be defective in the recognition of the G/T mispair due to deficiencies in either MutSα or MutLα, and similar to other MMR defective systems (bacteria and yeast), also showed increased spontaneous mutation rates. Reversion of the tolerant phenotype was accompanied by the recovery of the mismatch binding capacity and a return to a mutation rate similar to that of the parental cell lines (Branch *et al.*, 1993; Kat *et al.*, 1993; Hampson *et al.*, 1997). Sensitivity to S_N1-alkylating agents can be restored by chromosome transfer into cancer cell lines lacking functional MLH1 (chromosome 3) or MSH2 or MSH6 (both in chromosome 2) (Koi *et al.*, 1994; Umar *et al.*, 1997). Additionally, mouse embryonic stem cell lines where both copies of the MMR mouse gene *Msh2* were inactivated acquired a mutator phenotype and became tolerant to S_N1-alkylating agents (de Wind *et al.*, 1995). Moreover, MSH6 mutation have been associated with tumor progression and recurrence after O^6-alkylating treatment of patients with brain tumors (Hunter *et al.*, 2006; Cahill *et al.*, 2007).

1.3.4.4. Mechanisms of O^6MeG-induced cell death

O^6MeG is a covalent modification of guanine that if not repaired by MGMT persists in the DNA. Given the mispairing properties of this adduct (Parthasarathy & Fridey, 1986), replication of DNA containing this lesion leads to the formation of O^6MeG/C or O^6MeG/T mispairs (i.e. O^6MeG/Y). MutSα recognize both O^6MeG/C and O^6MeG/T mismatches (Duckett *et al.*, 1996) and it has been shown that this recognition is required for apoptosis induction (Hickman & Samson, 1999).

Different hypothesis of how MMR bound to mismatches containing O^6MeG trigger cell death have been proposed (Fig. 7). They are the direct signaling model, the abortive processing model and the nuclease attack model. These hypotheses will be discussed below.

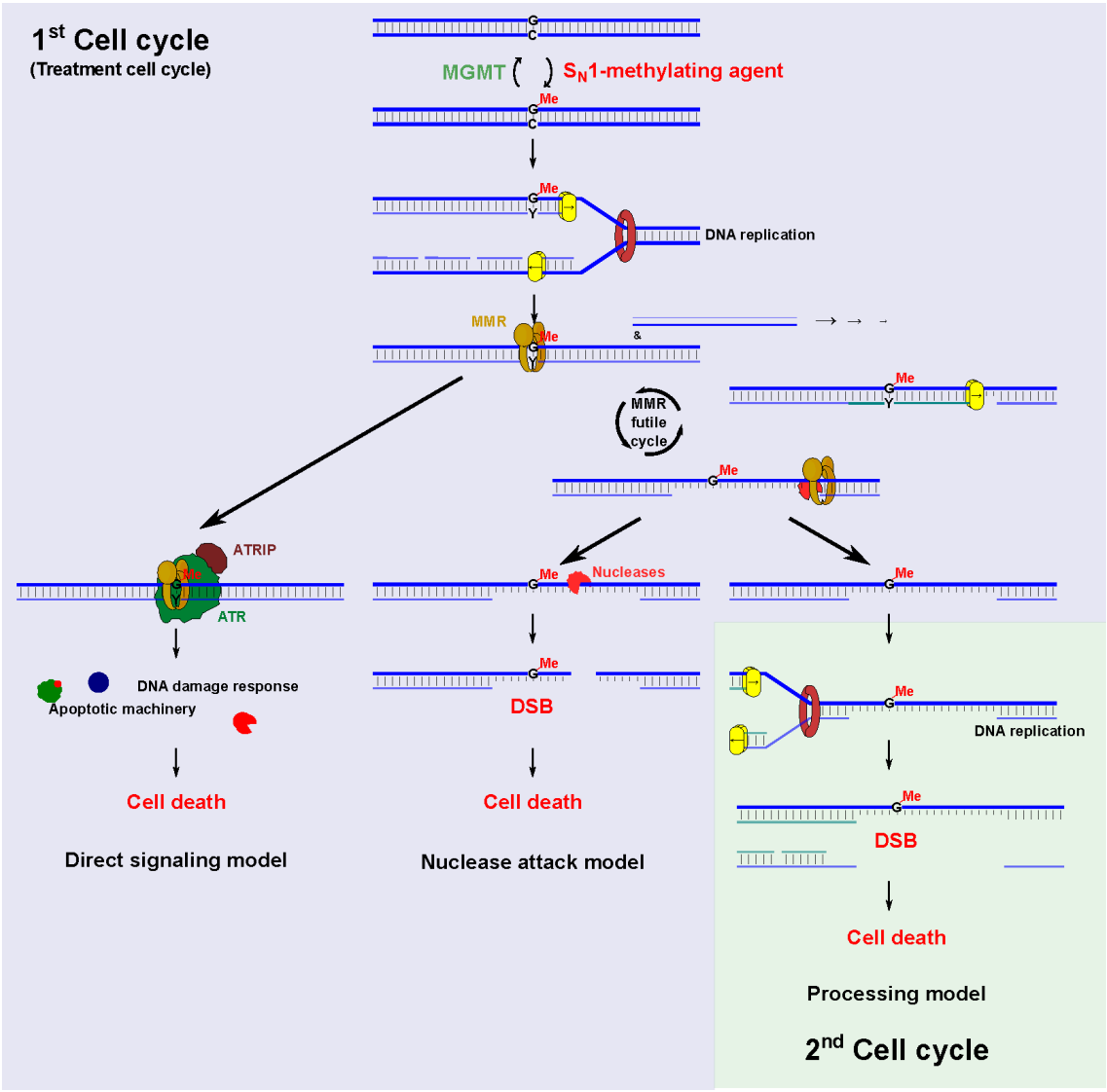

Figure 7. Models for O^{6}MeG-induced cell death. See Sections 1.3.4.4a to 1.3.4.4c for details. Modified from Kaina *et al*. (2007).

1.3.4.4a. Direct signaling model for O^{6}MeG-triggered toxicity

This model (Fig. 7, left) is based on the so-called sliding clamp signaling model for MMR (Modrich, 1997; Fishel, 1998), which proposes that once the heterodimeric MutSα recognizes the O^{6}MeG/Y mispair it forms an ATP bound hydrolysis-independent sliding clamp that signals the apoptotic machinery directly, with no requirement for processing of damage or modified sites by MMR.

Consistent with this model, a small percentage of the DDR transducer kinase ATR interacts constitutionally with MSH2. This physical interaction forms a signaling module that upon S_N1-methylating treatment leads to a direct phosphorylation of Structural maintenance of

chromosomes 1A [SMC1A] by ATR, with MSH6 functioning as an adapter for SMC1 binding. This phosphorylation was found to be required for cell survival (Wang & Qin, 2003).

Further support for the direct signaling model of MMR has come from studies showing ATR and serine/threonine-protein kinase CHK1 [CHK1] activation following S_N1-methylating treatment. This signaling was dependent on O^6MeG and occurred preferentially in the S-phase of the cell cycle. Using an *in vitro* system with nuclear extracts O^6MeG/T was shown to be preferentially recognized by MutSα over O^6MeG/C and G/T mismatches. This recognition resulted in recruitment of ATR/ATRIP to the damage site, ATR activation and subsequent CHK1 phosphorylation. RPA was not preferentially recruited to the damage site, arguing against activation through extensive DNA processing or formation of repair intermediates (Yoshioka *et al.*, 2006). In line with these observations, ATR activation and CHK1 phosphorylation is detected at very early time points after S_N1-methylating treatment (Caporali *et al.*, 2004; Stojic *et al.*, 2004), and human cells have been reported to arrest following the 1st S-phase after S_N1-methylating agent treatment (Carethers *et al.*, 1996).

A stronger support for a non-repair related function for MMR came from studies with missense mutations in the ATPase domain of MSH2 and MSH6 proteins in mice. These mutant proteins were capable of mismatch binding, but presented a DNA repair deficiency. Interestingly, and contrary to their MSH6-null mice counterparts, mouse embryonic fibroblasts obtained from these MSH6 mutants did not show any deficiency in the apoptotic response following S_N1-methylating agents (Lin *et al.*, 2004; Yang *et al.*, 2004).

1.3.4.4b. Processing model for O^6MeG-triggered toxicity

This model (Fig. 7, right) is based upon an early model proposed by Plant & Roberts (1971) and lately expanded on by Karran & Bignami (1994). In its current refined form, once recognized by MutSα the O^6MeG/Y mispair is processed by the repair activity of MMR (described in Section 1.1.2). Following recognition, the mismatch and a track of surrounding nucleotides are excised by the action of MutLα and EXO1. Giving the mispairing properties of O^6MeG, synthesis across the lesion again introduces a mispair. This mispair is again recognized by MutSα, restarting the MMR-dependent processing of the lesion. This self abortive processing, referred too as MMR futile repair cycle or loop, is unable to correct the lesion. As a result, single-stranded gaps persist in the DNA, and upon a second round of DNA replication leads to collapse of replication forks, DSB formation and cell death.

A body of evidence supports this model. O^6MeG-dependent SCE and CA are formed only at time points compatible with cells that have undergone two rounds of DNA replication (Kaina & Aurich,

1985; Kaina *et al.*, 1997). Apoptosis induction after S_N1-methylating agent treatment is a very late event after damage induction (Ochs & Kaina, 2000; Roos *et al.*, 2007; Naumann *et al.*, 2009), compatible with the kinetics of SCE and CA induction. Cell death triggered by S_N1-methylating agents is preceded by DSB formation (Ochs & Kaina, 2000), a DNA lesion that has been shown to be a potent inductor of apoptosis (Lips & Kaina, 2001), and which according to this model are proposed to be the final trigger of the apoptotic response after O^6MeG processing.

Also in line with the processing model, single-stranded gaps in the DNA have been evidenced following unsuccessful post-replicative processing of O^6MeG-induced mispairs by MMR. These gaps were even found far from the replication fork and remain in the DNA after completion of the 1st round of DNA replication. According to the processing model, these gaps are expected to cause collapse of replication forks in the 2nd cell cycle after treatment. The persistence of diffused chromatin bound PCNA staining after the 1st DNA replication and into the 2nd cell cycle have been taken to suggest post-replicative iterative attempts by the MMR machinery to fill these gaps even into the post-treatment cell cycle (Mojas *et al.*, 2007).

Moreover, compatible with processing of the O^6MeG-induced mismatch by the MMR complex, cell extracts from tolerant cells did not performed repair-dependent DNA synthesis after S_N1-treatment, but it was restored by reconstitution of the extract with the corresponding MMR purified protein. Extracts from normal cells, on the other hand, showed repair-dependent synthesis associated with incompletely repaired plasmids (Ceccotti *et al.*, 1996). Additionally, contrary to the report by Yoshioka *et al.* (2006), CHK1 phosphorylation by ATR have been reported to be dependent on RPA, suggesting the generation of ssDNA as part of the activation process, probably as a result of a repair intermediate (Wang & Qin, 2003). Finally, contrary to that reported by Carethers *et al.* (1996), an ATR and CHK1-dependent G_2 arrest has been reported to be compatible with cells in the 2nd cell cycle after treatment. Abrogation of ATR or CHK1 leaded to attenuation of the arrest, and an increase in cell death (Caporali *et al.*, 2004; Stojic *et al.*, 2004).

1.3.4.4c. Nuclease attack model for O^6MeG-triggered toxicity

This model (Fig. 7, middle) assume generation of DSB and toxicity as a result of cleavage of the template strand upon nuclease attack in areas of gaped DNA generated as a result of futile processing of the O^6MeG/Y mispair by MMR (Kaina *et al.*, 2007).

1.4. Glioblastoma multiforme

1.4.1. Description and classification

Gliomas are tumors that arise from glial cells, and include astrocytoma, glioblastoma, oligodendroglioma, ependymoma, mixed glioma, malignant glioma not otherwise specified, and other rare histologies. Glioblastoma (IDC-O 9440/3, *a.k.a.* glioblastoma multiforme [GBM]) is the most common and deadliest form of primary brain tumor. Belonging to the group of astrocytic tumors, it is graded with the highest category of malignity for primary tumors (code /3, i.e. primary infiltrative malignant neoplasia) and for aggressiveness (grade IV) according to the World Health Organization [WHO] classification of the tumors of the central nervous system (Louis *et al.*, 2007a; Louis *et al.*, 2007b).

GBM arise either from a progressive pathway from lower grade tumors (grade II and III astrocytoma) or occurs *de novo*, without detectable antecedent of malignant lesion. About 90% of the GBM are primary tumors (i.e. *de novo* occurrence), affecting mostly older patients above the age of 45 years. Secondary or progressive GBM, on the other hand, are found mostly in patients below this age, and comprise the remaining 10% of the cases. Independent of their primary or secondary origin, GBM are clinically indistinguishable. Nevertheless, both kinds of tumors represent two completely different genetic entities, with genetic alterations affecting similar molecular pathways. Genetic sub-classes within these entities have also been proposed, with potential prognostic implications (Furnari *et al.*, 2007).

1.4.2. Incidence

During 2008, 237 913 cases of brain and nervous system cancer were reported worldwide, corresponding to a rate of 3.5 per 100 000 person/year (3.7 and 3.3 per 100 000 person/year for males and females, respectively). Underregistration is expected for several countries (Ferlay *et al.*, 2010).

For the 2004-2007 period in the United States, GBM accounted for 16.7% of all primary brain and CNS tumors, with an incidence of 3.19 per 100 000 person/years, topped just by non-malignant meningioma. The incidence of GBM increases with increasing age (0-19 years: 0.14 per 100 000 person/year, 20-34 years: 0.41, 35-44 years: 1.22, 45-54 years: 3.71, 55-64 years: 8.22, 65-74 years: 13.27, 75-84 years: 14.49, 85+ years: 8.30), and is 1.6 times more common in males

than females (3.99 vs 2.53 per 100 000 person/year, respectively). GBM accounts for 53.7% of all gliomas, and together with astrocytoma make up 76% of all gliomas (Hinsdale, 2011).

1.4.3. Treatment

1.4.3.1. Current standard of care

There is no curative treatment for GBM. Standard of care for patients with this malignancy include symptomatic treatment with anticonvulsants and corticosteroids, and surgery followed by radiation therapy and chemotherapy. Antibiotic prophylaxis against *Pneumocystis jirovecii* pneumonia is also recommended during chemoradiotherapy.

Cytoreductive surgery not only alleviates symptoms by debulking of the tumoral mass, but the extend of resection has also been indicated as a factor in improving survival in primary malignant glioma by facilitating adjuvant chemoradiotherapy. Nevertheless, complete surgical resection of the tumor is invariably hampered by the inherent invasiveness of these malignancies into surrounding healthy brain tissue, thus weighting the role of chemoradiotherapy on the survival of patients (Ryken *et al.*, 2008).

Current standard first line chemoradiotherapy for newly diagnosed GBM patients consist of concomitant radiotherapy [RT] and chemotherapy with the methylating agent temozolomide [TMZ], followed by maintenance chemotherapy with TMZ alone. Primary combinatorial treatment consist of fractionated focal irradiation in daily fractions of 2 Gy given 5 days per week for 6 weeks, for a total of 60 Gy, plus TMZ at a dose of 75 mg/m^2 administered daily for 40 to 49 days. Maintenance TMZ therapy is administered for 6 cycles of 5 days every 4 weeks, at a dose of 150-200 mg/m^2 (Stupp *et al.*, 2005; Stupp *et al.*, 2007). Alternative schedules and longer periods of maintenance TMZ therapy are also practiced (Villano *et al.*, 2009).

1.4.3.2. Temozolomide

Temozolomide [TMZ] (code L01AX03 according to The Anatomical Therapeutic Chemical Classification System by the WHO Collaborating Centre for Drug Statistics Methodology) is an oral imidazotetrazine alkylating agent. Under physiologic condition it converts spontaneously into the highly reactive 5-(3-methyltriazen-1-yl)imidazol-4-carboxamid (MTIC) by a non-enzymatic, chemical degradation process. MTIC further breaks down to 4-amino-5-imidazole-carboxamide (AIC) and a methyl-diazonium cation (Tsang *et al.*, 1991; Denny *et al.*, 1994).

TMZ is absorbed rapidly and achieves a peak plasma concentration in 0.33 to 2.5 h. Maximal plasma concentration ranges between 25 and 85 μM for individuals receiving 100 to 200 mg TMZ/m^2/day. Elimination occurs with a half life of 1.4 to 2.1 h. TMZ or its metabolites are mainly eliminated in the urine, and a small amount in the feces (Baker *et al.*, 1999; Hammond *et al.*, 1999). TMZ readily penetrates the intact blood-brain barrier, with a cerebrospinal fluid:plasma ratio of 0.33 in non-human primates (Patel *et al.*, 2003).

TMZ is well tolerated. Common adverse effects of the combined regimen include thrombocytopenia, nausea, vomiting, anorexia, and constipation. TMZ exposure was additionally associated to alopecia, headache, fatigue and convulsions (Stupp *et al.*, 2005). Major hematologic adverse effects, mainly in the form of aplastic anemia, and also including agranulocytosis, aplasia, leukemia, myelodysplastic syndrome and lymphoma have been reported (Villano *et al.*, 2011).

1.4.4. MGMT promoter methylation status

MGMT constitutes the first line of defense against O^6-alkyl lesions (Section 1.1.1.2 and 1.3.3), and consequently, an important tumoral drug resistance marker. Although regulation of MGMT expression by different transcription factors has been reported, MGMT expression depends mainly on the methylation status of the 5^{th} carbon atom of cytosine residues in CpG islands located in the *MGMT* gene promoter. As a consequence of *MGMT* promoter methylation, MGMT expression is lost (Costello *et al.*, 1994a; Costello *et al.*, 1994b; Weller *et al.*, 2010; Christmann *et al.*, 2010).

Methylation of the *MGMT* promoter, as assessed by methylation-specific polymerase chain reaction (Herman *et al.*, 1996; Esteller *et al.*, 1999), has been used as a positive predictor of benefit upon TMZ treatment in GBM (Weller *et al.*, 2010).

MGMT promoter methylation has been found to predict prolonged progression-free survival and overall survival in patients treated with TMZ (21.7 months overall survival in patients treated with TMZ and RT as compared to 15.3 months in patients treated with RT alone), while in the absence of *MGMT* promoter methylation a much smaller and insignificant increase was found (11.8 months vs 12.7 months among patients treated with TMZ and RT as compared with RT alone) (Hegi *et al.*, 2005).

1.4.5. MGMT inhibitors

Although brain tumors usually express low levels of MGMT, a major fraction of these malignancies do indeed show clinically relevant expression levels of this repair enzyme (Citron *et al.*, 1995), making them non-responsible to treatment with chemotherapeutic S_N1-alkylating agents like TMZ. To overcome this problem, MGMT inhibitors have been envisioned as a tool for enhancing the effectiveness of this group of agents in MGMT expressing tumors (Kaina *et al.*, 2010).

The modified oligonucleotide O^6-benzylguanine [O^6BG] (Dolan *et al.*, 1990) is by far the most extensively studied MGMT inhibitor at pre-clinical and clinical level (Kaina *et al.*, 2010). MGMT inactivation by the pseudo-substrate O^6BG occurs by covalent transfer of the benzyl group of the inhibitor to the active site of the repair protein (Pegg *et al.*, 1993). O^6BG has been shown to completely deplete MGMT activity in cultured cell lines within 15 min of application, resulting in an increased toxicity of MGMT expressing cells treated with S_N1-alkylating agents (Dolan *et al.*, 1990). Since then, several *in vitro* and pre-clinical studies have demonstrate the applicability of this inhibitor to sensitize MGMT expressing cancer cells or tumors to the toxic effects of S_N1-alkylating agents (Kaina *et al.*, 2010). The O^6BG derivative O^6-(4-bromothenyl)guanine [O^6BTG] (Lomeguatrib, PaTrin-2) (McElhinney *et al.*, 1998) has also been shown to have these chemo-sensitizing properties (Middleton *et al.*, 2000; Kaina *et al.*, 2010). Both O^6BG and O^6BTG have reached Phase II clinical trials for the treatment of different tumors, including GBM, CNS tumors, myeloma multiple, metastatic melanoma and metastatic colorectal carcinoma in combination with TMZ or carmustine (http://clinicaltrials.gov) (Kaina *et al.*, 2010).

1.4.6. Prognosis

Prognosis of GBM patients is extremely poor, with the untreated individuals dying within 3-4 months after diagnosis. Post-operative RT has previously been shown to prolong the survival of GBM patients, as compared to surgery alone, from 3-4 to 7-12 months (Walker *et al.*, 1978). The addition of concomitant and maintenance TMZ to standard post-operative RT further improved the median survival from 12.1 to 14.6 months. Overall survival after combined therapy is 27.2% at 2 years, 16.0% at 3 years, 12.1% at 4 years, and 9.8% at 5 years, versus 10.9%, 4.4%, 3.0%, and 1.9% with RT alone (Stupp *et al.*, 2005; Stupp *et al.*, 2009). Recursive partitioning analysis showed significantly longer survival for patients grouped within the most favorable WHO performance status. Median survival times ranged from 10 to 17 months, corresponding to increase in survival of 1.1 to 7 months, depending on the performance status of the patients (Mirimanoff *et al.*, 2006). The almost invariable

tumor recurrence contributes greatly to the low survival even after following the complete therapeutic scheme.

Combination therapy of TMZ with other chemotherapeutic agents (carmustine, lomustine, cisplatin, hydroxyurea, doxorubicin, procarbazine, etoposide, topotecan, paclitaxel, fotemustine), tyrosine kinase-inhibitors (erlotinib, gefitinib, cediranib, cilengitide, sunitinib, lapatinib), monoclonal antibodies (bevacizumab, cetuximab, panitumumab) and other antitumor and metabolic agents (tamoxifen, thalidomide, celecoxib) have been investigated. Nevertheless, none of these combinations have shown any significant improvement in toxicity compare to TMZ alone (Dresemann, 2010).

1.5. Aims of the study

Chemotherapeutic S_N1-alkylating agents are important anticancer drugs widely used for the treatment of different types of tumors, including melanomas, lymphomas, sarcomas and gliomas. Nevertheless, despite their widespread used, the mechanisms of cell death trigger by this group of agents is not yet completely understood, and their therapeutic performance is low.

This study is aimed to investigate the mechanisms of O^6MeG-induced cell death. Different hypotheses of how O^6MeG trigger cell death have been proposed and will thus be considered in this study. Given that different hypotheses predict cellular events to occur in different phases of the cell cycle, and in different cell cycles after treatment, the cell cycle dependence of O^6MeG-triggered cell death will be analyzed in synchronized cells. Moreover, the knowledge accumulated on the mechanism of toxicity by this group of agents will be applied with the intention of improving the cytotoxic potential of chemotherapeutic S_N1-alkylating agents. This will be performed in a clinically relevant cell system, namely glioblastoma multiforme, the most common and deadliest form of primary brain tumor, for which the S_N1-alkylating agent temozolomide is the current first-line chemotherapeutic drug.

In order to investigate the mechanism of O^6MeG-triggered cell death, the following points will be addressed:

- Out of which cell cycle and cell cycle phase after treatment do cells activate the DNA damage response and cell cycle arrest after O^6MeG induction? When are DNA double-strand breaks formed in cells treated with O^6MeG-inducing agents?
- What is the kinetics of cell death induction after treatment with O^6MeG-inducing agents? How does the processing of O^6MeG adducts impacts on the extension of apoptosis induction? What could be the underlying reason for the observed late cytotoxic response after O^6MeG induction?

In order to analyze a strategy for improving the cell death response after treatment with O^6MeG-inducing agents, the following points will be addressed:

- Does DNA double-strand break repair inhibition sensitizes glioblastoma cells to treatment with the alkylating agent temozolomide? If cells are sensitized, is this sensitization related to toxicity trigger by O^6MeG?
- Does co-inhibition of N-alkylations repair and DNA double-strand break repair further sensitizes glioblastoma cells to treatment with the alkylating agent temozolomide?

2. Materials and methods

2.1. Equipment and software

2.1.1. Equipment

Description	Commercial name	Source
^{137}Cs-Source	Gammacell 2000	Molsgaard Medical. Copenhagen, Denmark
Analytical balance	Sartorius analytic	Sartorius. Göttingen, Germany
Bacteria Incubator	None	Heraeus. Munich, Germany
Biological safety cabinet	HERA safe	Thermo Fisher Scientific. Munich, Germany
Biological safety cabinet	NUAIRE	NuAire. Plymouth, MN, USA
Cell disruptor / homogenizer	Sonifier	Branson Ultrasonic. Danbury, CT, USA
Centrifuge	Megafuge 1.0	Heraeus. Munich, Germany
CO_2 incubator	Heracell 150	Thermo Fisher Scientific. Munich, Germany
Electrophoresis power supply	Power Pac 200/300	BioRad. Munich, Germany
Electrophoretic Transfer Cell	Mini Trans-Blot	BioRad. Munich, Germany
Flow cytometer	BD FACSCalibur	BD Biosciences. Heidelberg, Germany
Fluorescent microscope with automatic image analysis	Metafer Finder System	MetaSystems, Altlussheim, Germany
Freezer (-20°C)	Premium NoFrost	Liebherr. Ochsenhausen, Germany
Freezing Container	None	Nalgene, Rochester, NY, USA.
Heating block	Thermoststat 5320	Eppendorf. Hamburg, Germany
Heating block with shaking	Thermomixer compact	Eppendorf. Hamburg, Germany
Horizontal electrophoresis chamber	Mini-Sub Cell GT	BioRad. Munich, Germany
Inverted microscope	Wilovert A	Hund. Wetzlar, Germany
Laser Scanning Microscope	LSM 710	Carl Zeiss. Jena, Germany
Liquid scintillation analyser	TRI-CARB 2100TR	Canberra-Packard. Dreieich, Germany

Description	Commercial name	Source
Microplate photometer	Multiskan EX	Thermo Fisher Scientific. Munich, Germany
Refrigerated centrifuge	Centrifuge 5402	Eppendorf. Hamburg, Germany
Refrigerated centrifuge	Megafuge 10R	Heraeus. Munich, Germany
Refrigerated ultra centrifuge	Suprafuge 22	Heraeus. Munich, Germany
Refrigerated ultra centrifuge	Sorvall RC-5B	DuPont. Bad Homburg, Germany
Refrigerator	Premium	Liebherr. Ochsenhausen, Germany
Shaker with incubation hood	Certomat / Certomat H	Sartorius. Göttingen, Germany
Thermal cycler	MyCycler	BioRad. Munich, Germany
Ultralow temperature freezer (-86°C)	VIP Series -86°C freezer	Sanyo. Munich, Germany
UV-C-Source	NSE 11-270	Phillips. Hamburg, Germany
UV-transilluminator with image capture and manipulation software	InGenius	Syngene. Cambridge, UK
Vacuum pump	None	Brand. Wertheim, Germany
Vertical electrophoresis cell	Mini Protean	BioRad. Munich, Germany
Vortex	Vortex-Genie	Bender & Hobein. Zurich, Switzerland
Water bath	Wasserbad Köttermann	Köttermann. Uetze-Hänigsen, Germany

2.1.2. Software

Description	Commercial name	Source
Office software suite including word processing, spreadsheet, and presentation applications	LibreOffice	The Document Foundation. GNU Lesser General Public License
Reference management software	Bibus	Bibus developers. GNU General Public License
Graphing and statistics software	GraphPad Prism version 3.2, 2000	GraphPad Software, Inc. La Jolla, CA, USA

Description	Commercial name	Source
Acquisition and data analysis software for flow cytometry	CellQuest™Pro	Becton, Dickinson and Company. Franklin Lakes, NJ, USA
Flow cytometry data analysis software	WinMDI version 2.9	Joseph Trotter at The Scripps Research Institute. La Jolla, CA, USA
DNA cell-cycle analysis software for flow cytometry data	ModFit™	Verity Sofware House. Topsham, ME, USA
Refresh ratios in FCS list-files	Refresh Radio 1.10	Ron Hoebe at the University of Amsterdam, Netherlands
Image Analysis Systems	Multi-Analyst 1.1	BioRad. Munich, Germany
Automated imaging software	Metafer Finder System v. 3.1	MetaSystems. Altlussheim, Germany
Graphics editing program	Adobe® Photoshop® CS4	Adobe Systems Incorporated. San Jose, CA, USA
Graphic design software	Adobe® Illustrator® CS4	Adobe Systems Incorporated. San Jose, CA, USA
Vector graphics editor software	Inkscape	The Inkscape Team. GNU General Public License
Basic local alignment search tool	BLAST	National Center for Biotechnology Information. Bethesda, MD, USA (Altschul *et al.*, 1990) http://blast.ncbi.nlm.nih.gov/Blast.cgi.

2.2. Cell lines and cell culture conditions

2.2.1. Cell lines

Name	Abbreviation	Description	Reference / source
Capan-1	None	Pancreatic adenocarcinoma. Naturally selected inactivating BRCA2 mutation (6174ΔT and loss of the second allele)	ATCC® HTB-79™
Capan-2	None	Pancreatic adenocarcinoma. BRCA2 wild-type	ATCC® HTB-80™

Name	Abbreviation	Description	Reference / source
CHO-9	None	Chinese hamster (*Cricetulus griseus*) ovary cells	Wood & Burki, 1982
CHO-9-MGMT	None	CHO-9 cell line stably transfected for constitutive expression of MGMT protein Neomycin resistant	Kaina *et al.*, 1991
LN-229	None	Human derived glioblastoma cell line	ATCC® CRL-2611™
U87MG	None	Human derived glioblastoma (astrocytoma) cell line	ATCC® HTB-14™
T98G	None	Human derived glioblastoma multiforme cell line	ATCC® CRL-1690™
LN-229-MGMT	None	LN-229 cell line stably transfected for constitutive expression of MGMT protein Neomycin resistant	This work
LN-229-pSuper-empty	LpSe	LN-229 cell line stably transfected with circular pSuper vector	This work
LN-229-RAD51shRNA-4 (Correspondingly -8, -21, -22, -23)	LR51sh-4 (Correspondingly -8, -21, -22, -23)	LN-229 cell line stably transfected for intracellular production of shRNA against RAD51. Clone 4 (Correspondingly clones -8, -21, -22, -23) Neomycin resistant	This work
LN-229-XRCC2shRNA-1	LX2sh-1	LN-229 cell line stably transfected for intracellular production of shRNA against XRCC2. Clone 1 Neomycin resistant	This work
LN-229-MGMT-RAD51shRNA-3	LMR51sh-3	LN-229-MGMT cells stably transfected for intracellular production of shRNA against RAD51. Clone 3 Neomycin and puromycin resistant	This work

2.2.2. Cell culture conditions

2.2.2.1. General cell culture conditions

All cell lines were routinely cultured in humidified atmosphere with 7% CO_2 at 37°C. CHO-9 cells and stably transfected cells derived from this cell line were maintained in RPMI medium supplemented with 5% Fetal bovine serum [FBS]. Glioma cell lines (namely LN-229, U87MG and T98G) and all generated transfectants from these cell lines were routinely cultured in Dulbecco's

modified Eagle's medium (DMEM) containing 10% FBS. Pancreatic adenocarcinoma cell line Capan-1 was culture in DMEM medium supplemented with 20% FBS, while Capan-2 in McCoy's 5a medium supplemented with 10% FBS. Media was acquired from Gibco (Invitrogen. Karlsruhe, Germany) and FBS from PAA (Pasching, Austria). Plastic cell culture consumables were from Cellstar (Greiner Bio-One. Frickenhausen, Germany).

Cells stocks were prepared from logarithmically growing cultures. Harvested cells were centrifuged and resuspended in a mixture 90% FBS- 10% DMSO. Cells were aliquoted in cryo-vials at about $2x10^6$ cells/vial and frozen overnight to -80°C at a -1°C/min cooling rate making use of a Freezing Container (Nalgene®. Rochester, NY, USA). Frozen cells were transferred to and kept in liquid nitrogen.

Cell lines were screened for *Mycloplasma* contamination (namely *M. orale, M. hyorhinis, M. arginini, M. fermentans, M. salivarium, M. hominis, M. pneumoniae, Acholeplasma laidlawii, M. synoviae* and *Ureaplasma* species, among others) by hot-start Polymerase Chain Reaction (Venor®GeM-Mycoplasma Detection Kit. Minerva Biolabs, Berlin, Germany). Only uncontaminated cell lines were employed.

Cells lines were thawed at 37°C, rinsed in complete medium, and cultured under standard conditions. Cells were allowed to recover from cryopreservation and adjust to culture conditions for a period no shorter than 10 days before experiments were conducted. During this recovery period, cells were passaged twice.

During routine cell culture, cells were passage about twice a week at appropriated dilutions to avoid cells from reach confluence before new passage. Cell were passage by detachment of adherent cells with a 0.5 mg/ml Trypsin- 0.22 mg/ml EDTA- Phosphate buffered saline [PBS] solution (PAA. Pasching, Austria). Cell lines were maintained in culture for no longer than 2 months.

For experiments, and unless otherwise specified, cells were seeded 24 h before pre-treatments, treatments or transfections were performed. The seeding density was selected to assure cells would have the possibility to grow exponentially (if not impaired by treatments) at the time of end points measurement.

2.2.2.2. Synchronization of cells

Exponentially growing cells were seeded in complete medium in 75 cm^2 flasks and grown to high

density without reaching confluence. Cell monolayers were rinsed twice with PBS, and medium was changed to a 5% FBS supplemented RPMI medium lacking divalent cations (prepared in house, composition in Table Supp. 1). Prometaphasic cells were enriched for by growing the cultures for 4 h in the presence of colcemid (Sigma. Munich, Germany). 100 ng/ml colcemid was employed for CHO-9 cells and transfectants from this cell line. For LN-229 cells and its transfectants a dose of 50 ng/ml was used. The arrested mitotic cells were collected by shake-off (manual shaking of the cell culture flasks) and rinsed twice by centrifugation (1 000 revolutions per minute [rpm] for 4 min at room temperature [R.T.]) and resuspension rounds in complete medium prior to seeding in complete medium.

2.3. Drugs, irradiation and treatment of cells

Temozolomide [TMZ]: Stocks were prepared by dissolving TMZ (Schering-Plough. Kenilworth, NJ, USA) in DMSO and sterile dH_2O (1:2) to a 35 mM concentration. Aliquoted stocks were stored at -80°C.

1-methyl-2-nitro-1-nitrosoguanidine [MNNG]: A 10 mM stock solution was prepared by dissolving MNNG (Sigma. Munich, Germany) in dimethyl sulfoxide [DMSO] and then diluting it with sterile dH_2O (100-fold dilution). The MNNG were aliquoted and stored at -80°C until used.

Nimustine [ACNU]: ACNU (Sigma. Munich, Germany) stock solution was prepared by dissolving the drug in sterile dH_2O to 10 mM. ACNU aliquots were stored at -20°C.

Methyl methanesulfonate [MMS]: MMS (Sigma. Munich, Germany) was diluted in sterile dH_2O to a concentration of 100mM. Aliquoted stock solution was stored at -20°C for no longer than 2 weeks.

Cisplatin [CisPt]: A 1 mg/ml cisplatin stock in 0.90% NaCl solution was kept at -20°C.

O^6-benzylguanine [O^6BG]: The MGMT inhibitor O^6BG (Sigma. Munich, Germany) was dissolved to a 10 mM solution in DMSO and kept at -20°C. For MGMT depletion, 10 µM O^6BG was added to the cells 1 h prior to treatment.

NU7026: The DNA-PKcs inhibitor NU7026 (Sigma. Munich, Germany) was dissolved in DMSO to 5 mM, stored in aliquots at -20°C, and added to cells at a final concentration of 10 µM 6 h prior to

treatment or irradiation.

AZD2281 (*a.k.a.* olaparib): The PARP inhibitor AZD2281 (Selleck Chemicals. Houston, TX, USA) was dissolved in DMSO and PBS (1:10) to a 1 mM concentration. Aliquots were stored at -20°C. AZD2281 was added to the cells (0.1 to 1 μM.) 1 h before treatments.

Ionizing radiation [IR]: Adherent growing cells were irradiated in 60 mm dishes using a ^{137}Cs source at the indicated dose (Gy).

Ultraviolet radiation [UV]: Adherent growing cells were irradiated using an UV-C light source at the indicated dose (J/m^2). Medium was removed before irradiation and replaced thereafter.

2.4. Transfections

2.4.1. Plasmid DNA stable transfections

2.4.1.1. Transfections

Plasmid DNA (listed in Section 2.4.1.2) was transfected into cells with the Effectene transfection kit (Qiagen. Hilden, Germany), according to the manufacturer's specifications. Transfection of 2 μg of plasmid DNA were performed in 60 mm dishes. 24 to 48 h after transfection cells were passaged 1:10 into ten 60 mm dishes. Selector was added to media 24 h thereafter. Cells were selected for with 0.40 to 1.50 mg/ml G418 or 0.22 μg/ml puromycin (both from Invitrogen. Karlsruhe, Germany) until colonies formed. Selector-resistant clones were expanded and tested for protein expression by Western blot (for protocol see Section 2.10). In case of plasmids lacking a selector marker a co-transfection of the target plasmid and a selector plasmid was performed at a 10:1 w/w ratio.

2.4.1.2. Plasmids

Name	Description	Reference / Source
pSuper.basic	Vector system for expression of shRNA under control of the polymerase-III H1-RNA promoter	Brummelkamp *et al.*, 2002 / OligoEngine. Seattle, WA, USA

Name	Description	Reference / Source
pSuper.puro	Vector system for expression of shRNA under control of the polymerase-III H1-RNA promoter. Puromycin resistance cDNA under the control of a PGK promoter	OligoEngine. Seattle, WA, USA
pSV2.neo	Neomycin resistance cDNA under the control of a SV40 promoter	Southern & Berg, 1982
pSV2.MGMT	Human MGMT cDNA under the control of a SV40 promoter	Kaina *et al.*, 1991
pSuper-RAD51sh-Bia	pSuper.basic plasmid directing the expression of a shRNA against RAD51	This work (see Section 2.11)
pSuper-XRCC2sh-Sud	pSuper.basic plasmid directing the expression of a shRNA against XRCC2	This work (see Section 2.11)

2.4.2. siRNA transient transfections

2.4.2.1. Transfections

25 to 50 nM Small interfering RNA [siRNA] was transfected with Lipofectamine™ RNAiMAX (Invitrogen. Karlsruhe, Germany) following the manufactures protocol. Briefly, siRNAs and lipofectamine were independently diluted in FBS-free medium. Complexes lipofectamine-RNA were formed by mixing the diluted lipofectamine with the diluted siRNAs and incubating for 20 min at R.T. The complex were then added to cells growing in complete medium. Unless otherwise specified transfections were performed in 6-well plates. Nonsense siRNA (AllStars Negative Control siRNA, Qiagen. Hilden, Germany) were used as a control.

2.4.2.2. siRNAs

Target protein **(GenBank accession number)**	**Oligonucleotides *** * F = forward or sense nucleotide; R = reverse or antisense nucleotide Target sequence showed in uppercase.	**Sequence previously evaluated by**
RAD51 (NM_002875)	F: 5'-GAAGAAAUUGGAAGAAGCUtt-3' R: 5'-AGCUUCUUCCAAUUUCUUCtt-3'	Biard, 2007
BRCA2 (NM_005431)	F: 5'-CUGAGCAAGCCUCAGUCAAtt-3' R: 5'-UUGACUGAGGCUUGCUCAGtt-3'	Fan *et al.*, 2006

2.5. Colony Formation Assay

Cells growing in logarithmic phase were monodispersed and seeded at appropriated cell numbers (150 to 3 000 cells) on 60 mm dishes to yield about 100 colonies after appropriate incubation in presence or absence of treatment. The appropriate number of cells to seed were determined in preliminary experiments for each cell line and treatment combination. Cells were allowed to attach for 6 h, and then were irradiated or treated with increasing doses of the agents. After appropriated incubation times (12 to 15 days) medium was removed, attached cells were rinsed with PBS, and colonies were fixed in an acetic acid:methanol:H_2O (1:1:8) mixture for 30 min. Colonies were stained with 1.25% Giemsa and 0.125% violet crystal for 10 min. Colonies composed of at least 50 cells were scored. Survival was calculated relative to that of untreated control, taking into account the colony forming efficiency for each experiment.

In the case of DNA-PK inhibition, 10 µM NU7026 was added to cells upon seeding. In the case of PARP inhibition, AZD2281 was added 1 h before treatment. For Colony Formation Assay [CFA] of transiently transfected cells, CFAs were seeded from cells growing on 60 mm dishes 18 h after transfection with the corresponding siRNA (see Section 2.4.2 for transfection protocol), so that treatments were performed 24 h after transfection.

2.6. Flow cytometry

2.6.1. Sub-G_1 determination

At the end of the indicated incubation times after treatment, media containing detached cells were collected in 15 ml tubes. Adherent cells were harvested by trypsinization and combined with the detached cells. The total cell population was centrifuged (1 000 rpm for 4 min at R.T.) and resuspended in 200 µl PBS. Cells were fixed with 2 ml 70% ethanol at -20°C for at least 20 min and no more than 6 days. After fixation, cells were centrifuged (1 000 rpm for 4 min at R.T.) and resuspended in 333 µl PBS containing 30 µg/ml Ribonuclease A [RNase A]. After 1 h RNA digestion, DNA was stained with 167 µl 50 µg/ml propidium iodide (PI, 16.7 µg/ml end concentration). Flow cytometric aquisition of at least 10 000 cells was performed using a FACSCalibur (Becton Dickinson. Heidelberg, Germany). The proportion of cells with sub-diploid DNA content (Sub-G_1) were calculated with WinMDI 2.9 (The Scripps Research Institute. La Jolla, CA, USA).

2.6.2. Cell cycle distribution analysis

Samples were prepared as described for Sub-G_1 analysis (Section 2.6.1). Histograms depicting the DNA content distribution were generated with WinMDI 2.9 (The Scripps Research Institute. La Jolla, CA, USA) and ModFit™ (Verity Software House. Topsham, ME, USA).

2.6.3. Detection of phosphatidylserine exposure and membrane permeability in intact cells

At the end of the indicated incubation times, adherent cells were harvested by trypsinization and combined with the previously collected detached cells. The total cell population was centrifuged (1 000 rpm for 4 min at 4°C) and rinsed twice by resuspension in ice-cold PBS and centrifugation (1 000 rpm for 4 min at 4°C). Cell pellets were resuspended in 0.01 M HEPES (pH 7.4), 0.14 M NaCl, 2.5 mM $CaCl_2$, and incubated for 20 min in the presence of 2.5 µl Annexin V- FITC (BD Pharmingen™. Heidelberg, Germany). PI (1 µM end concentration) was added to the cell suspension prior to the analysis. Flow cytometric aquisition of 10 000 cells was performed with a FACSCalibur (Becton Dickinson. Heidelberg, Germany). Data was analyzed with WinMDI 2.9 (The Scripps Research Institute. La Jolla, California, USA).

2.6.4. Caspases activation

At the end of the indicated incubation times, cells were harvested as described above (Section 2.6.1) for Sub-G_1 analysis. The total cell population was centrifuged (1 000 rpm for 4 min at R.T.) and resuspended in 500 µl PBS. Cells were incubated for 20 min in the presence of 20 µM CaspACE™ FITC-VAD-FMK (Promega, Mannheim, Germany), in a humidified air- 7% CO_2 atmosphere at 37°C in the dark, and rinsed twice with PBS (resuspension in PBS followed by 4 min R.T. centrifugation at 1 000 rpm). Cells were ethanol fixed, RNA was digested and DNA was counterstained as described above (Section 2.6.1) for Sub-G_1 analysis. Flow cytometric aquisition of 20 000 events was performed using a FACSCalibur (Becton Dickinson, Heidelberg, Germany). Data was analyzed with WinMDI 2.9 (The Scripps Research Institute. La Jolla, CA, USA).

2.6.5. BrdU incorporation

Bromodeoxyuridine [BrdU] incorporation was analyzed by enhancement of DNA-bound TO-PRO-3

fluorescence, as described previously (Beisker *et al.*, 1999). At the end of the incubation times, detached and adherent cells were harvested, combined and centrifuged as for Sub-G_1 determination (Section 2.6.1). Cell nuclei were prepared and stained in a two step protocol, as follow: harvested cells were resuspended and incubated for 30 min at R.T. in 0.3 ml solution A (584 mg/l NaCl, 1 000 mg/l sodium citrate, 33 mg/l PI, 10 mg/l RNase A, 0.3 ml/l Nonidet NP-40), followed by addition of 0.3 ml solution B (1.5% citric acid, 0.25 M sucrose, 33 mg/l PI) and a further 30 min incubation at R.T. Immediately prior to flow cytometric analysis, 0.3 µM TO-PRO-3 (Invitrogen. Karlsruhe, Germany) was added to the samples. Cell nuclei preparation and staining was performed in the dark. 50 000 events were acquired per sample (FACSCalibur. Becton Dickinson. Heidelberg, Germany). The radio of TO-PRO-3/PI was calculated as a new parameter with the Refresh Radio 1.10 Software. The generated data was further analyzed with WinMDI 2.9 (The Scripps Research Institute. La Jolla, CA, USA).

2.6.6. Carboxyfluorescein succinimidyl ester (CFSE) proliferation Assay

Carboxyfluorescein diacetate succinimidyl ester [CFDA-SE] is an esterase-activable fluorescent dye. CFDA-SE diffuses passively into cell, where intracellular esterases remove the acetate groups to yield a fluorescent ester form, carboxyfluorescein succinimidyl ester [CFSE]. Through its succinimidyl ester group CFSE covalently reacts with intracellular amine groups, thus fluorescently labeling the cells. The label, and consequently its fluorescence, is halved between daughter cell following each cell division, therefore allowing to determine proliferation of cells (Lyons, 2000).

Cellular proliferation as determined by CFSE dilution was analyzed essentially as described (Lyons & Parish, 1994). Cells were synchronized as described above (Section 2.2.2.2), rinsed twice with PBS by resuspension and centrifugation (1 000 rpm for 4 min at R.T.), and resuspended in PBS to a density of $1x10^6$ cells/ml. Cells were labeled with 5 µM CFDA-SE (Sigma. Munich, Germany) added to the cell suspension for 8 min at R.T. in the dark. Thereafter, the excess CFDA-SE was quenched by adding 5 volumes complete RPMI medium. Cells were rinsed twice with PBS by resuspension and centrifugation as above, and seeded in complete medium. Staining and incubation were performed in the dark. After the indicated incubation times, detached and adherent cells were harvested, washed with PBS, and resuspended in 0.01 M HEPES (pH 7.4), 0.14 M NaCl, 2.5 mM $CaCl_2$. 100 000 events were acquired with a FACSCalibur (Becton Dickinson. Heidelberg, Germany). Events with decreased FSC-SSC were excluded from the analysis. Data was analyzed with the Proliferation Wizard module of ModFit™ (Verity Software House. Topsham, ME, USA). Dilution of CFSE by 50% was taken to be indicative for passage of cells through one cell cycle. The 1st generation after completion of mitosis of

the synchronized cells (about 2 h after synchronization and CFSE staining) was set as the parent population.

2.6.7. Detection of phosphatidylserine exposure and membrane permeability in CFSE-labeled cells

Cells were labeled with CFSE, cultured and harvested as described in Section 2.6.6. Harvested cells were resuspended in binding buffer (0.01 M HEPES (pH 7.4), 0.14 M NaCl, 2.5 mM $CaCl_2$), incubated for 20 min with either Annexin V- PE or Annexin V- APC (both from BD Pharmingen™. Heidelberg, Germany). The membrane impermeable DNA-binding dyes TO-PRO-3 (1 μM, Invitrogen. Karlsruhe, Germany) or alternatively PI (1 μM, Sigma. Munich, Germany) was added to the cells immediately prior to the analysis. Phosphatidylserine positive cells were classified according to their cell proliferation status (assessed as dilution of the cell-tracking dye CFSE) with the Proliferation Wizard module of ModFit™ (Verity Software House. Topsham, ME, USA), and further expressed relative to the total amount of phosphatidylserine positive cells.

2.7. Immunofluorescence microscopy

Glass cover slips were pretreated by sequential immersion in diethylether (10 min), 100% ethanol (5 min), 70% ethanol (5 min), H_2O (5 min), 1M HCl (30 min) and 70% ethanol (10 min and up to several months for storage). Pretreated cover slips were laid on 35 mm dishes and cells were cultured and treated on them. After the indicated incubation times, medium was removed and cells were fixed with 4% formaldehyde- PBS for 15 min at R.T., followed by 100% methanol for at least 20 min and up to 7 days at -20°C. Non-specific binding was prevented by blocking with 5% Bovine serum albumin [BSA]- 0.3% Triton-X100- PBS. Cells were incubated in the presence of the primary antibody (anti-P-H2A.X (S139) [γH2A.X], 1:1 000, Upstate Biotechnology. Lake Placid, NY, USA; anti-TP53BP1, 1:400, Cell Signaling Technology. Beverly, MA, USA) overnight at 4°C followed by a 2 h incubation with the secondary antibody (anti-mouse- Alexa Fluor 488, 1:500, Molecular Probes, Invitrogen. Karlsruhe, Germany; anti-rabbit-Cy™3, 1:500, Jackson ImmunoResearch Laboratories. West Grove, PA, USA) at room temperature. DNA was counterstained either with 100 nM DAPI or 1 μM TO-PRO-3 (Invitrogen. Karlsruhe, Germany) in 0.1% Tween 20- PBS for 15 min, and slides were mounted in 1% 1,4-diazabicyclo-[2,2,2]-octane (DABCO)- 50% glycerol- PBS. Three washing steps (5 min each) with 0.1% Tween 20- PBS were included after each incubation during the

immunostaining process. Foci formation was automatically scored by fluorescent microscopy with the Metafer Finder System v. 3.1 (MetaSystems. Altlussheim, Germany). Representative photomicrographs were acquired by laser scanning microscopy (LSM 710. Carl Zeiss MicroImaging. Jena, Germany).

2.8. Cell extracts and protein quantification

2.8.1. Total cell extract (in sonication buffer)

2.8.1.1. Extract

At the end of the incubation times, adherent cells were rinsed once with ice cold PBS and harvested with a rubber cell culture scraper. Cells were pelleted by centrifugation (4 000 rpm for 4 min at 4°C), and cell pellets were flash frozen in liquid nitrogen. Frozen pellets were collected and stored at -20°C. Pellets were resuspended and sonicated in sonication buffer (20 mM Tris-HCl pH 8.5, 1 mM EDTA, 5% glycerin, 1 mM 2-mercaptoethanol, 1 mM PMSF). The mixture was centrifuged for 10 min at 14 000 rpm at 4°C to remove non soluble components. Protein concentration was determined following the Bradford method (see Section 2.8.1.2). Samples were stored at -20°C.

2.8.1.2. Protein quantification by the Bradford method

Protein concentration was determined according to the method described by Bradford (1976). Protein extracts (10 µl at a 1:10 dilution in H_2O) were mixed with 200 µl Bradford reagent (8.5% phosphor acid, 4.75% ethanol, 1% Coomassie blue G250) in 96 well microtiter plates. Samples were incubated for 10 min at R.T., and their absorbance were measured at 595 nm. A calibration curve in the range of 0 to 5 mg/ml was generated with BSA for each experiment.

2.8.2. Total cell extract (in SDS-PAGE sample buffer)

2.8.2.1. Extract

At the end of the incubation times, medium was discarded and adherent cells were rinsed once with PBS at R.T. 95°C pre-heated SDS-PAGE sample buffer (62.5 mM Tris-HCl pH 6.8, 10% Glycerol, 2%

Sodium dodecyl sulfate [SDS], 5% 2-mercaptoethanol, 0.01% bromophenol blue) was added directly onto the cells. Samples were collected, sonicated and heated for 3 min at 50°C.

2.8.2.2. Protein semi-quantification by immunodetection of housekeeping proteins

A equal volume from each sample was resolved by SDS-PAGE (Section 2.9). A housekeeping protein was immunodetected by Western blot (Section 2.10) and its relative expression was quantified by densitometry of the scanned bands, either with the Multi-Analyst® Software for chemiluminescence detected blots or with the Odyssey® Infrared Imaging System (LI-COR Biotechnology. Bad Homburg, Germany) for infrared detected Western blots. Protein expression was expressed relative to a reference sample.

2.9. Sodium dodecyl sulfate polyacrylamide gel electrophoresis

Samples were resolved by Sodium dodecyl sulfate polyacrylamide gel electrophoresis [SDS-PAGE], according to the published methodology (Laemmli, 1970). Briefly, protein extracts were mixed with dH_2O and 4X SDS-PAGE loading buffer (250 mM Tris-HCl pH 6.8, 40% glycerol, 8% SDS, 20% 2-mercaptoethanol, 0.04% bromophenol blue) to give an appropriated volume of sample in 1X SDS-PAGE loading buffer. Samples were denatured for 5 min at 95°C or alternatively 3 min at 50°C in the case of immunodetection of proteins above 300 kDa. 30 µg protein was loaded on the stacking gel. Proteins were concentrated at 100 V in a 4% stacking gel (4% polyacrylamide, 125 mM Tris-HCl pH 6.8, 0.1% SDS, 0.05% Ammonium persulfate [APS], 0.005% Tetramethylethylenediamine [TEMED]) and resolved at 120 V in a separating gel (5-12% polyacrylamide, 375 mM Tris-HCl pH 8.8, 0.1% SDS, 0.05% APS, 0.005% TEMED). Gels were electrophoresed in SDS-PAGE running buffer (25 mM Tris-HCl, 192 mM glycine, 0.1% SDS). Electrophoresis was stopped before the front reached the bottom of the gel. Molecular weight markers were electrophoresed parallel to the samples.

2.10. Protein immunoblot

2.10.1. Western blot

SDS-PAGE resolved gels were blotted onto nitrocellulose membranes (Whatman. Dassel, Germany) based on the described methodology (Towbin *et al.*, 1979). Transfer was performed in blotting buffer

(25 mM Tris-HCl, 192 mM glycine, 20% methanol) at 4°C. Transfer was carried out overnight at 50 mA. Blocking of non-specific binding was performed for 30 min with 5% non fat milk [NFM]-0.1% Tween 20- Tris buffered saline [TBS] or 5% BSA- 0.1% Tween 20- TBS in the case of phospho-proteins. For immunodetection, membranes were incubated with the primary antibodies overnight at 4°C, and either peroxidase-conjugated or IRDye infrared secondary antibodies for 2 h at room temperature. Three 10 min washing steps with 0.1% Tween 20- TBS were performed after each antibody incubation. According to the selected secondary antibody, proteins were either detected using a chemiluminescence detection system (Amersham Biosciences. Uppsala, Sweden) or using the Odyssey® Infrared Imaging System (LI-COR Biotechnology. Bad Homburg, Germany). The antibodies used are listed in Section 2.10.2.

2.10.2. Antibodies

Target protein	Details	Dilution	Source
ATR	Goat polyclonal	1:1 000	Santa Cruz Biotechnology. Heidelberg, Germany
P-ATR (S428)	Rabbit polyclonal	1:1 000	Cell Signaling Technology. Beverly, MA, USA
ERK2	Rabbit polyclonal	1:3 000	Santa Cruz Biotechnology. Heidelberg, Germany
Cleaved CASP3 (D175)	Rabbit polyclonal	1:1 000	Cell Signaling Technology. Beverly, MA, USA
Cleaved CASP7 (D198)	Rabbit polyclonal	1:1 000	Cell Signaling Technology. Beverly, MA, USA
CHK1	Rabbit polyclonal	1:1 000	Cell Signaling Technology. Beverly, MA, USA
P-CHK1 (S317)	Rabbit polyclonal	1:1 000	Bethyl Laboratories. Montgomery, TX, USA
PARP1	Mouse polyclonal	1:1 000	BD Transduction Laboratories. Erembodegem, Belgium
Rabbit IgG	Peroxidase conjugate	1:3 000	GE Healthcare. UK
Mouse IgG	Peroxidase conjugate	1:3 000	GE Healthcare. UK
BRCA2	Rabbit polyclonal	1:1 000	Cell Signaling Technology. Beverly, MA, USA

Target protein	Details	Dilution	Source
MGMT	Mouse monoclonal	1:1 000	Chemicon, Millipore. Temecula, CA, USA
RAD51	Rabbit polyclonal	1:4 000	Calbiochem, Merck Chemicals Ltd. Nottingham, UK
XRCC2	Rabbit polyclonal	1:1 000	Millipore. Billerica, MA, USA
Rabbit IgG	IRDye 800 conjugated	1:10 000	LI-COR Biotechnology. Bad Homburg, Germany
Mouse IgG	IRDye 800 conjugated	1:10 000	LI-COR Biotechnology. Bad Homburg, Germany

2.11. shRNA plasmids

2.11.1. Plasmids construction

pSuper (OligoEngine. Seattle, WA, USA) constructs were generated to direct the intracellular synthesis of Short hairpin RNA [shRNA] against specific target proteins. The procedure recommended by the company was followed. Briefly, sense and antisense oligonucleotides (described in detail in Section 2.11.2) were synthesized to contain a BamHI 5`end, the target sequence in sense and antisense direction separated by a spacer sequence for loop formation, and a 3` HindIII end.

Target sequences were selected from the literature, and were analyzed with BLAST (Altschul *et al.*, 1990) to make certain they do not have significant sequence homology with other genes (potential off-targets). Software was run at http://blast.ncbi.nlm.nih.gov/Blast.cgi. The search parameters were adjusted to search for a short input sequence.

3 µg of each oligonucleotide was mixed in annealing buffer (100 mM NaCl, 50 mM HEPES pH 7.4), pre-heated 4 min at 90°C, annealed 10 min at 70°C and stepwise cooled down for 20 min at 37°C, 10 min at 10°C and then further cooled down to 4°C. 15 µg pSuper plasmid was HindIII and BglII digested in sequential steps (2 h of HindIII digestion alone, followed by 4 h concomitantly with BglII). HindIII was then heat inactivated for 20 min at 65°C. 0.24 µg annealed oligos (0.12 µg each) were ligated into 0.5 µg linearized pSuper plasmid. Reaction was performed overnight at R.T. with T4 DNA ligase (New England Biolabs. Frankfurt am Main, Germany) following the manufacturers recommendations. 1 h BglII digestion was performed after ligation in order to decrease background in

transformation given by potential undigested plasmids and re-ligated vectors with no target oligonucleotide insert (plasmid BglII site is destroyed upon ligation of BamHI oligonucleotide ends).

The ligation reaction was transformed into competent *Escherichia coli* DH5α according to the method described in Section 2.12.2. The presence of positive clones were checked by digestion of purified plasmids with EcoRI and HindIII, were the presence of the insert gave an increase of 54 bp (ligated oligos) in the shorter restricted fragment.

2.11.2. Inserts

Target protein **(GenBank accession number)**	**Oligonucleotides *** * F = forward or sense nucleotide R = reverse or antisense nucleotide Target sequence showed in uppercase.	**Plasmid name**	**Sequence previously evaluated by**
RAD51 (NM_002875)	F: 5'-gatcccc GAAGAAATTGGAAGAAGCT ttcaagaga AGCTTCTTCCAATTTCTTC ttttta-3' R: 5'-agcttaaaaa GAAGAAATTGGAAGAAGCT tctcttgaa AGCTTCTTCCAATTTCTTC ggg-3'	pSuper-RAD51sh-Bia	Biard, 2007
XRCC2 (NM_005431)	F: 5'-gatcccc GCTTCAAACTATACTACAAGG ttcaagaga CCTTGTAGTATAGTTTGAAGC ttttta-3' R: 5'-agcttaaaaa GCTTCAAACTATACTACAAGG tctcttgaa CCTTGTAGTATAGTTTGAAGC ggg-3'	pSuper-XRCC2sh-Sud	Sudo *et al.*, 2007

2.12. Transformation

2.12.1. Preparation of competent *Escherichia coli*

Competence in *E. coli* DH5α was induce by calcium chloride, according to the principle describe by Mandel & Higa (1970). *E. coli* was growth in LB medium at 37°C to early logarithmic phase (OD between 0.35 and 0.45 as assessed by spectrometry at 600 nm). Culture was inoculated from a starter overnight culture. Oxygen saturation in the culture was encouraged by continuous shaking of the culture flask at 200 rpm. Cells were pelleted at 4 000 rpm for 5 min at 4°C and then resuspended in ice-cold 50 mM $CaCl_2$. Cells were incubated for 20 min on ice and pelleted by centrifugation as above. Bacteria were aliquoted in stocks in a 50 mM $CaCl_2$ 10% glycerol solution, flash frozen in liquid nitrogen, and stored at -80°C.

2.12.2. Transformation of plasmid DNA into competent *E. coli*

Transformation of $CaCl_2$ competent cells was performed by heat shock. 100 µl of the bacteria suspension was incubated 5 min on ice with the plasmid DNA. Cells were heat shocked at 42°C for 1 min, and cooled back down on ice for 5 min. Bacteria were grown for 60 min at 37°C with continuous shaking of the culture flask at 200 rpm in 1 ml LB medium, and then plated onto LB agar plates containing the appropriate antibiotic for selection (Section 2.12.3). Agar plates were incubated at 37°C for 18 h for colonies to form.

2.12.3. Antibiotics

Antibiotic	Stock solution	Working concentration
Ampicillin	50 mg/ml in H_2O	50 µg/ml
Kanamycin	10 mg/ml in H_2O	50 µg/ml

2.13. Plasmid purification

2.13.1. Preparation

Single bacteria clones were picked and transferred into LB medium with the appropriated antibiotic selection (Section 2.12.3). Bacteria were grown overnight with continuous shake at 37°C and collected by centrifugation. DNA plasmid purification was performed by anion-exchange chromatography making use of commercial kits (NucleoBond® mini, midi or maxi gravity flow columns. Macherey-Nagel. Düren, Germany). Briefly, bacteria were lysed following the NaOH/SDS lysis method by Birnboim & Doly (1979). RNA digestion occurred during the lysis step. Lysate was neutralized with potassium acetate, that also caused the precipitation of proteins, chromosomal DNA and other debris bound to potassium dodecyl sulfate. The precipitate was remove by filtration and/or centrifugation, while plasmid DNA remained in solution. Plasmid DNA was bound to the silica resin by gravity force and/or centrifugation, washed, and then eluted with 5 mM Tris-HCl, pH 8.5 (final step for mini preparations) or under high-salt and alkaline conditions (midi and maxi preparations). In the case of midi and maxi preparations, plasmids were precipitated with isopropyl alcohol, washed with 70% ethanol, and finally resuspended in nuclease free-sterile dH_2O.

2.13.2. Nucleic acid quantification

Nucleic acids were quantified by spectrophotometry with the NanoDrop system (Thermo Scientific. Wilmington, DE, USA). The mode DNA-50 was selected for dsDNA, where 1 unit of absorbance at 600 nm along a path length of 10 mm correspond to 50 µg/ml. The ratio of sample absorbance 260 nm / 280 nm was used to asses purity of the nucleic acids (> 1.8 for DNA). The 260 nm / 230 nm ratio (> 2.0 for DNA) was also used as a measurement of nucleic acid purity.

2.14. Agarose gel electrophoresis

DNA electrophoresis was performed in agarose gels (0.7-1.0% agarose, 0.5 µg/ml ethidium bromide, 89 mM Tris, 89 mM boric acid, 2 mM EDTA pH 8.0). Samples were combined with 6X loading buffer (10 mM Tris-HCl pH 7.6, 0.03% bromophenol blue, 0.03% xylene cyanol, 60% glycerol and 60 mM EDTA) to give up to 0.5 µg DNA in 12 µl 1X loading buffer. Gels were electrophoresed in TBE buffer (89 mM Tris, 89 mM boric acid, 2 mM EDTA pH 8.0) at 5 V/cm until the bromophenol blue migration band had migrated 3/4 of the gel length. Ethidium bromide stained DNA was visualized and recorded with the InGenius system (Syngene. Cambridge, UK). Molecular weight markers were electrophoresed parallel to the samples.

2.15. MGMT activity assay

MGMT activity was determined following a modification of the method described by Myrnes *et al.* (1984). Briefly, ^{3}H-MNU-labelled calf thymus DNA was used as a substrate containing radioactive O^{6}MeG. Total cell extract (200 µg protein prepared as described in Section 2.8.1) was incubated with ^{3}H-labelled DNA (about 80 000 cpm) in 700 mM HEPES-KOH (pH 7.8), 10 mM DTT, 50 mM EDTA for 90 min at 37°C. DNA was hydrolyzed and protein was precipitated by 15 min incubation at 95°C in the presence of 13% trichloroacetic acid. Samples were cooled down on ice and protein was sedimented for 10 min at 14 000 rpm at 4°C. Protein was hydrolysed in the presence of a 0.2 M NaOH solution, and radioactivity was measured by liquid scintillation counting making use of a Liquid scintillation analyser (Canberra-Packard. Dreieich, Germany). Activity is expressed as fmol of radioactivity transferred from ^{3}H-labelled DNA to protein per mg of total protein in each sample.

2.16. DNA-PK activity assay

Total cell extracts were prepared as reported (Shao *et al.*, 2008). Briefly, cells were lysed through three cycles of freeze (liquid nitrogen) / thaw (30°C) in extraction buffer (50 mM NaF, 20 mM HEPES (pH 7.8), 450 mM NaCl, 25% glycerol, 0.2 mM EDTA, 0.5 mM dithiothreitol, in the presence of protease inhibitors (Complete. EDTA-free. Roche, Basel, Switzerland)). Extracts were centrifuged (12 000 rpm for 30 min at 4°C), and supernatants were shock frozen and stored at -80°C. Endogenous DNA was removed by Diethylaminoethyl Sepharose Fast Flow (GE Healthcare, UK). DNA-PK activity was determined by liquid scintillation counting using the SignaTECT DNA-Dependent Protein Kinase Assay System (Promega, Mannheim, Germany). Determinations were performed using a Liquid scintillation analyser (Canberra-Packard. Dreieich, Germany). The assay was carried out from three independent cell extracts for each cell line. Each sample was analyzed in the presence or absence of 10 μM of the DNA-PKcs inhibitor NU7026. For background control, reactions were performed in the absence of activator, as suggested by the assay manufacturer. Activity is expressed in arbitrary units as cpm per 10 μg of total protein in each sample.

3. Results

3.1. Part I: Mechanism of O^6MeG-induced cell death

3.1.1. Establishment of a method for synchronizing cells

Different models have been proposed to explain the role of MMR in O^6MeG-triggered cell death (Section 1.2.4.4). As suggested by the MMR processing model, the events leading to cell death after exposure to alkylating agents would be dependent on the progression of cells through two rounds of DNA replication. The direct signaling model, on the other hand, implies that cell death would occur in the treatment cell cycle, as no further processing would be required. Similarly, a hypothetical nuclease attack in areas of gaped DNA after initial processing by MMR would also lead to cell death directly from the treatment cell cycle. In order to test which one of these hypotheses holds true, the cell cycle dependence of O^6MeG-triggered cell death was analyzed.

Under normal culture conditions, exponentially growing cells progress through the cell cycle independently of the cell cycle stage of the neighboring cells, i.e., in an asynchronous way. Under these conditions, the measured end points are a mixture of responses created both by cells in different phases of the cell cycle at the moment of measurement and by responses originating from cells that were treated in different stages of the cell cycle. In order to improve the detection and characterization of the events leading to alkylating damage-induced toxicity, we established a method for synchronizing cells. The approach of mitotic shake-off was selected as synchronizing method. In order to increase the yield of the system, a pre-enrichment with a metaphase synchronizing agent was included. The method of shake off was selected to avoid any influence of the synchronization procedure on S-phase related events (Jackman & O'Connor, 2001). The ovarian fibroblast CHO-9 cell line was selected as an experimental mammalian system, given the great deal of information available about the response of this cell line to O^6-methylating agents. The prototypic S_N1-methylating agent 1-methyl-2-nitro-1-nitrosoguanidine [MNNG] was employed for the same reason.

The doubling time of the cell line under the specific culture conditions was determined (Fig. Supp. 1A). Based on it, two exposure times to the synchronizing agent (colcemid) were selected, corresponding to a third (4 h) and a full cell cycle (12 h). Colcemid, a microtubule-destabilizing agent, was assayed under a broad range of concentrations (50 to 400 ng/ml). In order to facilitate the shake-off process, the formulation of the growth media used during pre-enrichment with the metaphase synchronizing agent was modified to exclude divalent cations (Table Supp. 1). Lack of divalent cations prevent mitotic cells from re-attaching to the culture flask after their mitotic rounding

up. The synchrony efficiency was evaluated by measurement of the DNA content distribution in the cell population by flow cytometry. The final conditions (described in Section 2.2.2.2) were selected to obtain the major degree of synchronicity, without blocking cells from cycling or inducing any cell death. As shown in Fig. Supp. 1C, a very high degree of synchronization was achieved for a period lasting at least two full cell cycles. Metaphasic cells (Fig. Supp. 1C, 0 h) progressed to G_1 within 2 h, and thereafter through S and G_2/M to complete a 1st cell cycle (Fig. Supp. 1C, up to 12-14 h) and continued their migration through G_1-S-G_2/M of a 2nd cell cycle (Fig. Supp. 1C, up to 24-26 h).

3.1.2. Cell cycle progression of synchronized MGMT deficient and proficient cells following S_N1-alkylation damage

The effect of O^6-methylating agent treatment on the cell cycle progression was evaluated in the synchronized cell system. Cells were treated at the beginning of G_1 (from here on defined as time 0, corresponding to 2 h after seeding of mitotic cells) with different doses of MNNG.

Two low doses (0.5 and 1 μM) MNNG were first evaluated. These doses are known to be highly recombinogenic, but not significantly toxic or clastogenic in this cell line (Kaina *et al.*, 1991; Kaina *et al.*, 1997; Roos *et al.*, 2009) (Table Supp. 2). Treatment of MGMT deficient cells with these low doses caused no delay in the progression of cells through the S-phase of either the treatment or post-treatment cell cycle (Fig. 8A). A slight accumulation of cells in G_2/M of the 2nd cell cycle after treatment was observed (Fig. 8A). This accumulation was completely absent once O^6MeG was removed in the MGMT proficient cells (Fig. 8B). Similar to their MGMT deficient counterparts, MGMT proficient cells did not show any delay in the progression through S-phase (Fig. 8B).

A high MNNG dose (10μM) was thereafter used. This dose has been previously shown to be highly toxic and clastogenic in this cell line (Table Supp. 2). Under these treatment conditions, a slight delay in the progression of cells trough the 1st cell cycle was observed, evidenced as a delay in the entrance of cells in the 2nd G_1 and as a slight prolongation of the 1st S-phase (Fig. 9A). This effects were also evident in MGMT proficient cells (Fig. 9B), indicating that this delay is not caused by the O^6MeG lesion. Additionally, a dramatic accumulation of cells in the 2nd G_2/M after treatment was observed only in cells deficient for MGMT expression (Fig. 9A, B). This accumulation continued for the whole assayed time (Fig. 9A. See also Fig. 12A for data up to 72 h).

Beyond this G_2/M accumulation, there was a dramatic reduction in the amount of cells entering the 3rd G_1-phase, accompanied by a lack of clearly defined 3rd S-phase peak. As indicated, all these 2nd

S-phase and 2nd G_2/M related effects were completely absent in MGMT expressing cells, indicating the effects observed were caused by the O^6MeG lesion.

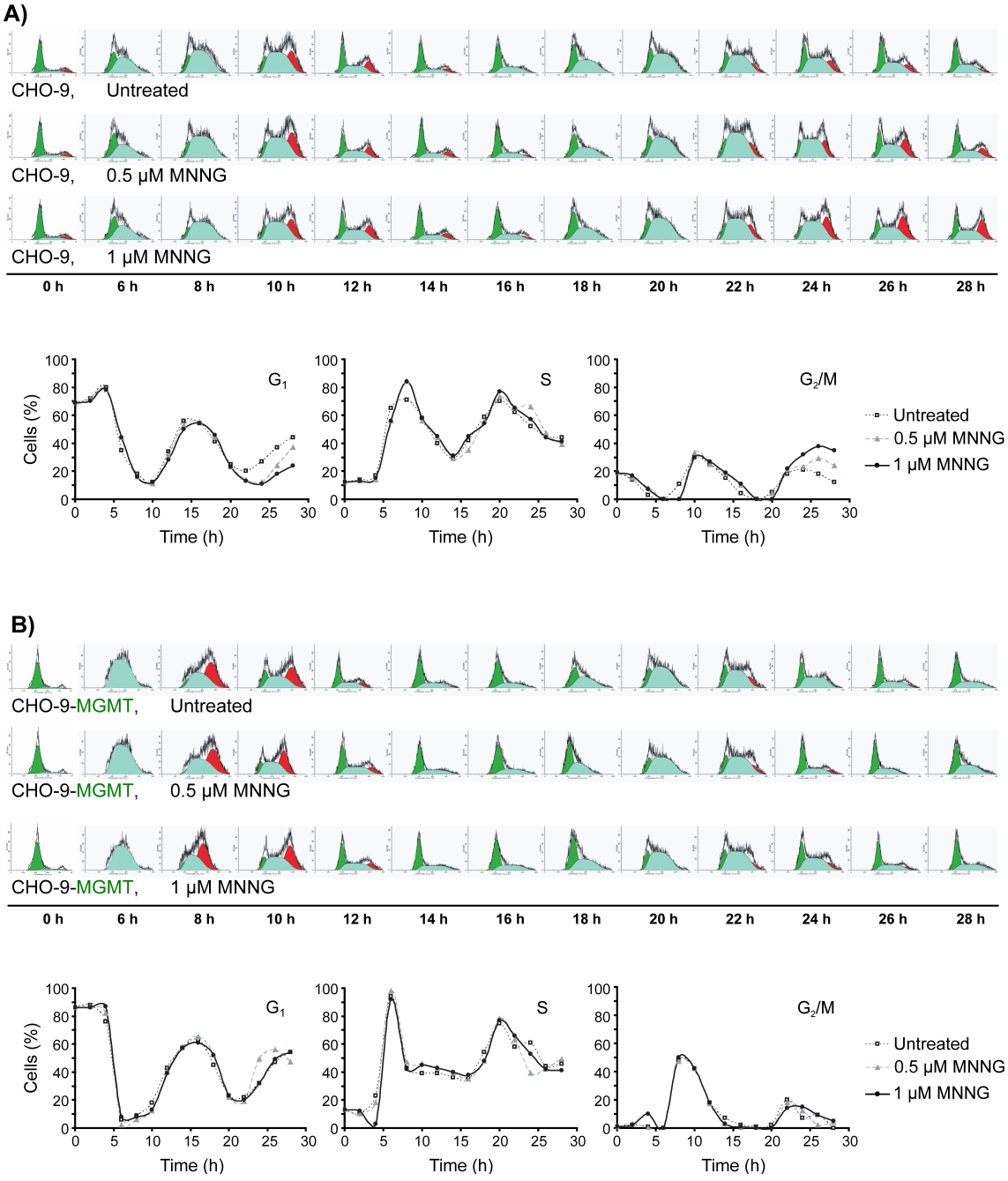

Figure 8. Cell cycle progression of synchronized cells following exposure to low dose MNNG. Synchronized CHO-9 cells (A) or CHO-9-MGMT transfected cells (B) were treated in G_1 with 0.5 or 1 µM MNNG, and their progression through the cell cycle was analyzed by flow cytometry. In the upper panels, DNA content histograms of the cell populations are shown as a function of time after MNNG treatment. In the lower panels, the proportion of cells in each phase of the cell cycle was quantified and presented for the same time points.

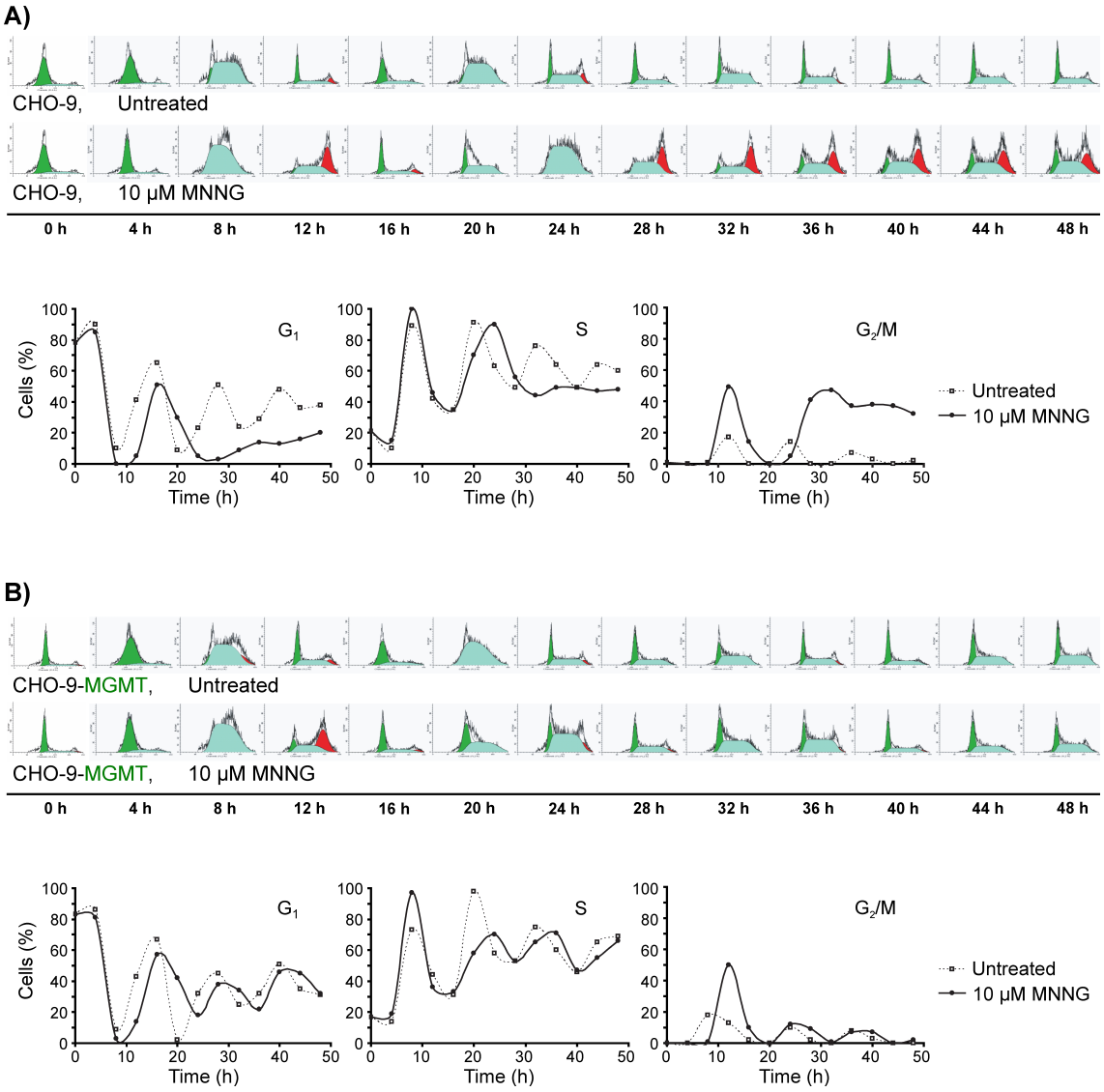

Figure 9. Cell cycle progression of synchronized cells following exposure to a high dose of MNNG. Synchronized CHO-9 cells (A) or CHO-9-MGMT transfected cells (B) were treated in G_1 with 10 µM MNNG, and their progression through the cell cycle was analyzed by flow cytometry. In the upper panels, DNA content histograms of the cell populations are shown as a function of time after MNNG treatment. In the lower panels, the proportion of cells in each phase of the cell cycle was quantified and presented for the same time points.

Collectively, the data indicate that after induction of a low level of O^6MeG in the DNA (which parallels a high level of recombination events, but not toxicity) there is no measurable impairment on S-phase progression. On the other hand, a high level of O^6MeG in the DNA (corresponding to a highly clastogenic and toxic dose) hinders the progression of cells through the 2nd S-phase. O^6MeG causes a dose-dependent accumulation of cells in the G_2/M-phase of the post-treatment cell cycle. Given that it was induced even at a sub-toxic dose, the data also indicates that a slight activation of the G_2/M checkpoint is not sufficient for triggering cell death.

3.1.3. Kinetics of ATR and CHK1 phosphorylation induced by MNNG in synchronized CHO-9 cells

Activation of the ATR/CHK1 axis by MutSα acting on O^6MeG has been suggested to trigger cell death after alkylating agent treatment (Yoshioka *et al.*, 2006). Additionally, processing of the O^6MeG lesion into DSB is also expected to activate these kinases (Stojic *et al.*, 2004).

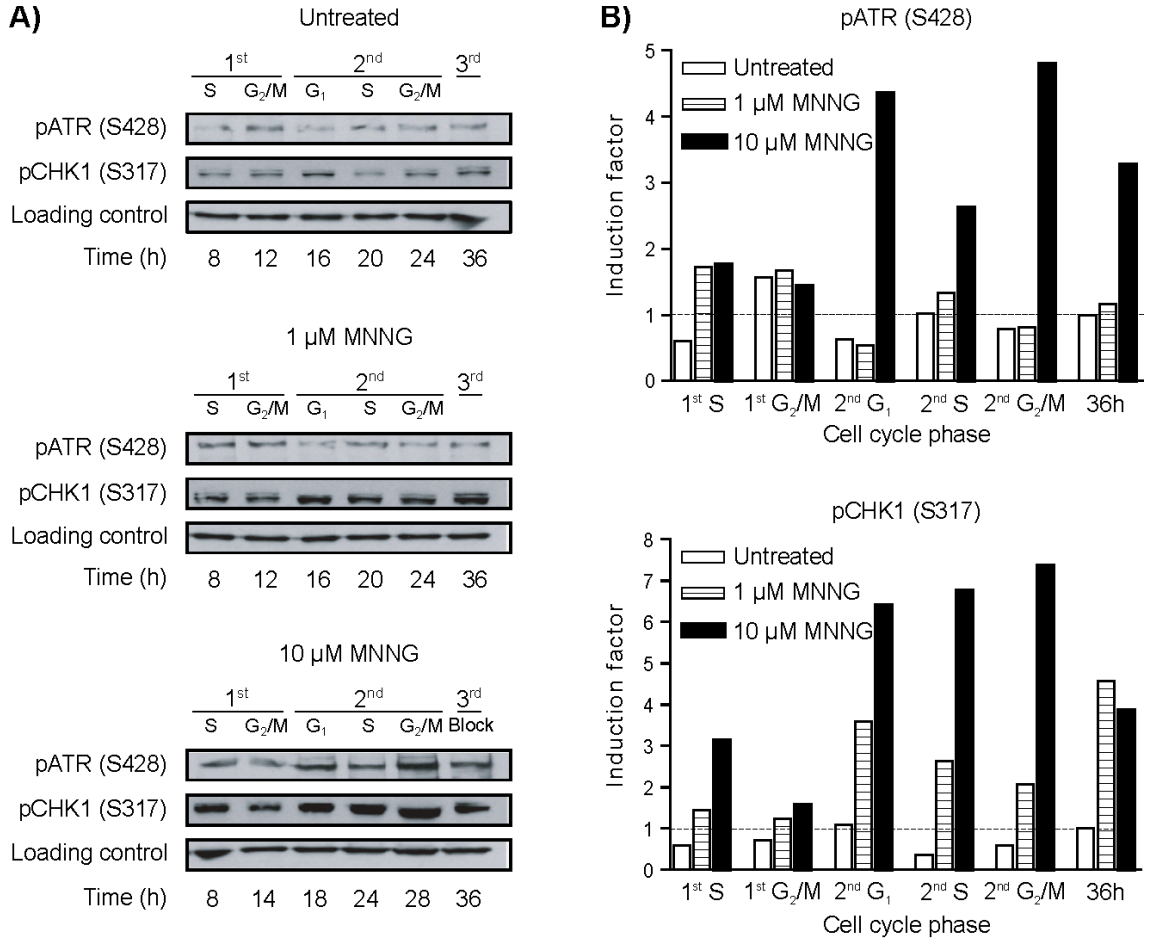

Figure 10. Kinetics of ATR and CHK1 phosphorylation induced by MNNG in synchronized CHO-9 cells. (A) Western blot analysis of P-ATR (S428) and P-CHK1 (S317) in synchronized CHO-9 cells non-treated or treated with 1 or 10 µM MNNG. Immunodetection of ERK2 was performed as a loading control. The time points correspond to those with an enrichment of the cell population in the cell cycle phases indicated on the top of the blots. (B) Quantification of the obtained data, using ERK2 as internal standard. Induction factors represent the fold-expression compared to the 36 h value of the untreated control.

In order to gain insight into the kinetics of ATR and CHK1 activation after O^6MeG induction, their kinetics of phosphorylation was evaluated by Western blot analysis (Fig. 10). Following 10 µM MNNG treatment (which is a toxic dose. See Fig. 12 and Table Supp. 2) a maximum of phosphorylation was observed during the 2nd cell cycle. A lower grade activation was also evident

during the 1st cell cycle. A 1 μM MNNG treatment (which is a sub-toxic dose. See Table Supp. 2) did not lead to a detectable ATR phosphorylation, while lead to a CHK1 phosphorylation mainly in the 2nd cell cycle at a lower grade than after treatment with a high dose (10 μM) MNNG.

The data corroborate the activation of this axis already in the 1st cell cycle. Nevertheless, it also shows that the ATR/CHK1 axis is more efficiently activated during the 2nd cell cycle after O^6MeG induction.

3.1.4. Kinetics of MNNG-induced DNA double-strand breaks formation in synchronized cells

DNA double-strand break [DSB] have been shown to precede the apoptotic response triggered by O^6-methylating agents (Ochs & Kaina, 2000) (Section 1.2.4.4b). Although this observation supports the processing model, it has never been shown in which cell cycle phase these DSB form. In order to scrutinize the kinetics of DSB formation, the induction of γH2A.X foci, a sensitive marker for DSB (Rogakou *et al.*, 1998), was assessed by fluorescence microscopy (Fig. 11). A slight increase in the amount of γH2A.X foci was detected for treated (10 μM MNNG) cells already during the 1st cell cycle after treatment. However, this increase was of very low level and was present both in cells deficient and proficient for MGMT, therefore indicating they were not caused by the processing of the O^6MeG lesion. During the 2nd S-phase, however, a far more prominent increase in the amount of γH2A.X foci was detected in cells deficient for MGMT, which persisted to the 2nd G_2/M-phase. This γH2A.X foci accumulation was completely absent in MGMT expressing cells, indicating its dependence on the O^6MeG lesions.

In conclusion, the data corroborate the hypothesis that O^6MeG adducts have to undergo two rounds of DNA replication in order to be converted into DSB.

3.1.5. Kinetics of apoptosis induction by S_N1-alkylating agents

Although it has been previously shown that toxicity induced in response to O^6MeG is a delayed event ensuing DSB formation (Ochs & Kaina, 2000; Roos *et al.*, 2007; Naumann *et al.*, 2009) (Section 1.2.4.4b), the detailed kinetic of apoptosis induction in relation to the cell cycle is still unclear. Primarily, it has not been elucidated in which cell cycle after treatment and out of which cell cycle phase cells undergo death. This is a key point of disagreement among the different models attempting to explain O^6MeG-induced toxicity. Making use of the synchronized cell system, MGMT deficient cells were treated with a toxic dose of 10 μM MNNG.

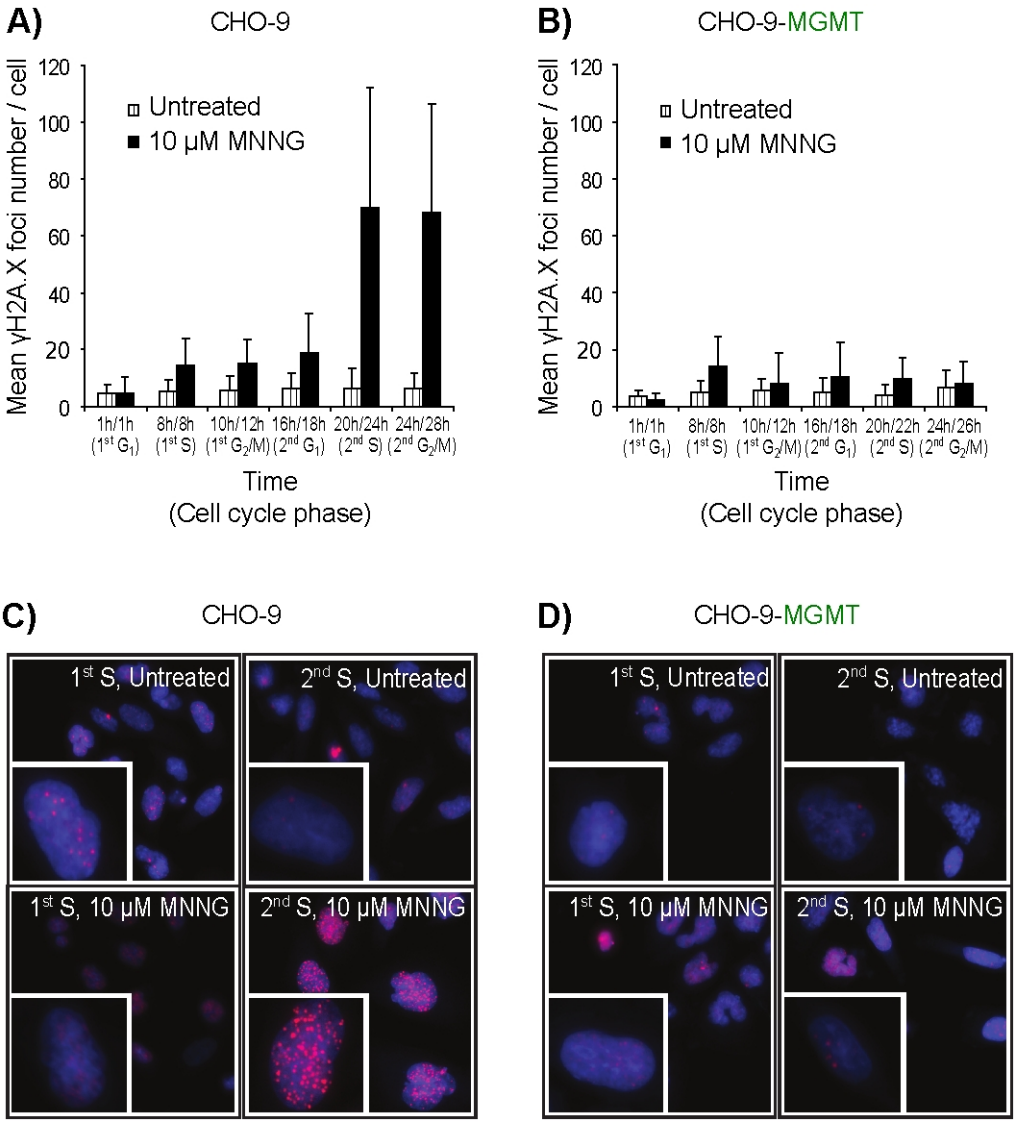

Figure 11. Kinetics of MNNG-induced DNA double-strand break formation in synchronized cells. Nuclear γH2A.X foci were analyzed by immunofluorescence microscopy of cellular nuclei. Foci were quantified in control or MNNG treated synchronized CHO-9 cells (A) and CHO-9- MGMT transfected cells (B). The time points correspond to those with an enrichment of the cell population in a particular phase of the cell cycle (indicated in brackets on the bottom of the graphs). At least 40 nuclei were scored per time point. (C and D) Representative nuclear γH2A.X foci photomicrographs for the 1st and 2nd S-phases of MGMT deficient and proficient cells are shown. Nuclear staining (shown in blue) was performed with TO-PRO-3 and γH2A.X foci were detected with anti-**P**-H2A.X (S139), using an Alexa Fluor 488 conjugated antibody (shown in red) as secondary antibody.

As evidenced from the analysis of cells with sub-diploid DNA content (Fig. 12A, red line), an increase in the amount of apoptotic cells relative to untreated cells started at about 36 h after treatment, several hours after the onset of the G_2/M accumulation in the post-treatment cell cycle. Thereafter, cell death continued to increase steadily with time, at least up to the last analyzed time point 72 h after treatment. MGMT proficient cells did not show any increase in toxicity after MNNG treatment.

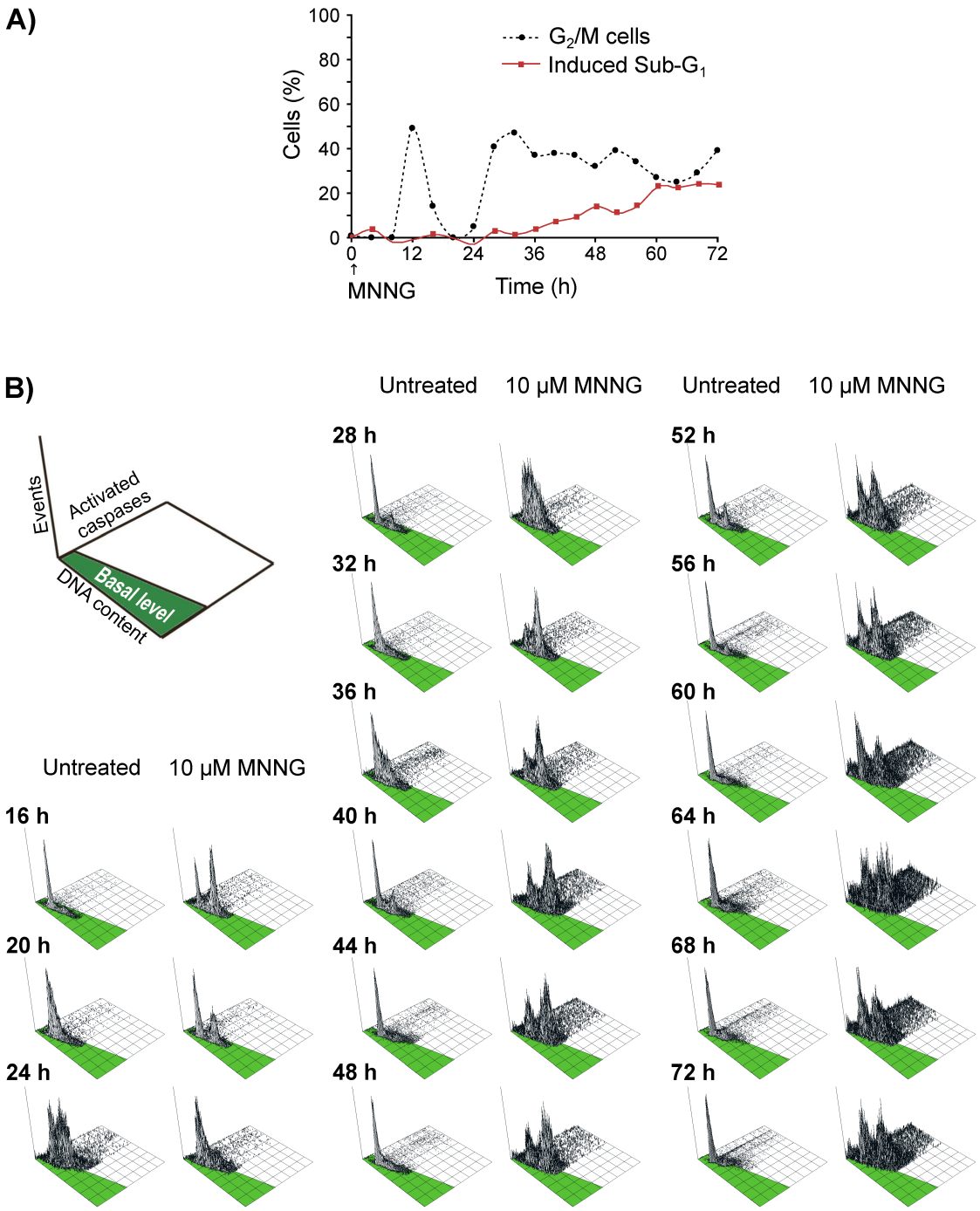

Figure 12. Kinetics of apoptosis induction by MNNG in synchronized CHO-9 cells.
(A) Time course of induction of apoptosis after 10 µM MNNG treatment, measured as percentage of induced Sub-G_1 fraction. The distribution of cells with G_2/M DNA content is also shown as a reference for cell cycle progression of the same cell population. (B) Time course of total caspases activation following MNNG treatment as determined by flow cytometric analysis of FITC-VAD-FMK staining. Caspases activation, shown as a positive shift in the Activated caspases axis, is presented relative to DNA content histograms for the indicated time points. The basal level of caspases activation (green area) was defined relative to the signal of untreated controls.

In order to corroborate these findings, activation of total caspases was analyzed by flow cytometry. Cell cycle distribution was also analyzed simultaneously (Fig. 12B). A positive shift in the activated caspases axis was evident for MGMT deficient cells around 36 to 40 h after treatment, some hours after the cells had gone through the 2nd S-phase and started to accumulate in G_2/M.

In order to established in more detail the precise phase of death activation, Western blot analysis of cleaved caspase-3 (CASP3), caspase-7 (CASP7) and PARP1 (as markers of apoptosis activation) was performed in samples enriched for particular phases of the cell cycle (Fig. 13). For the analyzed proteins, cleavage was detected from the 2nd S-phase on after treatment with 10 µM MNNG. In the untreated control, no cleavage of CASP3 and a very slight cleavage of CASP7 and PARP1 was observed.

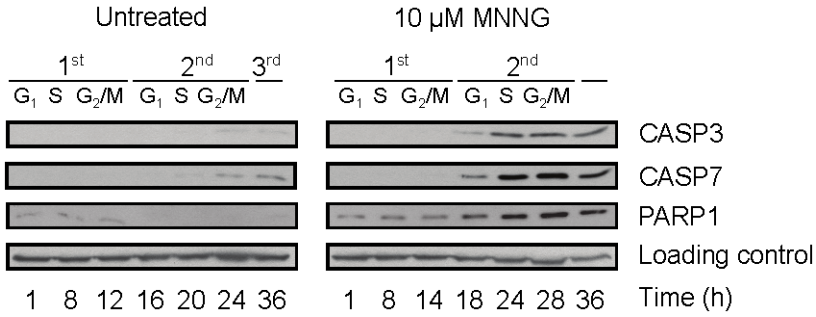

Figure 13. Cell cycle dependency of apoptosis activation in synchronized CHO-9 cells after MNNG treatment.
Apoptosis activation was determined by Western blot analysis of cleaved fragments from CASP3, CASP7 and PARP1. The time points were selected to achieve an enrichment of the cell population in the indicated phases of the cell cycle. ERK2 was used as loading control.

Collectively, the data show that following O^6MeG induction apoptotic cell death becomes activated after two rounds of DNA replication, and continue for several hours thereafter.

3.1.6. DNA replication and proliferation of cells beyond the second G_2/M after MNNG treatment

Although the above data indicate that O^6MeG-triggered apoptosis occurs after two rounds of DNA replication (Fig. 13), it was not clear why there was such an extra delay in the onset of apoptosis for a sub-fraction of the cell population. Namely, the apoptotic population continued to increase even beyond 24 h after the onset of apoptosis (Fig. 12). At least two possible scenarios were considered. In the first scenario, all cells die out of the 2nd cell cycle after a prolonged arrest, which differed in

duration among different cells. In an alternative scenario cells die after undergoing additional replication cycles.

In order to address these possibilities, the incorporation of BrdU after the 2nd G_2/M accumulation was analyzed by flow cytometry. In principle, if cells die out of the G_2/M arrest or as a result of a mitotic failure, cells should not demonstrate additional DNA synthesis. Conversely, cells progressing beyond the arrest and successfully reentering the cell cycle should exhibit DNA synthesis. As shown in Fig. 14, it was possible to determine BrdU incorporation, and by extension DNA synthesis, not only in untreated, but also in MNNG treated cells. In the latter case, incorporation was considerably reduced compared to control, but its presence is suggestive of cells recovering from or escaping the G_2/M arrest and progressing through at least the 3rd cell cycle.

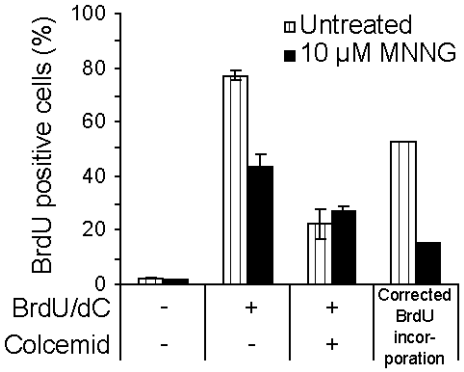

Figure 14. Replication of cells beyond the 2nd G_2/M after MNNG treatment.
BrdU incorporation was analyzed by enhancement of DNA-bound TO-PRO-3 fluorescence using flow cytometry (see Section 2.6.5 for details). BrdU incorporation was determined in cells that were transiently arrested in the 2nd cell cycle following MNNG treatment. Synchronized CHO-9 cells treated with 10 µM MNNG were incubated in the presence of BrdU/dC (60 µM each) at the beginning of the 2nd G_2/M (30 h post MNNG treatment). The percentage of cells that incorporated BrdU was measured by flow cytometry at 72 h post MNNG treatment. In a set of samples, 100 ng/ml colcemid was added with the BrdU to correct for BrdU incorporation by cells that had already passed the M-phase of the cell cycle. Data represents the mean ± SD of three independent experiments.

To further substantiate this observation, the division status of the cells was assessed with the cell tracker CFSE (Fig. 15). CFSE is a intracellularly-activated fluorescent ester that covalently binds to amine groups. Intracellular CFSE-labeled macromolecules are equally distributed into daughter cells following each cell division, hence reducing the cellular fluorescence of each successive cellular generation by a half (Lyons, 2000). Determination of fluorescence intensity thus allows for proliferation determination. Measuring the dilution of CFSE in MNNG treated cells, it was possible to determine the presence of cells not only in the first two, but also in the 3rd and 4th cell cycles after O^6MeG induction, confirming the proliferation of cells beyond the 2nd G_2/M (Fig. 15B).

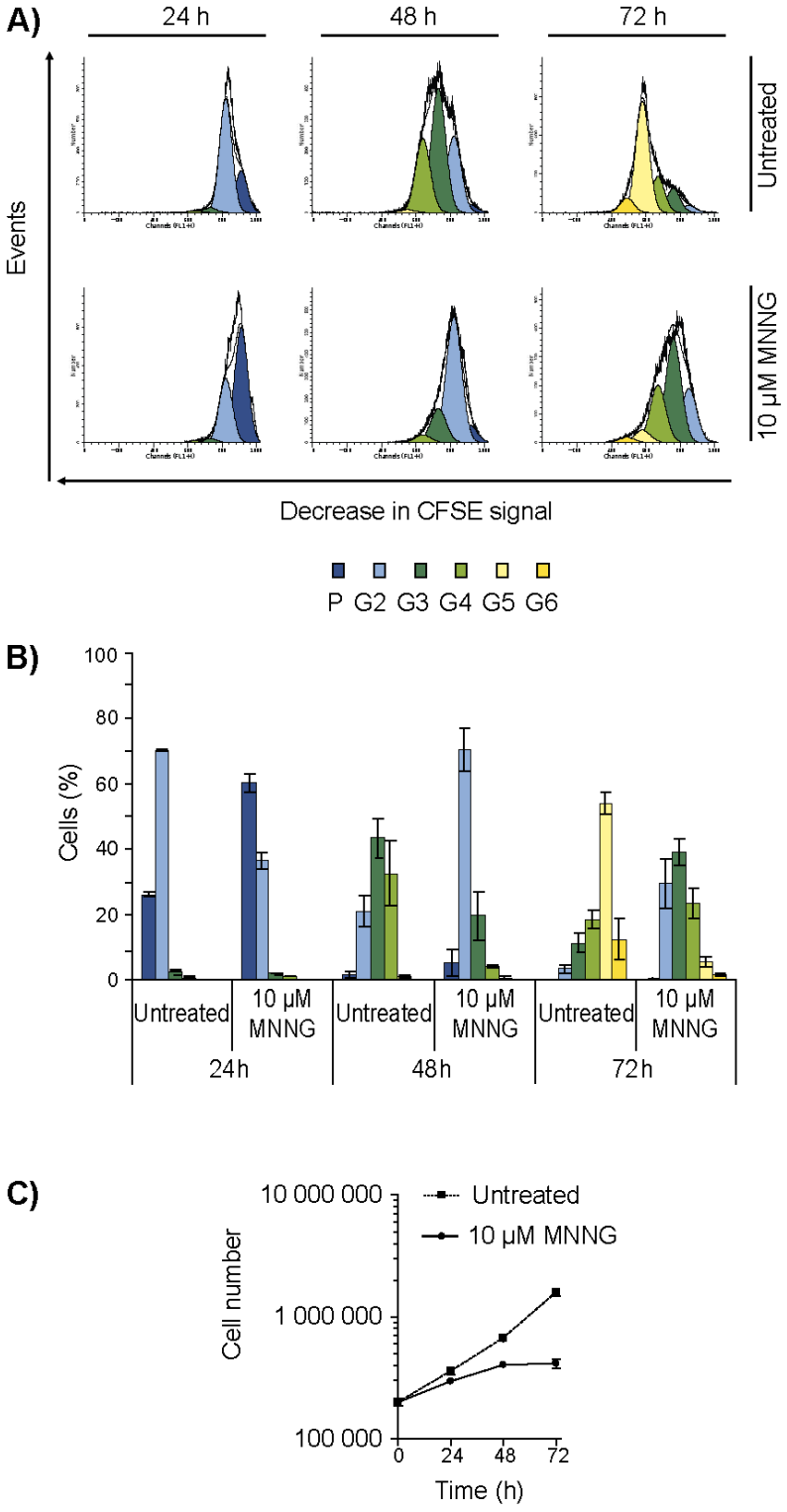

Figure 15. Proliferation of cells after MNNG treatment.
Synchronized CHO-9 cells were labeled with CFSE, seeded, and treated in G_1 with 10 µM MNNG. The proliferation status of the cell population was measured by dilution of the cellular CFSE fluorescence using flow cytometry (see Section 2.6.6 for details). Representative CFSE histograms (A) and the quantification (mean ± SD) of three independent experiments (B) are presented for the indicated time points. P = parent population, i.e. 1st cell cycle after treatment; G2 to G6 = Generations 2 to 6, i.e. 2nd to 6th cell cycle after treatment. (C) Cellular counts (mean ± SD) of the cells depicted above were performed with a Neubauer microscope counting chamber at the indicated time points after seeding.

With the CFSE proliferation assay, it was also possible to corroborate the MNNG-induced delay in the proliferation of cells, consistent with that observed on the DNA distribution analysis presented in Fig. 9. The delay was detected already 24 h after treatment, and was even more pronounced at later time points.

Consistent with these results, cell numbers of treated cells did not show any decrease at time points were there was significant cellular death, suggesting that the removal of cells by apoptosis was counteracted by the generation of new cells via proliferation (Fig. 15C). Additionally, the cell numbers at 48 h after treatment demonstrated an increase in the number of cells corresponding to at least two cell divisions, i.e., successful completion of the 2^{nd} mitosis.

Collectively, the data indicate that following O^6MeG induction cells are temporarily arrested in the G_2/M-phases following the 2^{nd} DNA replication cycle, but are then able to recover or escape from the arrest and proceed into following generations.

3.1.7. Apoptosis induction of cells beyond the second G_2/M after MNNG treatment

The survival data for CHO-9 cells shows that a 10 μM MNNG treatment leads to a reduction of survival to <0.1%, as measured by CFA (Table Supp. 2) (Kaina *et al.*, 1991). Consequently, it could be inferred that most of the cells proliferating beyond the 2^{nd} G_2/M following treatment with this dose of MNNG are bound to die (it should be noted that the CFA compiles all death events, irrespective of the cell cycle phase). Nevertheless, some proliferating cells could be survivors that outgrow the arrested cells, or cells that pass the checkpoint before its activation.

To analyze the destiny of those cells that proliferate past the 2^{nd} cell cycle, the flip of phosphatidylserine to the outer membrane and the permeabilization of the plasma membrane were determined by flow cytometry in CFSE stained cells. This allows for assessment of apoptosis as a function of the number of cell divisions the cells had undergone. As shown in Fig. 16, apoptotic cells were detected not only in the 2^{nd}, but also in the 3^{rd} and 4^{th} cell cycles after MNNG treatment, as determined 72 h after treatment.

Collectively, the data demonstrate that after a toxic dose of MNNG, a fraction of the cells undergoes apoptosis in the post-treatment cell cycle, after two rounds of DNA replication. Some cells are able to overcome the G_2-block, continue to proliferate, and trigger the apoptotic response in subsequent cell cycles.

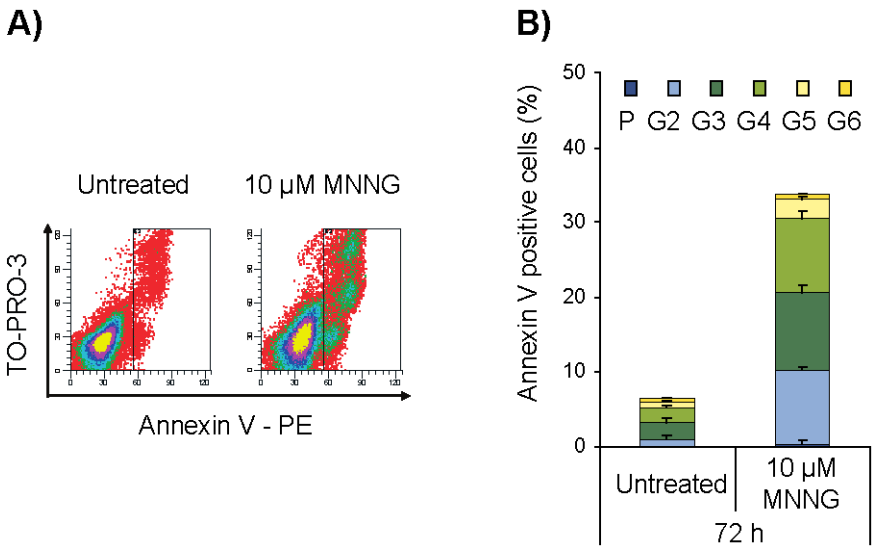

Figure 16. Apoptosis induction of cells beyond the 2nd G_2/M after MNNG treatment.
Synchronized CHO-9 cells were labeled with CFSE, seeded, and treated in G_1 with 10 µM MNNG. (A) Representative density blots depicting Annexin V/TO-PRO-3 staining 72 h after treatment. (B) Quantification of the proliferation status, determined by the extent of dilution of the incorporated CFSE (as in Fig. 15), for the Annexin V positive fraction (shown enclosed in a rectangle in (A)). Data represents the mean ± SD of three independent experiments. P = parent population, i.e. 1st cell cycle after treatment; G2 to G6 = Generations 2 to 6, i.e. 2nd to 6th cell cycle after treatment.

3.1.8. Towards a mechanistic explanation for O⁶MeG-induced cell death beyond the second generation

Cell death occurring out of the 2nd generation is compatible with the processing model for O⁶MeG-triggered apoptosis. For those cells where apoptosis occurs out of the subsequent generations two main possibilities are envisioned. First, persistence of unrepaired O⁶MeG lesions could lead to further MMR futile cycles and DSB formation in following S-phases, which would then trigger apoptosis. Second, in a non mutually exclusive alternative, cell death could be triggered by an uncontrollable increase in genomic instability caused by accumulation of faulty or non-repaired DNA damage.

To analyzed whether O⁶MeG contributes to toxicity beyond the 2nd cell cycle, MGMT expression was regulated in such a manner in order to induce repair at time points corresponding to cells in the 3rd or latter generations (see Fig. Supp. 2 for details). As shown in Fig. 17, removal of O⁶MeG at these late time points significantly reduced apoptosis induction.

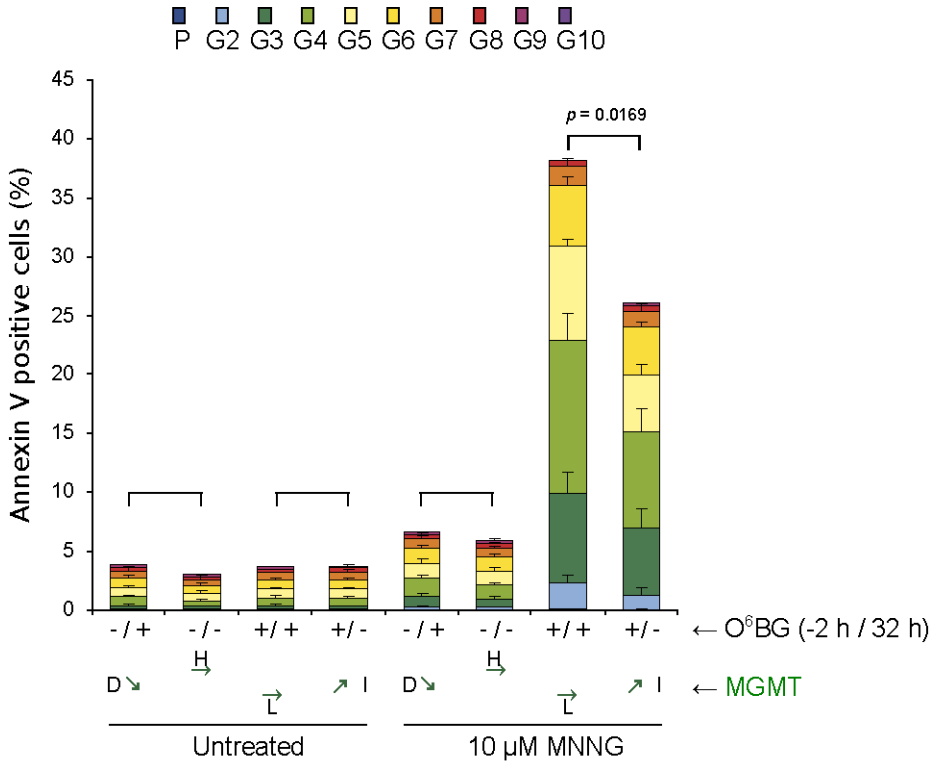

Figure 17. Role of O^{6}MeG in apoptosis induction following the 2nd generation after treatment. Synchronized CHO-9-MGMT cells were seeded in the presence (+) or absence (-) of the MGMT inhibitor O^{6}BG and then treated in G_1 with 10 µM MNNG. Medium was changed 32 h thereafter with (+) or without (-) replenishing the inhibitor to the cells. Apoptosis and cell proliferation was measured as in Fig. 16 120 h after treatment. The arrows with letters indicate the behavior of MGMT activity relative to media change. L (low): MGMT remains inhibited as before, H (high): MGMT remains active as before, D (decrease): loss of or I (increase) recovery of activity after medium change. Data represents the mean ± SD of three independent experiments. Line over bars indicates groups which were compared. *p* values were calculated using the Student's t-test. *p* values above 0.05 are not shown.

If the second alternative is also true, induction of cell death in following generations after treatment should not be a phenomenon restricted to O^{6}MeG-induced toxicity, but a more general phenomenon after genotoxic insult. Indeed, progression with unrepaired DNA damage have been reported for human cells irradiated with IR (Syljuåsen *et al.*, 2006) (discussed in detail in Section 4. Discussion).

To test this hypothesis, toxicity was measured after a wide range of genotoxic treatments (namely S_N1-methylating, S_N1-chloroethylating and S_N2-methylating agents, cisplatin and IR) and represented relative to the proliferative status of the cells. As shown in Fig. 18, although there are clear differences between the apoptosis induction profile for the analyzed agents, treatment with non-related genotoxic agents induce cell death not only in the treatment cell cycle but also in the following generations.

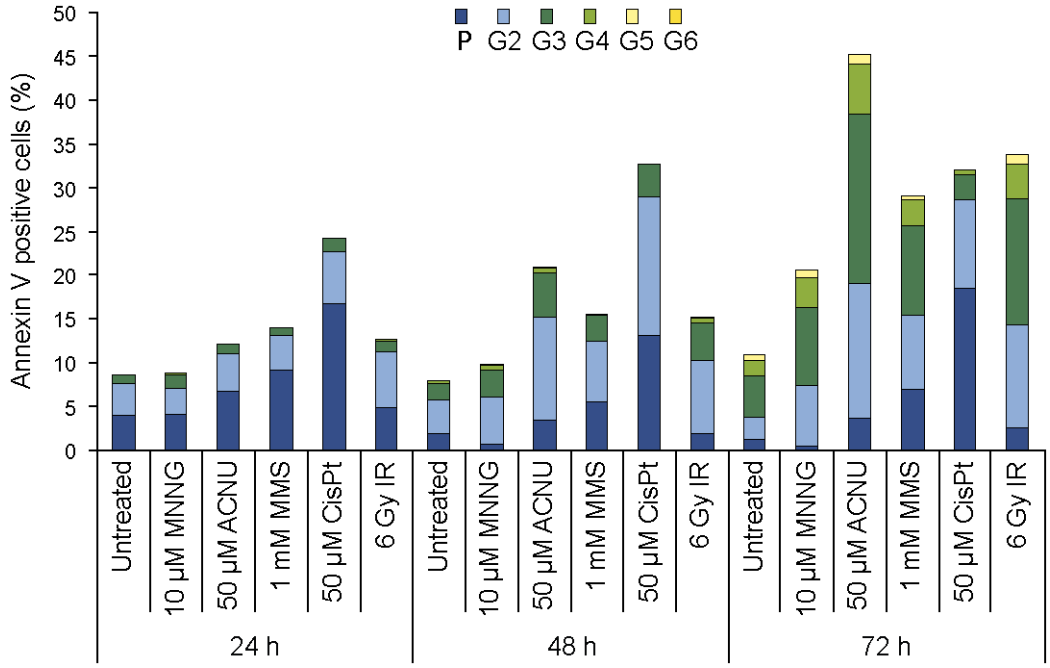

Figure 18. Apoptosis induction after genotoxic treatment according to the proliferative status of the cells. Synchronized CHO-9 cells were CFSE labeled, seeded, and pulse-treated (1 h) or irradiated in G_1 with the indicated dose of genotoxic agents. Toxicity was measured as in Fig. 16 at the indicated time points. Three independent experiments were performed. A representative experiment is shown.

Together, the data indicate that O^6MeG processing is able to trigger apoptosis several cell cycles after adduct formation. Nevertheless, as MGMT re-expression did not lead to complete abolition of apoptosis induction (Fig. 17), an O^6MeG-independent mechanism may also play a role in cell death triggered at these late time points.

3.1.9. Extension into a clinically relevant cell system

Toxicity that is triggered several cell cycles after DNA damage induction has important implications for cancer treatment (detailed in Section 4. Discussion). Even thought all observations made so far using this mammalian cell system have held true when translated into clinically relevant systems (e.g. glioblastoma and melanoma cell systems treated with the O^6-alkylating chemotherapeutics), it was analyzed whether the cell cycle dependence of cell death was not restricted to this cell type. Working with synchronized glioblastoma LN-229 cells treated with the O^6-methylating agent temozolomide [TMZ], it was possible to detect dying cells out of the 2nd and following generations (Fig. 19).

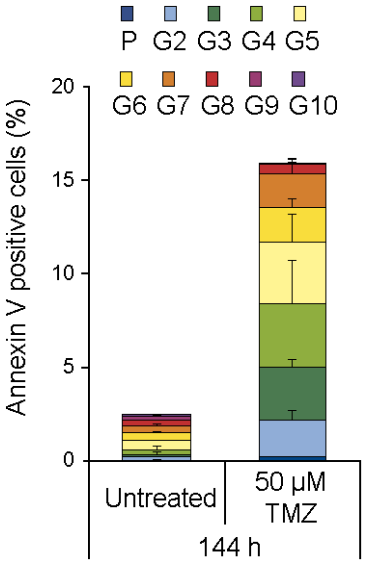

Figure 19. Apoptosis induction in glioblastoma LN-229 cells after TMZ treatment.
Synchronized LN-229 cells were labeled with CFSE, seeded, and treated in G_1 with 50 µM TMZ. The proliferation status, determined by CFSE dilution (as in Fig. 15), is presented for the Annexin V positive fraction. Data represents the mean ± SD of three independent experiments.

3.2. Part II: Mechanistic translation into a clinically relevant application

Inhibition of Homologous recombination as a strategy for tumor cell sensitization

Despite the widespread use of O^6-methylating agents in cancer chemotherapy, their therapeutic performance is only limited. Finding ways to improve the response to chemotherapeutic agents by rationally translating basic mechanistic knowledge into clinical applications is a key endeavor in the field of cancer research.

The dose-dependency of genotoxic effects observed after O^6-methylating agent treatment (Figs. 1-2, Table Supp. 2, discussed in detail below in Section 4. Discussion), together with other observations from our group (Kaina, 2004; Roos *et al.*, 2009) stresses the existence of a threshold toxic dose, which would be determined in part by the formation and persistence of DSB. Given the central role of DSB formation on toxicity, it would be expected that an impairment in the repair of those DSB triggered by the O^6-lesion would overcome this threshold, leading to a decrease in survival.

Parallel work performed in our group (Roos *et al.*, 2009) showed the importance of homologous recombination (HR) on the repair of secondary lesions induced by alkylating agents. In that work, rodent cells defective in HR were much more sensitive to cell death cause by O^6-methylating agents compared to the corresponding wild-type cells.

The mutant cell lines used in that study completely lack the expression of functional proteins involved in these repair pathways. Functional deficiency in HR is very rare for most cancer cell types, with mammalian and ovarian cancer being the exception. In order to translate these observations into a clinically relevant setting, a RNA interference approach directed to key players of the homologous recombination pathway was performed in glioblastoma cell lines. Given that the O^6-methylating agent temozolomide is the current first-line chemotherapeutic for glioblastoma patients, experiments were performed using this agent.

3.2.1. Establishment of stable HR down-regulated glioblastoma cells

Human glioblastoma LN-229 cells were stably transfected with a vector directing the intracellular synthesis of a shRNA against RAD51 (here designated as LN-229-RAD51sh). The corresponding vector with no target-sequence insert was used as a control (LN-229-pS-empty). Clones with more

than 70% suppression in RAD51 expression, as assessed by Western blot analysis (Fig. 20), were selected for further analysis.

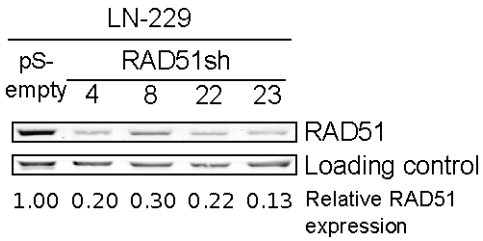

Figure 20. Stable down-regulation of RAD51 in LN-229 glioblastoma cells.
LN-229 glioblastoma cells were stably transfected either with a vector expressing a shRNA directed against RAD51 (LN-229-RAD51sh) or with the corresponding vector with no target insert (LN-229-pS-empty). RAD51 protein expression was assessed in the generated clones by Western blot analysis. ERK2 signal was used as loading control. RAD51 protein expression was quantified, corrected for loading and expressed relative to LN-229-pS-empty control.

3.2.2. Kinetics of DSB formation and repair after TMZ treatment in HR down-regulated glioblastoma cells

Down-regulation of HR is expected to lead to an impairment of repair of O^6-methylating agents derived DSB (Roos *et al.*, 2009). To verify this hypothesis, the kinetics of DSB formation and repair was analyzed by fluorescent microscopy of γH2A.X foci (Fig. 21A, B), a sensitive marker of DSB (Rogakou *et al.*, 1998). Treatment with a relatively low clinically achievable dose of TMZ (10 μM, see Section 1.3.3.2) lead to an increase in the foci formation already 24 h after damage induction. Foci number continued to increase with time for the next hours. Control cells showed repair (observed as a decrease in γH2A.X foci) already 72 h after treatment. The decrease in foci number continued steadily to values almost comparable to that of untreated cells 144 h after damage induction. Contrasting to this, cells showing the highest degree of down-regulation, presented a further increase in the number of γH2A.X foci till 72 h, and there was no evident reduction in its number by 144 h after treatment. Remarkably, cells presenting an intermediate level of RAD51 protein expression showed an intermediate phenotype, with delayed repair that was far from reaching normal levels even 144 h after treatment. Indeed, the impairment of DSB repair as determined by γH2A.X foci 96 h after treatment showed an inverse and significant correlation with RAD51 protein expression (Fig. 21C). To further investigate the theory that these TMZ-induced γH2A.X foci are DSB, a second DSB marker was used, namely Tumor protein p53 binding protein 1 [TP53BP1]. As shown in Fig. 22, TMZ also induced the formation of TP53BP1 foci, which co-localized with γH2AX in control (left panel) and RAD51 down-regulated cells (right panel).

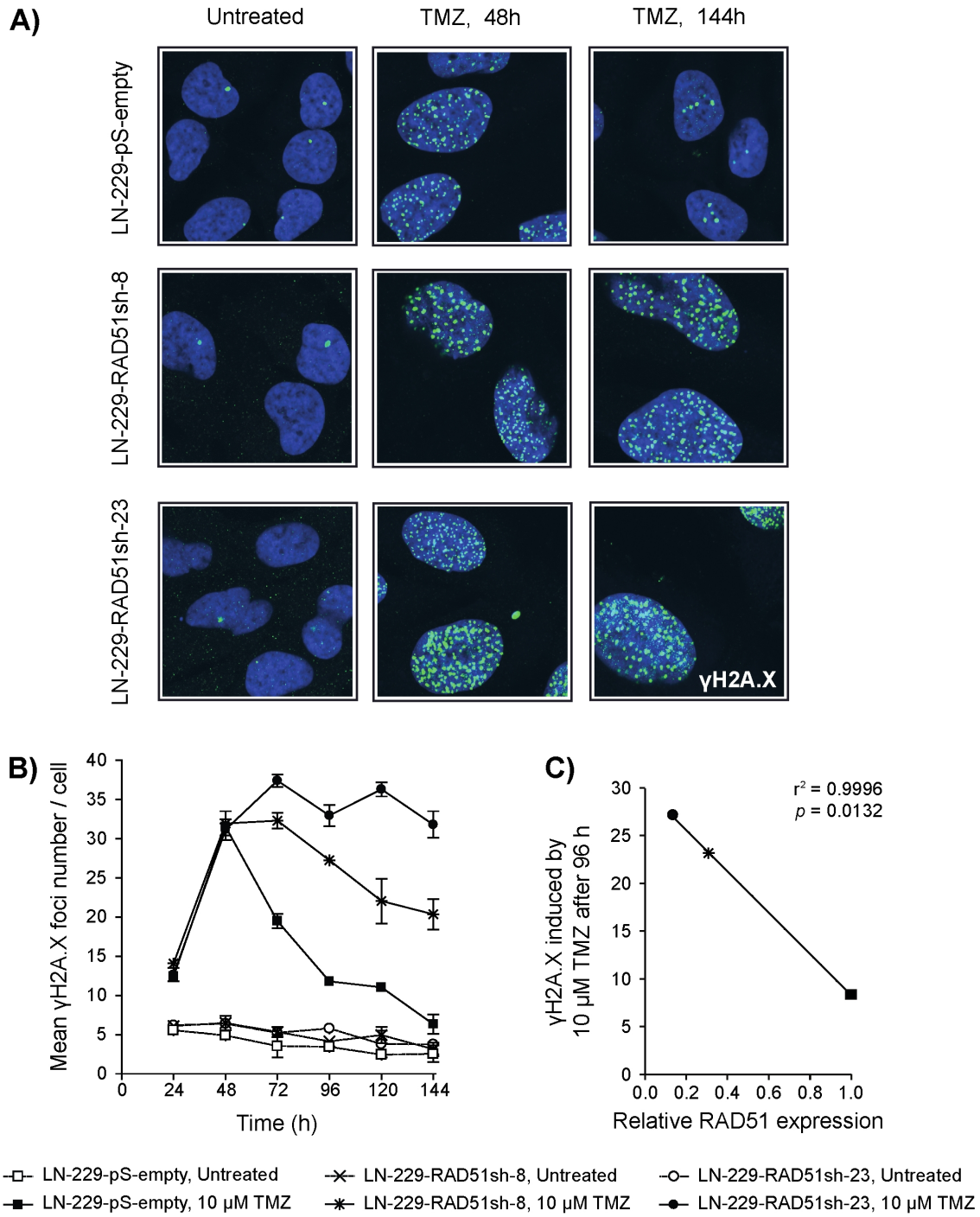

Figure 21. Kinetics of DSB formation and repair after alkylating damage in HR down-regulated LN-229 glioblastoma cells.
Kinetics of TMZ-induced γH2A.X foci formation and repair in RAD51 down-regulated LN-229 glioblastoma cells (see Fig. 20 for description of the cells) treated with 10 μM TMZ. Foci were analyzed by immunofluorescence microscopy of cell nuclei. Representative photomicrographs for two given time points are presented in (A) and quantification in (B). Data represents the mean ± SD of two independent experiments. At least 200 nuclei were counted per experiment. Nuclear staining (shown in blue) was performed with TO-PRO-3. γH2A.X was detected using Alexa Fluor 488 conjugated antibodies (shown in green) as secondary antibody. (C) Correlations between RAD51 expression, determined from Fig. 20, and γH2A.X foci number per cell 96 h after TMZ treatment, determined from (B) in this Figure.

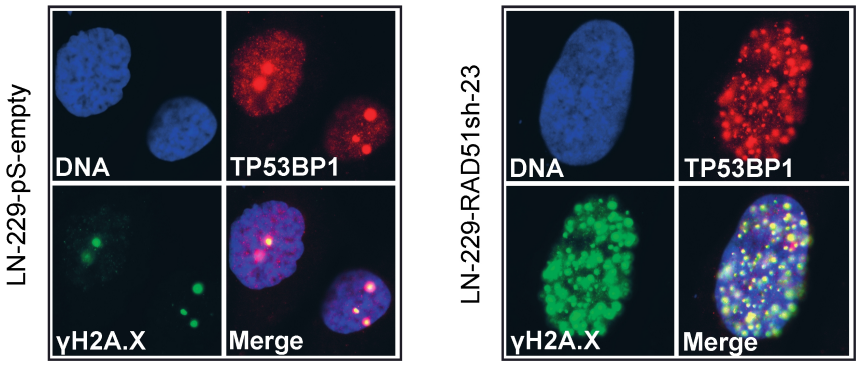

Figure 22. Co-localization of TP53BP1 with γH2A.X as a second marker for DSB in HR down-regulated LN-229 glioblastoma cells.
TP53BP1 and γH2A.X foci formation in RAD51 down-regulated LN-229 glioblastoma cells (see Fig. 20 for description of the cells) treated with 10 μM TMZ. Foci were analyzed by immunofluorescence microscopy of cell nuclei. Representative photomicrographs are shown. Nuclear staining (shown in blue) was performed with TO-PRO-3. γH2A.X and TP53BP1 were detected, respectively, using Alexa Fluor 488 and Cy™3 conjugated antibodies (shown in green and red respectively) as secondary antibodies.

The data show that HR down-regulation in glioblastoma cells leads to an accumulation and persistence of DSB after O^6-methylating agents treatment. This effect is proportional to the degree of knockdown in HR.

3.2.3. Sensitization of glioblastoma cells to chemotherapeutic alkylating agents by down-regulation of HR

The defect in DSB repair observed in HR down-regulated cells is expected to be accompanied by an increased TMZ-induced toxicity.

In order to evaluate the total cytotoxic effect on the RAD51 down-regulated glioblastoma cells, colony formation assays (CFA) were performed after genotoxic treatment. This assay also allowed us to rule out potential growth dissimilarities among control and HR deficient cells. RAD51 down-regulated glioblastoma cells showed a significant increase in toxicity after treatment with increasing doses of TMZ (Fig. 23A). Remarkably, this increase in toxicity was proportional to the decrease in RAD51 protein expression, and showed a threshold from which toxicity increases linearly to the degree of knockdown (Fig. 23B). Importantly, the induction on toxicity was also dose-dependent. The clone with the lower knockdown (LN-229-RAD51sh-8, about 30% RAD51 expression) showed no significant difference in survival relative to the control up to 5 μM TMZ (Fig. 23A). Differences emerged at

higher doses though. Almost an order of magnitude decrease in survival was seen at 15 µM for this HR deficient clone. For the clone with the highest knockdown (LN-229-RAD51sh-23, about 13% RAD51 expression) even the lowest analyzed dose of TMZ resulted in increased sensitivity. At some doses, HR down-regulation lead to about two orders of magnitude decrease in survival.

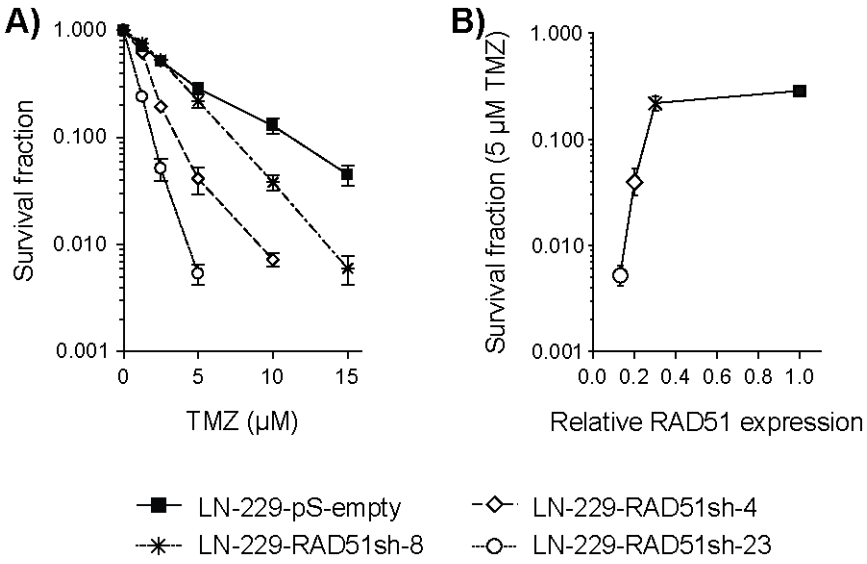

Figure 23. Sensitization of LN-229 glioblastoma cells to TMZ by down-regulation of RAD51.
(A) Clonogenic survival (CFA) for RAD51 down-regulated LN-229 glioblastoma cells (see Fig. 20 for description of the cells) following TMZ treatments. Treatments were performed 6 h after seeding. Data represents the mean ± SD of four independent experiments. (B) Dependence of TMZ-induced toxicity on RAD51 expression. Toxicity induced by 5 µM TMZ, determined from (A) in this Figure, is shown relative to RAD51 expression, determined from Fig. 20.

Together, the results shows that the toxic effects of TMZ are dose-dependent, and that saturation of HR must occur before cell death is trigger.

The impact of HR down-regulation on toxicity induced by the chloroethylnitrosurea nimustine (ACNU) and IR were also examined. Nimustine is used as second line therapeutic in GBM patients and IR is part of the standard of care for patients with these malignancies.

Similar to TMZ, down-regulation of RAD51 lead to a dramatic decrease in survival after ACNU treatment (Fig. 24A), highlighting the applicability of this sensitizing approach not only for O^6-methylating but also for O^6-chloroethylating agents. These effects were also dependent on the degree of RAD51 down-regulation and ACNU dose. Conversely, the increase in toxicity after IR of RAD51 down-regulated cells was far less prominent than for the other two agents (Fig. 24B), suggesting a less important role of HR in the repair of IR-induced DSB, which are known to be mainly

repaired by NHEJ.

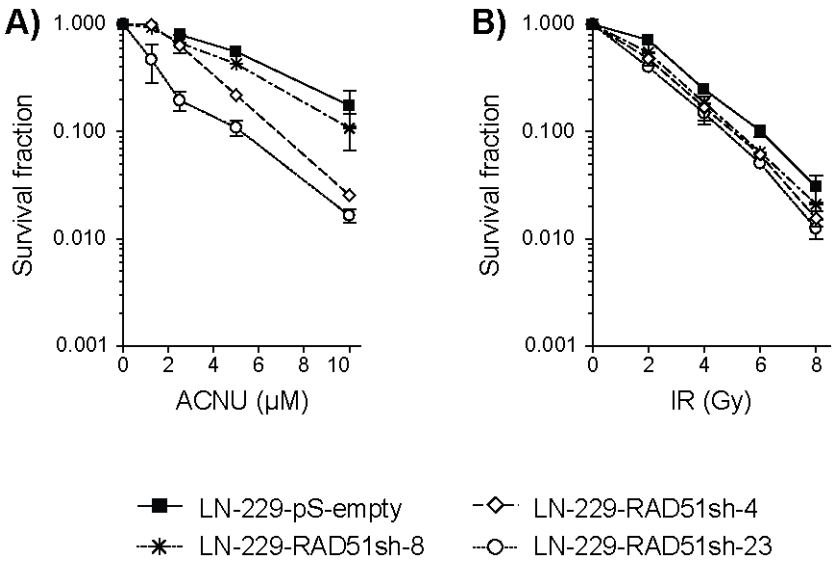

Figure 24. Sensitization of LN-229 glioblastoma cells to therapeutic agents by down-regulation of RAD51.
Clonogenic survival (CFA) for RAD51 down-regulated LN-229 glioblastoma cells (see Fig. 20 for description of the cells) following ACNU (A) and IR (B) treatments. Treatments and irradiation were performed 6 h after seeding. Data represents the mean ± SD of three independent experiments.

Cell death induced by O^6MeG in glioma cells is due to apoptosis (Roos *et al.*, 2007). Down-regulation of HR would be expected to increase the total cytotoxic response, with no impact on death pathway selection.

In order to verify this hypothesis, the apoptotic response was first analyzed in RAD51 stable down-regulated clones by Annexin V staining 144 h after 10 µM TMZ treatment (Fig. 25A). Control cells treated with this low dose TMZ showed only marginal induction of apoptosis, as compared to untreated cells. On the other hand, all RAD51 down-regulated clones showed a higher apoptotic response after treatment (Fig. 25A).

To further corroborate this observation, a 2nd cell line (namely U87MG glioma cells) was transiently down-regulated for RAD51 expression, and apoptosis was evaluated by Sub-G_1 analysis 144 h after 10 µM TMZ treatment. As before, following TMZ treatment a higher induction of apoptosis was observed in HR down-regulated cells relative to nonsense siRNA transfected cells (Fig. 25B).

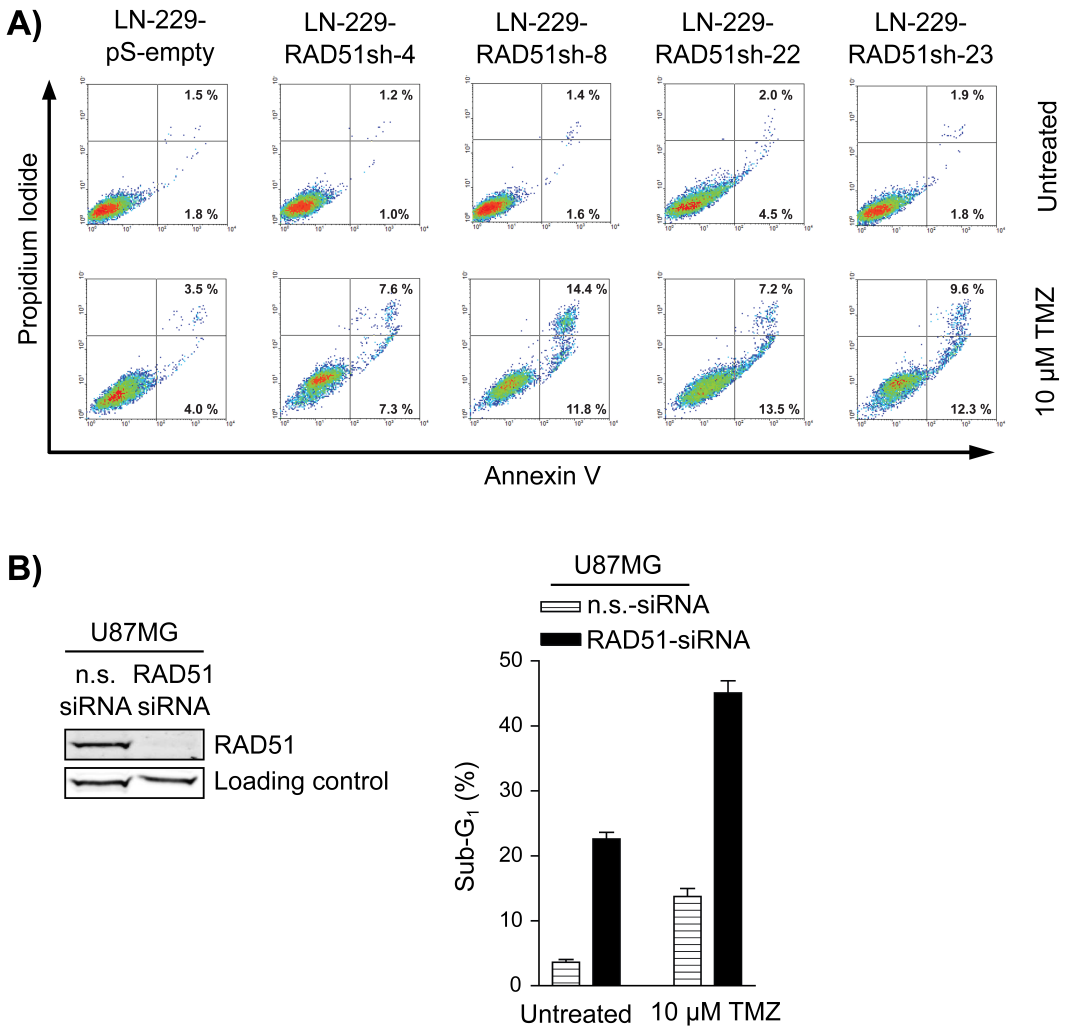

Figure 25. Apoptotic response after alkylating agent treatment in glioblastoma cells down-regulated for RAD51.
(A) Apoptosis induction after TMZ treatment in RAD51 stable down-regulated LN-229 glioblastoma cells, as assessed by Annexin V/PI assay performed 144 h after 10 µM TMZ treatment. The cells are described in Fig. 20. (B) Apoptosis induction after TMZ treatment in U87MG glioma cells transiently down-regulated for RAD51. Transfections were performed 24 h before TMZ treatment. Toxicity was assessed by Sub-G_1 determinations 144 h after treatment. Nonsense siRNA (n.s.-siRNA) transfected cells were used as control. Knockdown in protein expression was evaluated by Western blot (shown in the upper panel). ERK2 was immunodetected as loading control. Data represents the mean ± SD of three independent experiments.

Following O^6-methylating treatment, increased toxicity caused by HR down-regulation is executed via apoptosis. It is also important to note that the data also show that the chemo-sensitization is not cell line specific (see also Fig. 28B for data on T98G cells).

In order to extend the principle of chemo-sensitization to HR proteins other than RAD51, we performed survival assays after transient down-regulation of BRCA2 in LN-229 glioblastoma cells

(Fig. 26A-C). CFAs were performed from mass cultures transfected with the corresponding siRNAs. A similar picture of increased sensitivity towards the alkylating agents TMZ and ACNU, and to a much lower extend, towards IR was observed. Stable down-regulation of the HR protein XRCC2 (Fig. 26D) also lead to increased sensitivity towards TMZ treatment.

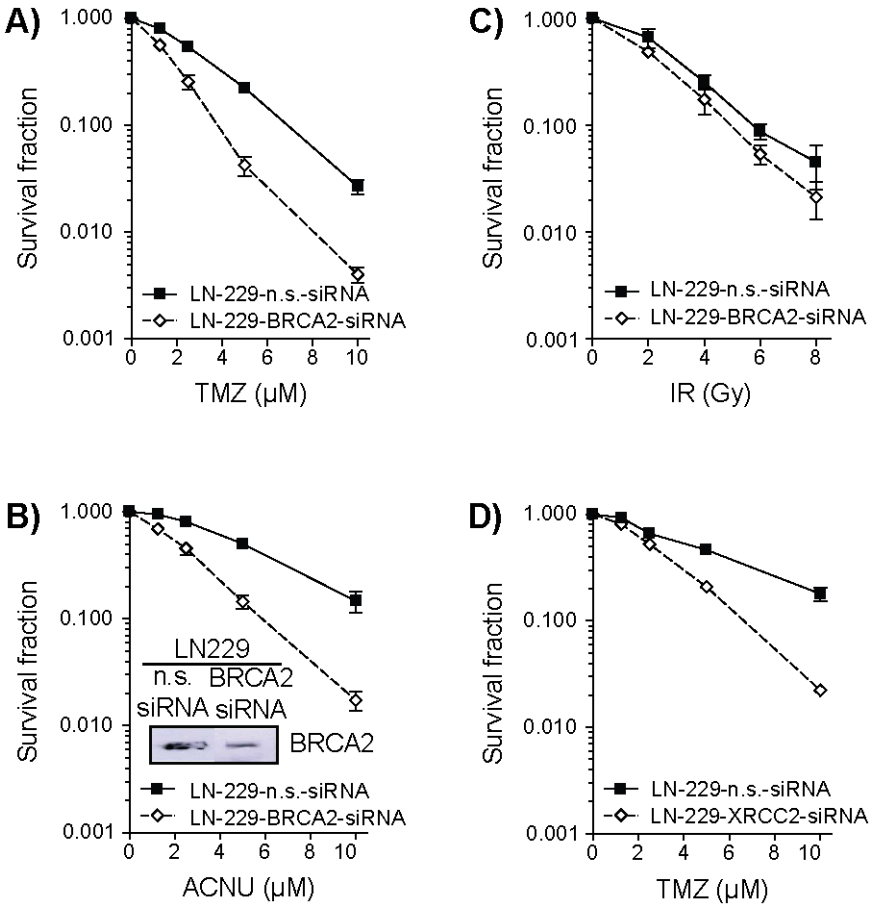

Figure 26. Sensitization of LN-229 glioblastoma cells to therapeutic agents by down-regulation of HR proteins other than RAD51.
(A-C) BRCA2 or (D) XRCC2 were down-regulated in LN-229 glioblastoma cells by siRNA or shRNA, respectively, and clonogenic survival was performed after genotoxic treatments. Transient transfections were performed 18 h before CFA seeding. Treatments and irradiation were performed 6 h after seeding. Nonsense siRNA (n.s.-siRNA) or empty vector transfected cells were used as control. Data represents the mean ± SD of three independent experiments.

Collectively, down-regulation of the HR pathway leads to an increase in death of glioblastoma cells treated with the O^6-alkylating agents TMZ and ACNU, and to a lesser extend with IR.

3.2.4. Sensitivity of HR deficient cancer cells, other than glioblastoma, to alkylating agents

O^6-alkylating agents are used for the treatment of several malignancies other than glioblastoma. Proteins of the HR pathway (namely BRCA) are occasionally defective in some neoplasms, and down-regulation of this repair pathway on those malignancies were normal expression occurs could be beneficial for patients. In order to analyze whether the chemo-sensitization principle could be extended to other cancers, the human pancreatic adenocarcinoma cell line Capan-1 (BRCA2-deficient) was selected. This cell line harbors a naturally selected inactivating BRCA2 mutation with loss of the second allele. As shown in Fig. 27, after treatment with the S_N1-methylating agent MNNG, that induces O^6MeG and N-methylpurines, toxicity was substantially higher than for the BRCA2 wild-type counterpart.

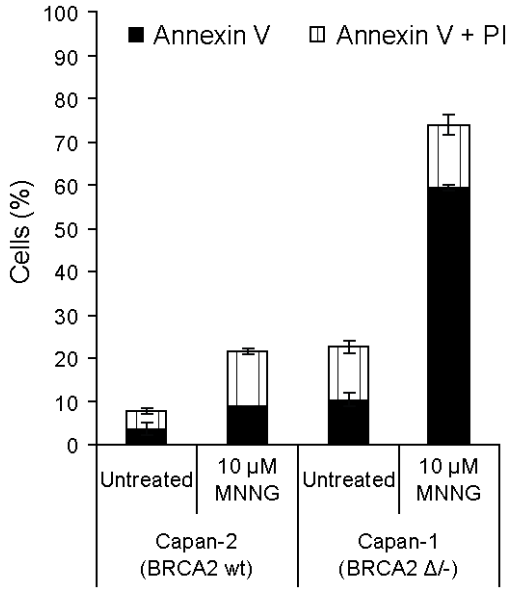

Figure 27. Apoptosis induction in pancreatic Capan-1 and Capan-2 cells after MNNG treatment.
Capan-1 (BRCA2 6174ΔT/-) and Capan-2 (BRCA2 wild-type) were treated with 10 µM MNNG. Treatments were performed after an 1 h pre-treatment with the MGMT inhibitor O^6BG (10 µM). Apoptosis determination was performed by Annexin V/PI assay 144 h after MNNG treatment.

In conclusion, chemo-sensitization to O^6-alkylating agents by reduced HR activity can be observed for cancers other than glioblastoma.

Once the feasibility of down-regulation of HR as a sensitizing strategy towards therapeutic agents was demonstrated, we scrutinized the impact of HR down-regulation on TMZ treatment, given it is the current first-line chemotherapeutic for glioblastoma patients.

3.2.5. Effect of MGMT expression and inhibition on the sensitization of glioblastoma cells to TMZ and effect of HR down-regulation

S_N1-methylating toxicity is triggered by conversion of the O^6MeG adduct into DSB (Ochs & Kaina, 2000). Cells expressing the repair enzyme MGMT are able to remove this adduct, thereby hindering DSB formation and toxicity (Kaina *et al.*, 1991) (see Section 3.1). Therefore, sensitization caused by HR down-regulation (Figs. 15-17) was expected to be due to faulty processing of O^6MeG-triggered secondary lesions. Nevertheless, HR has also been shown to be a major protection mechanism against DNA N-alkylations (Nikolova *et al.*, 2010). To determine whether HR down-regulation sensitizes towards O^6MeG derived lesions, glioblastoma cells were first transfected in order to let them constitutively express MGMT, and were then knocked-down for RAD51 expression (Fig. 28A, upper panel). Survival was evaluated after TMZ treatment for MGMT transfected control and RAD51 down-regulated cells (Fig. 28A, lower panel). In the presence of MGMT expression, no chemo-sensitization to TMZ was achieved despite down-regulation of RAD51 (compare with results from Fig. 23A). This provides evidence that following TMZ treatment HR down-regulation sensitizes to cell death triggered by processing of the DNA adduct O^6MeG.

As mention previously (Section 1.4.5), a fraction of brain tumors present clinically relevant expression of the repair enzyme MGMT (Citron *et al.*, 1995), making them non-responsible to treatment with O^6-methylating agents. MGMT inhibitors are being tested in clinical trials for those tumors where MGMT is expressed (Kaina *et al.*, 2010), in order to enhance the effectiveness of TMZ and related agents. In order to simulate this situation, a combinatorial approach (MGMT inhibition and HR transient down-regulation concomitant with TMZ treatment) was assayed in a cell line expressing endogenous MGMT, namely T98G. In the presence of MGMT, T98G cells were completely resistant to TMZ, irrespective of RAD51 knockdown. However, combining RAD51 knockdown with MGMT inhibition greatly sensitized the cells to TMZ, far beyond what was achieved by MGMT inhibition alone and no inhibition of HR activity (Fig. 28B).

Collectively, the data indicates that the increased sensitivity to TMZ provided by HR down-regulation is caused by the processing of O^6MeG. Additionally, it also shows that resistance to TMZ renders by MGMT, both in the presence or absence of HR down-regulation, can be overcome by MGMT inhibition. Finally, given that T98G is p53 mutated (the above used LN-229 and U87MG cell lines being p53 proficient), the data shows that chemo-sensitization by HR down-regulation can be achieved independently of the p53 status of the cells.

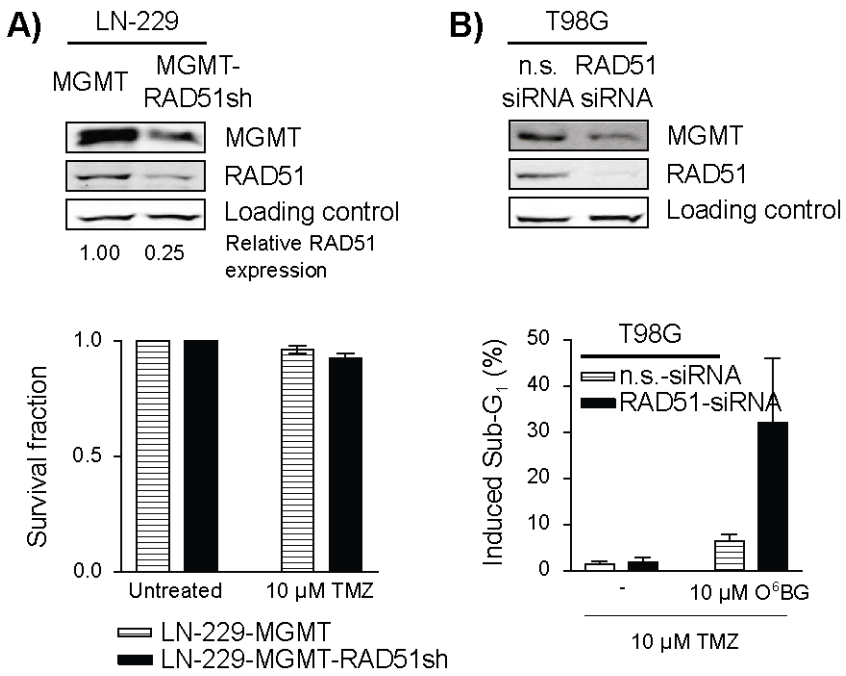

Figure 28. Effect of MGMT expression and inhibition on the sensitization of glioblastoma cells to TMZ mediated by HR down-regulation.
(A) LN-229 glioblastoma cells were stably transfected to express MGMT (LN-229-MGMT). The resulting cells were stably transfected to knockdown RAD51 (LN-229-MGMT-RAD51sh). Protein expression was assessed by Western blot. ERK2 immunodetection served as control of protein loading. Relative protein expression was calculated as in Fig. 20. Clonogenic survival (CFA) was determined after TMZ treatment. Treatments were performed 6 h after seeding. (B) T98G glioblastoma cells were transiently down-regulated for RAD51 (or transfected with nonsense siRNA), treated 24 h thereafter with 10 µM TMZ, and their apoptotic fractions (as assessed by Sub-G_1 analysis) determined 144 h after treatment. Treatment was performed with or without an 1 h pre-treatment with the MGMT inhibitor O^6BG (10 µM). Data represents the mean ± SD of three independent experiments.

3.2.6. Effect of DNA-PKcs dependent NHEJ inhibition on sensitivity of glioblastoma cells to alkylating agents

Together with HR, NHEJ plays a prominent role in DSB repair. To determine whether repression of NHEJ leads to an increased sensitivity towards TMZ, DNA-PKcs was inhibited with the specific inhibitor NU7026 (See Fig. Supp. 3 for measurement of DNA-PKcs inhibition in the presence of NU7026). Survival was evaluated after TMZ and IR treatments (Fig. 29). To facilitate comparison, equitoxic TMZ and IR doses producing about 30 to 40% toxicity in the absence of DNA-PK inhibition were selected (doses given in the legend of Fig. 29). For LN-229 glioblastoma cells (cells transfected with a empty vector, showing no RAD51 down-regulation. Fig. 29, dark bars), there was no significant increase in toxicity towards TMZ if DNA-PK was inhibited by NU7026. Conversely, and opposed to that seen for HR down-regulation, DNA-PK inhibition by NU7026 lead to a significant decrease in survival (about a third) after IR treatment.

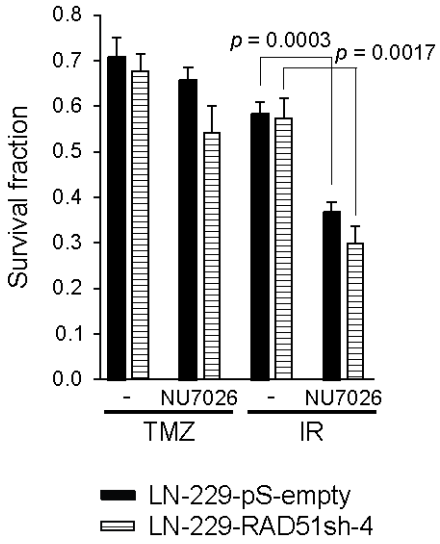

Figure 29. Effect of DNA-PKcs dependent NHEJ inhibition on sensitivity of LN-229 glioblastoma cells to alkylating agents.
Clonogenic survival (CFA) for glioblastoma cells after TMZ or IR treatments in the presence and absence of 10 μM of the DNA-PKcs inhibitor NU7026. Equitoxic TMZ and IR doses producing about 30 to 40% toxicity in the absence of DNA-PK inhibition were selected for RAD51 down-regulated and control cells, based on survival curves from Fig. 23 and Fig. 24. TMZ/IR selected doses were as follow: LN-229-pS-empty: 2.7 μM / 2.7 Gy; LN-229-RAD51sh-4: 1.5 μM / 1.9 Gy. NU7026 was added upon CFA seeding, and was then present throughout the experiment. Treatments and irradiation were performed 6 h after seeding. Data represents the mean ± SD of five independent experiments. *p* values were calculated using the Student's t-test. *p* values above 0.05 are not shown.

These results reaffirm that DNA-PKcs dependent NHEJ plays an important role in the repair of IR-induced DNA lesions, and that this pathway, however, is much less important for protection against TMZ-induced than for IR-induced DNA lesions.

Thereafter, we tested whether concomitant HR and NHEJ suppression (in the form of RAD51 k.d. and DNA-PKcs inhibition, respectively) has an additive sensitization effect towards TMZ and IR. Like their empty-transfected counterparts, HR down-regulated cells (Fig. 29, dashed bars) also presented a significant decrease in survival after IR treatment, but not after TMZ treatment. Nevertheless, following IR or TMZ treatment, DNA-PKcs inhibition by NU7026 did not show any significantly additive decreased in survival of RAD51 down-regulated cells, as compared to empty-transfected cells (compare darks and dashed bars for each combination of treatments).

Although it is worth mentioning that none of the repair pathways was completely silenced in our cell system, the results suggest a rather divergent repair pathway importance for these two agents, with HR playing the most prominent role in the repair of TMZ derived lesions, and DNA-PKcs dependent NHEJ playing a major role in the repair of IR derived lesions.

3.2.7. Combinatory effect of HR down-regulation and PARP inhibition in glioblastoma cells treated with TMZ

The synthetic lethality caused by PARP inhibitors in HR-deficient cells (Bryant *et al.*, 2005; Farmer *et al.*, 2005) have paved the way for several clinical trials for the use of these inhibitors in HR-deficient tumors (Sandhu *et al.*, 2010). Analogously, we speculated similar synthetic lethality in HR down-regulated glioblastoma cells. For this purpose we used olaparib (AZD-2281), a PARP inhibitor currently (as of December 2011) in Phase II clinical trials for breast, ovarian and colorectal cancer (http://clinicaltrials.gov).

As shown in Fig. 30, in the absence of any genotoxic treatment (black-filled markers/solid lines), PARP inhibition resulted in a much noticeable toxicity in those cells down-regulated for RAD51 throughout the range of evaluated concentrations of the PARP inhibitor, as compared to control transfected cells. We also evaluated the effect of PARP inhibition in combination with TMZ treatment (Fig. 30, empty markers/dashed line). The co-treatment reduced the survival in both control and RAD51 down-regulated cells, with the effect much more prominent in the latter.

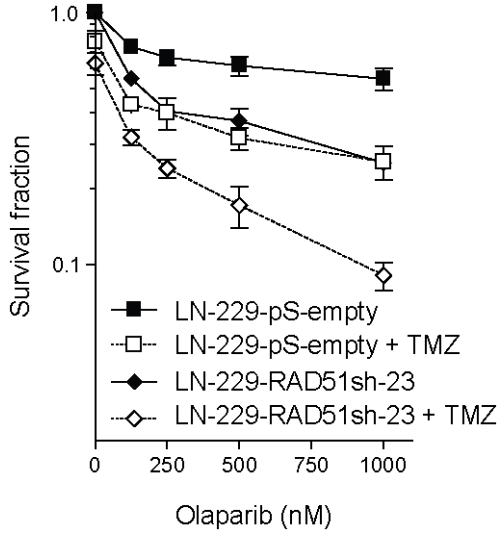

Figure 30. Combination effect of HR down-regulation and PARP inhibition in LN-229 glioblastoma cells treated with TMZ.
Clonogenic survival (CFA) for RAD51 down-regulated or control glioblastoma cells in the presence of PARP inhibition (AZD2281, *a.k.a.* olaparib). TMZ co-treatment (+TMZ) was also evaluated. Roughly equitoxic TMZ doses producing about 30 to 40% toxicity in the absence of PARP inhibition were selected for LN-229-RAD51sh-23 (0.8 μM) and control cells (2.5 μM), based on survival curves from Fig. 23 and Fig. 24. Survival in the absence of AZD2281 was set as 100% in order to compare the combinatorial effect of the inhibitor with TMZ. AZD2281 was added to cells 5 h after seeding, and was then present throughout the experiment. TMZ treatments were performed 6 h after seeding. Data represents the mean ± SD of three independent experiments.

The data indicate a significant impediment for the glioblastoma cells in repairing the TMZ-induced DNA damage when PARP is inhibited, which is exacerbated when HR is down-regulated by RAD51 knockdown.

4. Discussion

4.1. Part I: Mechanism of O^6MeG-induced cell death

Cancer is a generic term for over a 100 different diseases characterized by uncontrolled growth of abnormal cells in the body, invasion into adjacent tissues and metastasis. These diseases may be life threatening, specially if not or inappropriately treated. For example, the 5-year relative survival rate for all cancers diagnosed in the USA in the 1996-2004 period was about 66% (American Cancer Society, 2009). Besides lethality, patients usually suffer from physical, psychological and emotional complications derived from these diseases and their treatments.

Not only potentially devastating for patients and their relatives, cancer has a tremendous economical impact. The estimated 2008 overall cancer costs in USA raised to US$228.1 billion, from which US$93.2 billion are directly for medical costs, and US$18.8 billion and US$116.1 billion for indirect morbidity (loss of productivity due to illness) and mortality (loss of productivity due to premature death) costs, respectively (American Cancer Society, 2009).

Alkylating agents constitute a wide and heterogeneous class of substances able to alkylate macromolecules. Humans are constantly and virtually inevitably exposed to endogenous and exogenous alkylation sources, which are potentially clastogenic, mutagenic, carcinogenic and cytotoxic. Given its toxic effects and following a path of serendipity and keen medical observation during the first half of the last century, alkylating agents became the very first systemic chemotherapeutic anticancer agents. Since then, alkylating agents have been in use as anticancer drugs as stand alone agents or as part of combination regimes. Consequently, the biological effects following exposure of living organism to this group of agents have been in the spotlight of research for several decades. Nevertheless, the mechanisms of toxicity induced by these agents have not yet been fully elucidated. Although the constant discovery of new molecular players in repair and damage response pathways puts the research community a step closer to a clearer understanding of the biological effects of this group of toxins, a complete panorama is currently bewildering.

For S_N1-methylating agents (e.g. MNNG, TMZ), the O^6MeG lesion has been proven to be a highly cytotoxic, apoptotic, mutagenic, recombinogenic and clastogenic DNA adduct (Kaina *et al.*, 2007). Once induced in the DNA the damage is either repaired by MGMT or becomes converted by replication into the mispairs O^6MeG/T and O^6MeG/C, both substrates for MMR. As detailed in Section 1.2.4.4, several models have been proposed to explain toxicity induced by these agents. The processing hypothesis proposes toxicity to be a consequence of DSB formation associated with

replication fork collapse after encountering regions of single-stranded DNA (gaps or MMR related blocking lesions) formed by futile processing of the O^6MeG/Y by MMR (Karran & Bignami, 1994). The direct signal hypothesis proposes a model where MMR, acting as a sensor of DNA damage, is able to directly activate DDR and the downstream apoptotic cascade after O^6MeG/Y recognition (Modrich, 1997; Fishel, 1998). Additional alternatives have been proposed without much experimental support. Notably it has been suggested that nuclease attack at gaped DNA formed upon processing by MMR of the O^6MeG/Y mispair might lead to DSB formation and cell death.

As working hypothesis, if the direct signaling model or the nuclease attack model holds true, then DDR and apoptosis are expected to be activated in the treatment cell cycle upon DNA damage induction and passage through one S-phase (Fig. 7, left and middle). Additionally, in the nuclease attack model, DSB should be formed during this 1st treatment cell cycle (Fig. 7, middle). According to the processing model, DSB formation as well as DDR activation and cell death are expected to occur in cells that have undergone two rounds of DNA replication following O^6MeG induction (Fig. 7, right).

To addressed these issues, the response of cells to O^6MeG was determined as to cell cycle dependence. Cells were synchronized and then treated with a pulse (1 h) of the model S_N1 agent MNNG in the 1st G_1-phase after synchronization. In order to be able to assign effects to the methylation in the O^6-position of guanine, the response of an isogenic pair of cell lines deficient and proficient for the repair of O^6MeG was used.

Treatment with a highly toxic dose of MNNG (10 μM. < 0.1% survival. See Table Supp. 2) induced an O^6MeG-dependent delay in the progression of cells through the S-phase of the post-treatment cell cycle and an accumulation of cells in the 2nd G_2/M-phases. The accumulation of cells in the 2nd G_2/M-phases after O^6MeG induction is in accordance with previous data (Fig. 9) (Stojic *et al.*, 2004). Furthermore, this dose of MNNG induced a dramatic increase in the level of γH2A.X foci in the 2nd S/G_2/M-phases (a marker of DSB formation) (Fig. 11). This was paralleled by the activation of the checkpoints kinases ATR and CHK1 in the 2nd cell cycle (Fig. 10).

That all these critical events, i.e. inhibition of cell cycle progression, DDR activation and DSB formation, occurred preferentially in the 2nd cell cycle provides a strong support for the model where the initial O^6MeG adduct has to be processed through two rounds of replication in order to be converted into a killing lesion, in the form of DSB, which provide a strong signal for triggering the ATR/CHK1 damage response and cell cycle arrest in the 2nd cell cycle.

Some delay in the progression of cells through the 1st cell cycle and a low level γH2A.X foci formation was detected in the treatment cell cycle (Fig. 9, 11). Nevertheless, these events were of much lower level than those occurring in the post-treatment cell cycle and were not related to O^6MeG, as they were also detectable in MGMT expressing cells. N-alkylation lesions are very likely the cause of these effects. Importantly, the fact that MGMT expressing cells did behave like their MGMT deficient counterparts to these early events, but are completely refractory to cell death at this dose indicates that these effects are transitory and do not directly contribute to toxicity.

In the same way that histone H2A.X was phosphorylated already during the 1st S-phase, albeit at much lower level than during the 2nd S-phase, ATR and CHK1 was also phosphorylated already during the 1st round of DNA replication (Fig. 10). This low level of activation of the ATR axis could be caused both by those events triggered by N-alkylations and/or by recruitment to O^6MeG/T mismatches in a MutSα and MutL-dependent mechanism, as proposed by the signaling model (Yoshioka *et al.*, 2006). This not withstanding, cell death is activated first in the 2nd cell cycle (elaborated on below), arguing against a direct role of this 1st cell cycle DDR activation on toxicity.

In MGMT deficient cells, apoptosis occurred several days after DNA damage induction, in accordance with what was observed in previous reports (Fig. 12) (Ochs & Kaina, 2000; Roos *et al.*, 2007; Naumann *et al.*, 2009). More revealing, a detailed determination of the cell cycle dependence of apoptosis induction demonstrated that the activation of apoptosis markers started in the 2nd S-phase (Fig. 13), strongly supporting the assumption proposed by the processing model, that cell death is activated not immediately after damage induction, but late in the 2nd cell cycle. Additionally, the data strongly argues against models indicating cell death to be activated directly in the 1st cell cycle, as assumed by the direct signaling model or by a potential nuclease attack at single-stranded DNA formed as a consequence of futile MMR cycles.

Interestingly, a detailed analysis of the kinetics of apoptosis activation showed that the increase in cell death was still detectable at very late time points (Fig. 12). Although the basic assumption would be that this is explained by cells dying out of a very prolonged arrest in the 2nd cell cycle, it was possible to determine significant DNA replication and proliferation of cells after the 2nd G_2/M at doses known to kill over 99.9% of the cells (Fig. 14-15, Table Supp. 2), arguing against all cells dying from or immediately after the arrest. In this sense, scrutiny of apoptosis induction as a function of proliferation of the cells showed apoptotic cells originating not only in the 2nd post-treatment cell cycle, but also in the 3rd and 4th cycles after damage induction (Fig. 16).

Apoptosis is activated already in the 2nd cell cycle following induction of O^6MeG (Fig. 13, 16).

Chromosomal aberrations are formed after S_N1-methylating agent treatment at time points corresponding to the 2nd mitosis (Kaina *et al.*, 1997). This implies that treated cells are able to go beyond the G_2-block into M-phase, and would explain cells dying out of the 3rd generation after catastrophic mitotic events. Nevertheless, dying cells are also detected in later generations, implying that additional mechanisms are involved.

O^6MeG is a stable lesion that, in the absence of MGMT, is not eliminated from the DNA (Beranek, 1990). If cells are able to overcome the G_2-block in the 2nd generation and complete mitosis successfully, the original lesion would still be present in the DNA of daughter cells. In subsequent cycles of DNA replication O^6MeG could induce mismatches anew, whose futile repair attempts would lead to DSB formation and a new death signal in the following generations.

In line with this, de-repression of MGMT activity at time points where treated cells are beyond the 2nd generation lead to a significant reduction in apoptosis (Fig. 17). Thus, removal of the original lesion after the 2nd cell cycle gives the cells the possibility to recover and survive, indicating that the presence of O^6MeG does induce cell death after the 2nd cell cycle. MGMT can repair O^6MeG lesions when paired to C as well to T (Toorchen *et al.*, 1984), thus MGMT expression at any point after treatment can repair the original lesion.

After a pulse treatment with S_N1-methylating agents the amount of O^6MeG induced in the DNA will not increase. In fact the opposite is true, as cells undergo cell division the amount of O^6MeG would half for every division. Less O^6MeG would lead to less MMR futile cycles, less DSB and less cell death as cells continue to divide. Nevertheless, although O^6MeG is diluted with every cell division the yield of apoptosis remains similar in later generations (Fig. 16), suggesting the possibility of an additional mechanism of toxicity. Since cells progressing out of the 2nd cell cycle harbors a high yield of chromosomal aberrations (about 4 aberrations/cell after 10 μM MNNG. See Table Supp. 2) it is reasonable to assume that genomic instability provokes apoptosis in later generations. Thus, it is conceivable to speculate that in every cell cycle new aberrations will be formed, genomic instability increases, resulting in a decreased potential for accurate repair, and thus decrease potential for survival, at least for those cells that do not undergo malignant transformation. This continuous accumulation of genomic instability after several rounds of futile MMR processing and DSB formation would lead to an increase in cell death, counteracting the dilution of O^6MeG.

In line with a role for genomic instability as a trigger of cell death, pulse treatment of cells with genotoxic agents acting through different mechanisms (namely S_N1-chloroethylating, S_N2-methylating, cisplatin and ionizing radiation) induced apoptosis in the 1st and subsequent generations (Fig. 18).

Although some agents showed a marked preference for inducing cell death directly, all tested agents showed a strong tendency to be toxic several generations after DNA damage induction. This suggests that cells progress through the cell cycle with unrepaired DNA damage, which would allow for genetically unstable cells to propagate.

The concept of cells progressing into new generations harboring potentially lethal DNA damage have been addressed previously (see below), as explained by two different lines of thinking, namely checkpoint adaptation and threshold of checkpoint release.

Checkpoint adaptation is a genetically regulated process where a checkpoint arrest is transgressed before the checkpoint inducing signal have been completely removed. Adaptation of the G_2/M checkpoint was initially observed in yeast that has the ability to divide following a sustained checkpoint arrest despite the presence of damaged DNA (Sandell & Zakian, 1993; Toczyski *et al.*, 1997). The biological importance was assumed to be that for a single cell organism division in the presence of persistent DNA damage is preferable to permanent arrest. In a multicellular organism, S-phase checkpoint adaptation was first suggested in aphidicolin-treated *Xenopus* egg extracts (Yoo *et al.*, 2004) and, more significantly, G_2 checkpoint adaptation was also claimed to occurs in human osteosarcoma cells following IR (Syljuåsen *et al.*, 2006). Besides the potential risk of carcinogenesis caused by the accumulation of genetically unstable cells harboring DNA damage, it was speculated that adaptation could be a mechanism to initiate DNA repair in other phases of the cell cycle, or to be a preliminary step in inducing cell death, although probably in a stochastic manner rather than through a decision making program (Yoo *et al.*, 2004; Lupardus & Cimprich, 2004; Syljuåsen *et al.*, 2006; Syljuåsen, 2007). Mechanistically, the core of adaptation seems to involve Polo like kinase [PLK1]-mediated phosphorylation of claspin, (an adapter protein required for CHK1 activation by ATR (Freire *et al.*, 2006)) that causes the dissociation of claspin from the chromatin and down-regulates CHK1 activity, thus inactivating the checkpoint (Clémenson & Marsolier-Kergoat, 2009).

Another line of support for the progression of cells through the cell cycle following DNA damage comes from work showing the existence of a threshold for checkpoint initiation and for checkpoint release (Deckbar *et al.*, 2007). Within the concept of a negligent G_2 checkpoint (Deckbar *et al.*, 2007; Löbrich & Jeggo, 2007), checkpoint activation after IR only occurs after doses that induce more than 10-20 DSB per cell. Correspondingly, after higher doses of IR checkpoint release occurs before the completion of DSB repair in cells harboring about 10-20 DSB. Cells released from the arrest enter mitosis harboring 1-2 chromosomal breaks per cell (Deckbar *et al.*, 2007). Additionally, the threshold level after IR was found to be similar for both S-phase ATR- or G_2-phase ATM- evoked checkpoints

(Krempler *et al.*, 2007).

Both the checkpoint adaptation and checkpoint threshold models support our observations that cells could progress into new generations with potentially lethal DNA damage.

A **model for O^6MeG-triggered toxicity,** based on the available data (Karran & Bignami, 1994; Kaina *et al.*, 1997; Ochs & Kaina, 2000; Mojas *et al.*, 2007; Quiros *et al.*, 2010; other references cited in Section 1.2.4 and data from this work), is presented in Fig. 31. In the absence of the repair protein MGMT and in the presence of functional MMR, replication of DNA containing the O^6MeG adduct generates O^6MeG/C or O^6MeG/T mispairs (O^6MeG/Y). Both mispairs are recognized by MMR, whose enzymatic activities introduce a nick that is promptly enlarged to a single-stranded gap. Giving the mispairing properties of O^6MeG, synthesis across the lesion by repair polymerases again generates a mispair, which is again recognized and acted on by MMR. The ensuing self abortive processing is unable to correct the lesion and results in persistence of single stranded gaps in the DNA, that upon a 2^{nd} round of DNA replication leads to collapse of replication forks, DSB formation, G_2 checkpoint activation and cell death. Some of the DSB are only transiently formed and repaired by HR, which introduces recombination events manifesting as SCE, while non-repaired DSB contribute to CA formation and apoptosis activation. O^6MeG persist in the DNA and upon the 2^{nd} round of DNA replication causes new self abortive MMR cycles and single-strand gaps, which produce new DSB and related toxic response upon a further round of DNA replication in the next cell cycle. The same process repeats itself in the following generations. In parallel, those cells where cell death is not activated accumulate mis-repaired DNA damage they must deal with, which eventually is no longer tolerated and contribute to cell death.

The mixture of MMR futile cycles in later generations and accumulation of genomic instability in part explain the late response previously observed after treatment with this class of agents in glioma and melanoma cell systems (Roos *et al.*, 2007; Naumann *et al.*, 2009). In line with these observations, it was possible to demonstrate death in the 2^{nd} and later generations in a clinically relevant cell system, namely after treatment of glioblastoma cells with the first line chemotherapeutic TMZ (Fig. 19).

As a consequence of the formation, accumulation and removal of DNA damage, each subsequent cell cycle will activate the DDR with a completely different intracellular milieu that will influence the final response to the insult. Not only differences in the level of accumulated DNA damage but also the level of activation of particular DDR pathways will have an impact on which effector pathway is activated.

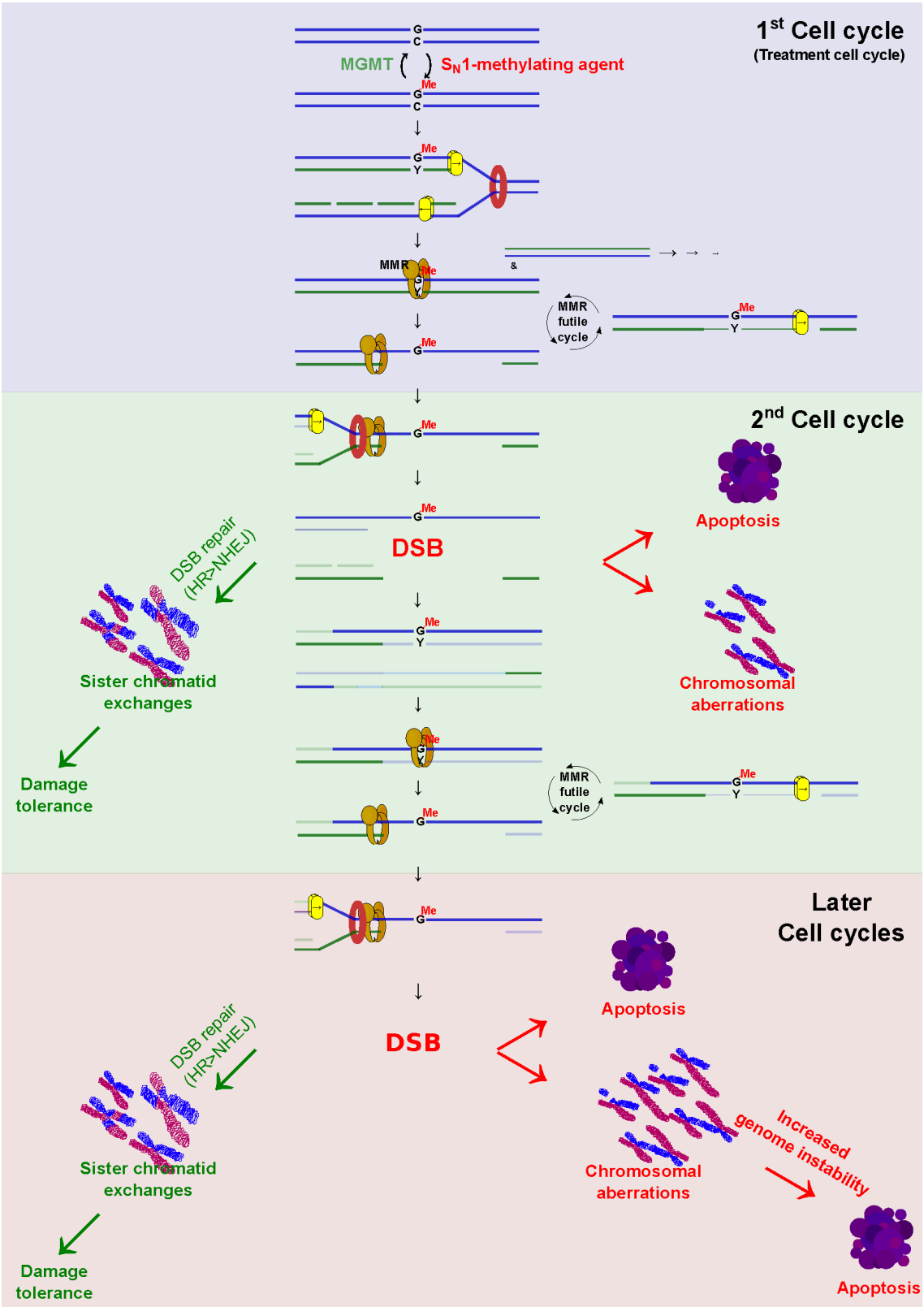

Figure 31. Proposed model for O^{6}MeG-triggered toxicity. Modified from Quiros *et al.* (2010). See text above for details.

Individual cells derived from the same culture have been reported to differ in the probability and timing of apoptosis induction. This phenomenon has been explained in the context of a natural cell-to-cell variability deriving from differences in the expression levels or activities of proteins involved in cell death pathways (Spencer *et al.*, 2009; Spencer & Sorger, 2011). In this sense, even in genetically identical cells differences in expression levels of DDR players will influence when cell death is activated. It is then conceivable to hypothesize that even the same level of damage can lead to different cell decisions, based on the intracellular availability of the DDR effectors.

An important inference drown from this concept is that for cancer cells treated with S_N1-methylating agents, where apoptosis is triggered several generations after damage induction, a therapeutic effect is not expected to occur immediately after treatment.

MGMT inactivating drugs are being tested in trials for those tumors were MGMT expression hampers the applicability of this group of agents (Kaina *et al.*, 2010). The fact that O^6MeG triggers toxicity several generations after treatment implies that their effectiveness will depend on the duration of inhibition and length of the cell cycle. Cancer cells whose MGMT activity is inhibited for treatment but are given enough time to recover from the inhibition could potentially correct the lesion and survive, even with an increased genomic instability. Further clonal expansion could generate heterogeneous sub-populations of modified cells, more resistant to these and other groups of therapeutic agents, and with an elevated carcinogenic potential.

Treatment with low dose MNNG (0.5 μM and 1 μM MNNG) did not inhibit the passage of cells through the 1st and 2nd post-treatment S-phases. A slight dose-dependent accumulation of cells in the 2nd G_2/M-phases, which seems to only be transitory, was observed for these doses. MNNG at a dose of 0.5 μM is known to be highly recombinogenic, without inducing CA or cell death (Fig. 8, Table Supp. 2).

Processing of the O^6MeG/Y secondary lesion by homologous recombination results in SCE formation in the 2nd S-phase after treatment (Roos *et al.*, 2009). The data suggests that bypass of this secondary lesion by homologous recombination is a rapid and highly efficient process. This bypass appears to take place without slowing down DNA replication, and efficiently protects against chromosomal aberrations and cell death.

The data supports the view that the biological effects of S_N1-methylating agents are dose-dependent, with the existence of a no-effect threshold for cell death and CA formation and a lineal response for SCE formation (Kaina, 2004). Low doses of S_N1-methylating agents are tolerated by the cells at the

expense of recombination events, which represent a survival mechanism for the cells.

DSB are at the center of S_N1-methylating agents-triggered toxicity, and HR is a key defense mechanism against this group of agents. Therefore, inhibition of this repair pathway should be a powerful strategy to augment the effect of O^6MeG-inducing chemotherapeutic agents. This possibility was carefully scrutinized in this work, as discussed in the next section.

4.2. Part II: Mechanistic translation into a clinically relevant application

Inhibition of Homologous recombination as a strategy for tumor cell sensitization

O^6-alkylating chemotherapeutics are widely employed as standalone agents or as part of regimes for the treatment of different tumors, including glioma, malignant melanoma, Hodgkin's and non-Hodgkin lymphoma, sarcoma and islet cell carcinoma of the pancreas. One of these malignancies, glioblastoma multiforme (GBM), constitute the deathliest and most common form of primary malignant brain tumor. The standard of care for this form of cancer combines cytoreductive surgery and post-operative chemoradiotherapy employing the O^6-methylating agent TMZ. Largely due to the poor completeness of resection caused by its inherent invasiveness into healthy tissue, concomitant and maintenance chemoradiotherapy are of utmost importance to prolong the survival of patients. Nevertheless, despite front-line treatment median survival rates for patients suffering from this condition is below 15 months.

Treatment of GBM or other malignancies where complete surgical removal of the neoplasm is not a feasible alternative presents a major therapeutic challenge. Hence, finding ways to potentiate the response to chemotherapeutics by rationally translating basic mechanistic knowledge into a potential clinical application is of paramount importance.

Along with other small molecules, e.g. imatinib mesylate (Gleevec, the first kinase inhibitor approved for use in cancer, targeting the fusion protein BCR-ABL in chronic myeloid leukemia) (Druker *et al.*, 2001), and antibodies, e.g. trastuzumab (Herceptin, the first clinically approved monoclonal antibody, indicated in Receptor tyrosine-protein kinase HER-2/neu [ERBB2]-positive metastatic breast cancer) (Slamon *et al.*, 2001), RNA interference [RNAi] have been envisioned as an appealing alternative for stand alone or complementary therapy.

Since the first successful *in vivo* pre-clinical therapeutic application of RNAi (siRNAs targeted to Fas in a mouse model of induced hepatitis, resulting in protection of the treated animals against liver fibrosis (Song *et al.*, 2003)), a myriad of *in vitro* and *in vivo* studies have been reported in models resembling a wide variety of medical conditions. Research efforts are ongoing in order to circumvent the inherent limitations in the use of RNAi as therapeutic agents, specially those concerning its stability, administration and delivery in clinical applications (Castanotto & Rossi, 2009; Pecot *et al.*, 2011; Petrocca & Lieberman, 2011).

Phase I and II clinical trials using RNAi are ongoing for different medical conditions (http://clinicaltrials.gov), including five phase I clinical trials for the use of RNAi in solid cancer and lymphoma. These trials involve the use of liposomes and nanoparticle delivered siRNA, a locked nucleic acid, and a biodegradable polymeric matrix placed in tumor for slow siRNA release (http://clinicaltrials.gov) (Petrocca & Lieberman, 2011). Promising early results have been obtained for systemic administration of siRNA using a targeted nanoparticle delivery system, where targeted RNAi mediated knockdown of the target protein was achieved in tumors of patients with metastatic melanoma (Davis *et al.*, 2010). Significant targeted down-regulation of BCR-ABL activity have also been reported after systemic liposomal delivery of a siRNA targeting this fusion transcript in a female patient suffering from chronic myeloid leukemia resistant to standard treatment (Koldehoff *et al.*, 2007).

Knowledge of potential therapeutic use of siRNA in the CNS comes mainly from studies working with neurodegenerative disorders *in vitro* and in rodent models. Much effort is directed towards stabilizing and directing the nucleotides into and throughout the brain, a matter of special difficulty given the challenge imposed by the blood-brain barrier. Viral vectors expressing shRNA are also limited by the ability of viruses to diffuse within the tissue and transduce target cells. Studies for naked or complexed siRNAs with liposomes, nanoparticles or cell penetrating peptides have been reported, and the use of brain homing antibodies have also been assayed (Boudreau & Davidson, 2010; Boudreau *et al.*, 2011; Bowers *et al.*, 2011). At a pre-clinical level, reports for successful RNAi in brain cancer in rodent models include direct administration of shRNA expressing plasmids by a mini-osmotic pump (Gondi *et al.*, 2004), intravenous shRNA plasmid delivered by a pegylated double immuno-targeted liposome (transferrin receptor to target vascular cancer endothelium and insulin receptor for receptor mediated endocytosis by cancer cell) (Zhang *et al.*, 2004), and intravenous administration of a biotinylated siRNA conjugated to a monoclonal antibody targeting the transferrin receptor via a biotin streptavidin linker (Xia *et al.*, 2007).

Given the central role of HR in the repair of O^6MeG-derived secondary lesions, its inhibition is expected to sensitize cancer cells to the killing effects of S_N1-methylating agents, making this repair pathway an attractive druggable target (Roos *et al.*, 2009; Rajesh *et al.*, 2010; Short *et al.*, 2011; Quiros *et al.*, 2011). Nevertheless, a direct correlation between patients survival and GBM tumoral RAD51 expression in primary and in recurrent tumors, independent of tumor proliferation, patient age, gender and performance status has been reported (Welsh *et al.*, 2009). In this sense, the lower survival for patients (an extension of higher survival of tumoral cells) with low tumoral RAD51 expression is at odds with a potential chemo-sensitization by HR inhibition.

Aimed at determining whether inactivation of HR would lead to increased sensitivity of glioma cells to O^6-alkylating agents, stable and transient RNAi transfections targeting HR were performed in GBM cells *in vitro*, as an indispensable early stage validation preceding a future translation into a clinical setting.

Collectively, the data demonstrates a massive increase in the sensitivity of glioma cells treated with O^6-methylating (TMZ) and O^6-chloroethylating (ACNU) chemotherapeutics once HR was knocked-down by RNAi (Fig. 23-24, 26). This was demonstrated for several key HR proteins (RAD51, BRCA2, XRCC2) (Fig. 23-24, 26), indicating the inhibition of the HR pathway at different levels sensitizes to these groups of agents. HR down-regulated GBM cells died mainly by apoptosis (Fig. 25), similar to what has been reported for glioma cells treated with S_N1-methylating agents (Roos *et al.*, 2007), indicating that the knockdown of HR proteins have no impact on death pathway selection. Significantly, the RNAi mediated chemo-sensitization was achieved in cell lines proficient (LN-229 and U87MG) and mutated (T98G, Capan-1) in p53 (Fig. 23-24, 26-28). Accordingly, it is known that p53 impacts the O^6MeG-triggered apoptotic response in glioma cells by regulating the executing pathway, but it is not involved in DSB formation or repair (Roos *et al.*, 2007).

The increased sensitivity to this group of agents (Fig. 23) was accompanied by an accumulation of DSB (Fig. 21). Both effects were proportional to the decrease in RAD51 protein expression. Importantly, these results also emphasizes the dose-dependence of the biological effects triggered by S_N1-methylating agents, as discussed previously in Section 4.1. This results are thus compatible with previous observations (Kaina, 2004; Roos *et al.*, 2009) indicating that a saturation of the HR system over a particular threshold must occur before DSB formation and cell death is trigger. The lower the activity in the HR system given its down-regulation, the faster becomes saturated, DSB form and trigger cell death.

In the light of these results, it is tempting to interpret the direct correlation between patients survival and GBM tumoral RAD51 expression in primary and in recurrent tumors observed by Welsh *et al.* (2009) in the sense that the elevated RAD51 expression represents some genetic instability in these tumor cells (indeed an alternative interpretation suggested by them), reflecting cells with a propensity to die after genotoxic insult. This might make up for the increased patient survival Welsh *et al.* observed in patients carrying tumors with high RAD51 expression. Expanding on this, it is tempting to speculate that the tumor cells with low HR activity might be adapted to grow under this condition of low repair, and might even up-regulate some survival pathways or have increased procarcinogenic pathways. Theoretically, a further inhibition of DNA repair (e.g. by RNAi) concomitant with alkylating chemotherapy would impose a challenge the cells might not have time to adapt to. Whether

a sub-population of cells can indeed survive this challenge, remains to be evaluated with the proper model systems.

It is important to note that chemo-sensitization was also demonstrated for pancreatic adenocarcinoma cells harboring naturally selected inactivating BRCA2 mutations (Fig. 27), remarking the applicability of this principle not only for glioma but also for other cell systems. It is also important to note that patients with neoplasms presenting inactivating mutations in HR genes, common in ovarian and breast cancer, are expected to directly profit from treatment with O^6-alkylating agents.

Expression of the repair protein MGMT completely abolished chemo-sensitization achieved by HR knockdown, indicating the strict dependence on O^6MeG processing into DSB. This is a non trivial observation, as HR has also been shown to be a resistance marker against N-alkylation induce toxicity (Nikolova *et al.*, 2010). Of great significance, pharmacological inhibition of MGMT restored the therapeutic benefit brought about by HR down-regulation (Fig. 28). Because of this, in patients with MGMT expressing GBM, a combinatorial targeted approach involving inhibition of both MGMT and HR would enhance the therapeutic effect of O^6-alkylating agents. For both inhibitors, either local administration directly to the tumor (as previously shown for MGMT (Koch *et al.*, 2007)) or a tumor targeting strategy would be desirable in order to avoid an exacerbation of the toxic side effect of TMZ in patients. RNAi targeting was discussed in this section, and tumor targeting strategies for MGMT inhibitors are also in development (Kaina *et al.*, 2010). Conjugates of the MGMT inhibitor O^6BG, namely, O^6BG-folate conjugates (Nelson *et al.*, 2004) or O^6BG-glucose conjugates (Reinhard *et al.*, 2001a; Reinhard *et al.*, 2001b; Kaina *et al.*, 2004) are based on the fact that cancer cells expose high levels of folate receptors or have increased glucose consumption, respectively. Promising *in vitro* results have been reported for these agents. Parallel to local administration or targeting strategies, MGMT-based myeloprotective gene therapy approaches are also envisioned as an alternative to reduce the dose limiting myelosupression associated with alkylating agent treatment (Kaina *et al.*, 2010).

To my knowledge, as of December 2011, there is only one report of inhibitors specifically targeting HR (Martinez *et al.*, 2010), namely three nucleic acid aptamers directed against RAD51. These aptamers, selected *in vitro* by the technique of Systematic Evolution of Ligands by Exponential Enrichment, affect the first step of the strand exchange reaction by promoting the dissociation of DNA from the ATP/RAD51/DNA complex (Martinez *et al.*, 2010). Their potential use for sensitizing tumor cells to chemotherapeutic agents has however not yet been demonstrated.

Other molecules have been reported to have an unspecific effect on HR. Imatinib (Gleevec), an established c-Abl tyrosine kinase inhibitor, has been shown to reduce RAD51 expression in tumor

cells (Russell *et al.*, 2003; Choudhury *et al.*, 2009). Erlotinib (Tarceva) and Gefitinib (Iressa), two Epidermal growth factor receptor [EGFR] tyrosine kinase inhibitors, have been shown to attenuate HR repair, probably at least in part by enhancing RAD51 mRNA instability by decreased phosphorylation of the PI3K-AKT and MKK1/2-ERK1/2 signaling pathways and by enhancing RAD51 protein instability through 26S proteasome mediated degradation (Li *et al.*, 2008; Ko *et al.*, 2008a; Ko *et al.*, 2008b; Ko *et al.*, 2009). The cyclin-dependent kinase inhibitor Flavopiridol (Alvocidib) has also been shown to transcriptionally suppress RAD51 expression, although only in p53 wild-type cells (Ambrosini *et al.*, 2008). RAD51 protein levels have also been shown to decrease after treatment with two histone deacetylase inhibitors (Adimoolam *et al.*, 2007; Rosato *et al.*, 2008). Whether the combined effect of HR inhibition plus all these other activities caused by these molecules indeed results in a better response after TMZ treatment in glioma cells remains to be evaluated in detail, especially as some of these agents might induce alterations in cellular proliferation, an aspect that might limit the killing effect of S_N1-methylating agents. An additional important consideration for such combination therapy is the potential undesirable toxicity brought about by the systemic concomitant modulation of HR and the targets they were originally designed for, as it might exacerbate the dose limiting toxicity of these agents.

This study (see also Quiros *et al.* (2011)) provides proof of principle evidence that RNAi targeting the HR pathway is a reasonable strategy for increasing O^6-alkylating agent efficacy, which may prove beneficial for patients treated with these groups of agents. Among the alternatives discussed (RNAi, aptamers, inhibitors), both nucleic acid aptamers and RNAi have the potential of targeting the GBM tissue by neurotrophic and cancer-targeting approaches, as those described above in this section. This is important to note since systemic administration of any of these substances might contribute to increased side effects.

The data is also in accordance with previous reports indicating a mild IR sensitivity in HR impaired cells, as compared to cross-linkers and alkylating agents (Godthelp *et al.*, 2002). The results also give support to previous observations indicating a minor role of NHEJ in the repair of O^6MeG-triggered DSB (Fig. 29) (Roos *et al.*, 2009). Even though NHEJ inhibition does not seems to play a significant role in the repair of O^6MeG-derived DSB, this data corroborates its role in the repair of IR-derived lesions. In this sense, NHEJ inhibitors could be of benefit following ionizing irradiation, as is the case of the standard of care of GBM patients, specially if administered around the days the patients receive radiotherapy.

Finally, the data also indicates a potential use for PARP inhibitors to further enhance TMZ-induced toxicity in glioma cells down-regulated for HR (Fig. 30). In the wake of the initial observations of

synthetic lethality triggered by PARP inhibition in BRCA deficient cells (Bryant *et al.*, 2005; Farmer *et al.*, 2005), the use of PARP inhibitors as monotherapy has been exploited in BRCA deficient ovarian and breast cancer, where positive results from clinical trial are starting to be reported (Fong *et al.*, 2009; Audeh *et al.*, 2010; Tutt *et al.*, 2010). The applicability of PARP inhibition concomitant with TMZ treatment has also been shown at pre-clinical level (Curtin *et al.*, 2004; Cheng *et al.*, 2005; Liu *et al.*, 2008; Horton *et al.*, 2009), and this combinatorial approach finds itself in phase I clinical trials for several malignancies (including acute leukemia, metastatic melanoma, metastatic prostate cancer, breast cancer, ovarian cancer, CNS tumors and other advanced solid tumors), as well as phase II for GBM, breast cancer, hepatocellular carcinoma and colorectal cancer (http://clinicaltrials.gov) (Mangerich & Bürkle, 2011). To my knowledge, our data shows for the first time (see also Quiros *et al.* (2011)) that a combinatorial approach of TMZ plus HR and PARP inhibition would optimize S_N1-alkylating agent-induced cell kill, as both the processing of O^6MeG and the misrepair of N-alkylations would lead to SSBs formation, collapse of replication forks upon DNA replication and DSB formation, which could not be repaired given the inhibition of HR. As discussed above, a proper tumor targeting strategy might be fundamental for optimizing the therapeutic index of this approach. Future work is intended in this direction.

5. Summary

Summary

Chemotherapeutic S_N1-methylating agents are important anticancer drugs widely used for the treatment of different cancers. S_N1-methylating agents induce several covalent modifications in the DNA, from which O^6-methylguanine (O^6MeG) is the main toxic lesion. Different hypotheses have been proposed to explain the mechanism of O^6MeG-triggered cell death, each of them predicting the cellular events triggered by O^6MeG to occur in different phases of the cell cycle, and in different cell cycles after treatment. In this work, these hypotheses were tested by making use of synchronized cells.

The results of this work provides evidence that support the abortive processing model, which states that abortive post-replicative processing of O^6MeG-driven mispairs by the DNA mismatch repair (MMR) machinery results in single-strand gaps in the DNA that, upon a 2nd round of DNA replication, leads to collapsed replication forks, DNA double-strand break (DSB) formation, G_2 checkpoint activation and cell death. In this work, it was shown that O^6MeG induces a delay in the progression of cells through the 2nd S-phase and an accumulation of cells in the 2nd G2/M-phase after treatment. This was accompanied by an increase in DSB formation in the 2nd S/G2/M-phase, and paralleled by activation of the checkpoint kinases ATR and CHK1. While apoptosis was also activated in the 2nd cell cycle, apoptosis induction was still detected several days after treatment. It is shown that a portion of cells continue proliferating past the 2nd cell cycle, and triggers apoptosis in the subsequent generations. An extension to the original model is therefore proposed, where the persistence of O^6MeG in the DNA causes new abortive MMR processing and single-strand gap formation in the 2nd and subsequent generations, where new DSB are produced triggering the toxic response. Interestingly, removal of O^6MeG at time points where treated cells are beyond the 2nd generation lead to a significant, but not complete, reduction in apoptosis, pointing to the involvement of mechanisms other than the persistent processing of O^6MeG as a cause of apoptosis induction at late time points. We therefore propose that an increase in genomic instability resulting from accumulation of mis-repaired DNA damage plays a role in cell death induction.

The fact that O^6MeG triggers toxicity several generations after treatment has important clinical implications. First, after S_N1-methylating agents based chemotherapy, a therapeutic effect is not expected to occur immediately. Second, for those tumors expressing O^6-methylguanine-DNA methyltransferase (MGMT), the effectiveness of chemotherapy will depend on long lasting MGMT inhibition. Cancer cells treated with S_N1-methylating agents like temozolomide, whose MGMT activity recovers after transient inhibition, could potentially correct the lesion and survive.

Given the central role of DSB formation in toxicity triggered by chemotherapeutic S_N1-methylating agents, it was aimed in the second part of this thesis to determine whether inhibition of DSB repair by homologous recombination (HR) or non-homologous end joining (NHEJ) is a reasonable strategy for sensitizing glioblastoma cells to O^6-alkylating agents.

The results of this work show that HR down-regulation in glioblastoma cells impairs the repair of temozolomide (TMZ)-induced DSB. HR down-regulation greatly sensitizes cells to cell death following O^6-methylating (TMZ) or O^6-chlorethylating (nimustine) treatment, but not following irradiation with ionizing radiation. The RNAi mediated inhibition in DSB repair and chemo-sensitization was proportional to the knockdown of the HR protein RAD51. Chemo-sensitization was demonstrated for several key HR proteins (RAD51, BRCA2, XRCC2), in glioma cell lines proficient (LN-229 and U87MG) and mutated (T98G) in p53. Similar to their non-knocked-down counterparts, HR down-regulated glioblastoma cells died mainly by apoptosis, indicating that the knockdown of HR proteins has no impact on death pathway selection. Evidence is also provided showing that O^6MeG is the primary lesion responsible for the increased sensitivity of glioblastoma cells following TMZ treatment, and that inhibition of the resistance marker MGMT is a feasible strategy for restoring the chemo-sensitization achieved by HR down-regulation. Data are also provided to show that inhibition of DNA-PK dependent NHEJ does not significantly sensitized glioblastoma cells to TMZ treatment. Finally, the data also show that PARP inhibition with olaparib additionally sensitized HR down-regulated glioma cells to TMZ.

Collectively, the data show that processing of O^6MeG through two rounds of DNA replication is required for DSB formation, checkpoint activation and apoptosis induction, and that O^6MeG-triggered apoptosis is also executed in subsequent generations. Furthermore, the data provide proof of principle evidence that down-regulation of HR is a reasonable strategy for sensitizing glioma cells to killing by O^6-alkylating chemotherapeutics.

6. References

References

Abbott PJ, Saffhill R. DNA synthesis with methylated poly(dC-dG) templates. Evidence for a competitive nature to miscoding by O(6)-methylguanine. Biochim Biophys Acta. 1979; 562:51-61.

Adimoolam S, Sirisawad M, Chen J, Thiemann P, Ford JM, Buggy JJ. HDAC inhibitor PCI-24781 decreases RAD51 expression and inhibits homologous recombination. Proc Natl Acad Sci U S A. 2007; 104:19482-19487.

Altschul SF, Gish W, Miller W, Myers EW, Lipman DJ. Basic local alignment search tool. J Mol Biol. 1990; 215:403-410.

Ambrosini G, Seelman SL, Qin L, Schwartz GK. The cyclin-dependent kinase inhibitor flavopiridol potentiates the effects of topoisomerase I poisons by suppressing Rad51 expression in a p53-dependent manner. Cancer Res. 2008; 68:2312-2320.

American Cancer Society. Cancer Facts & Figures 2009.

Andersen PL, Xu F, Xiao W. Eukaryotic DNA damage tolerance and translesion synthesis through covalent modifications of PCNA. Cell Res. 2008; 18:162-173.

Audeh MW, Carmichael J, Penson RT, Friedlander M, Powell B, Bell-McGuinn KM, Scott C, Weitzel JN, Oaknin A, Loman N, Lu K, Schmutzler RK, Matulonis U, Wickens M, Tutt A. Oral poly(ADP-ribose) polymerase inhibitor olaparib in patients with BRCA1 or BRCA2 mutations and recurrent ovarian cancer: a proof-of-concept trial. Lancet. 2010; 376:245-251.

Baker SD, Wirth M, Statkevich P, Reidenberg P, Alton K, Sartorius SE, Dugan M, Cutler D, Batra V, Grochow LB, Donehower RC, Rowinsky EK. Absorption, metabolism, and excretion of 14C-temozolomide following oral administration to patients with advanced cancer. Clin Cancer Res. 1999; 5:309-317.

Baute J, Depicker A. Base excision repair and its role in maintaining genome stability. Crit Rev Biochem Mol Biol. 2008; 43:239-276.

Becker K, Dosch J, Gregel CM, Martin BA, Kaina B. Targeted expression of human O(6)-methylguanine-DNA methyltransferase (MGMT) in transgenic mice protects against tumor initiation in two-stage skin carcinogenesis. Cancer Res. 1996; 56:3244-3249.

Becker K, Gregel CM, Kaina B. The DNA repair protein O6-methylguanine-DNA methyltransferase protects against skin tumor formation induced by antineoplastic chloroethylnitrosourea. Cancer Res. 1997; 57:3335-3338.

Becker K, Gregel C, Fricke C, Komitowski D, Dosch J, Kaina B. DNA repair protein MGMT protects against N-methyl-N-nitrosourea-induced conversion of benign into malignant tumors. Carcinogenesis. 2003; 24:541-546.

Beisker W, Weller-Mewe EM, Nüsse M. Fluorescence enhancement of DNA-bound TO-PRO-3 by incorporation of bromodeoxyuridine to monitor cell cycle kinetics. Cytometry. 1999; 37:221-229.

Beranek DT. Distribution of methyl and ethyl adducts following alkylation with monofunctional alkylating agents. Mutat Res. 1990; 231:11-30.

Biard DSF. Untangling the relationships between DNA repair pathways by silencing more than 20 DNA repair genes in human stable clones. Nucleic Acids Res. 2007; 35:3535-3550.

Birnboim HC, Doly J. A rapid alkaline extraction procedure for screening recombinant plasmid DNA. Nucleic Acids Res. 1979; 7:1513-1523.

Boudreau RL, Davidson BL. RNAi therapeutics for CNS disorders. Brain Res. 2010; 1338:112-121.

Boudreau RL, Rodríguez-Lebrón E, Davidson BL. RNAi medicine for the brain: progresses and challenges. Hum Mol Genet. 2011; 20:R21-7.

Bowers WJ, Breakefield XO, Sena-Esteves M. Genetic therapy for the nervous system. Hum Mol Genet. 2011; 20:R28-41.

Bradford MM. A rapid and sensitive method for the quantitation of microgram quantities of protein utilizing the principle of protein-dye binding. Anal Biochem. 1976; 72:248-254.

Branch P, Aquilina G, Bignami M, Karran P. Defective mismatch binding and a mutator phenotype in cells tolerant to DNA damage. Nature. 1993; 362:652-654.

Briegert M, Enk AH, Kaina B. Change in expression of MGMT during maturation of human monocytes into dendritic cells. DNA Repair (Amst). 2007; 6:1255-1263.

Briegert M, Kaina B. Human monocytes, but not dendritic cells derived from them, are defective in base excision repair and hypersensitive to methylating agents. Cancer Res. 2007; 67:26-31.

Bronstein SM, Hooth MJ, Swenberg JA, Skopek TR. Modulation of ethylnitrosourea-induced toxicity and mutagenicity in human cells by O6-benzylguanine. Cancer Res. 1992a; 52:3851-3856.

Bronstein SM, Skopek TR, Swenberg JA. Efficient repair of O6-ethylguanine, but not O4-ethylthymine or O2-ethylthymine, is dependent upon O6-alkylguanine-DNA alkyltransferase and nucleotide excision repair activities in human cells. Cancer Res. 1992b; 52:2008-2011.

Brummelkamp TR, Bernards R, Agami R. A system for stable expression of short interfering RNAs in mammalian cells. Science. 2002; 296:550-553.

Bryant HE, Schultz N, Thomas HD, Parker KM, Flower D, Lopez E, Kyle S, Meuth M, Curtin NJ, Helleday T. Specific killing of BRCA2-deficient tumours with inhibitors of poly(ADP-ribose) polymerase. Nature. 2005; 434:913-917.

Buck D, Malivert L, de Chasseval R, Barraud A, Fondanèche M, Sanal O, Plebani A, Stéphan J, Hufnagel M, le Deist F, Fischer A, Durandy A, de Villartay J, Revy P. Cernunnos, a novel nonhomologous end-joining factor, is mutated in human immunodeficiency with microcephaly. Cell. 2006; 124:287-299.

Cahill DP, Levine KK, Betensky RA, Codd PJ, Romany CA, Reavie LB, Batchelor TT, Futreal PA, Stratton MR, Curry WT, Iafrate AJ, Louis DN. Loss of the mismatch repair protein MSH6 in human glioblastomas is associated with tumor progression during temozolomide treatment. Clin Cancer Res. 2007; 13:2038-2045.

Campisi J. Cellular senescence: putting the paradoxes in perspective. Curr Opin Genet Dev. 2011; 21:107-112.

Caporali S, Falcinelli S, Starace G, Russo MT, Bonmassar E, Jiricny J, D'Atri S. DNA damage induced by temozolomide signals to both ATM and ATR: role of the mismatch repair system. Mol Pharmacol. 2004; 66:478-491.

Carethers JM, Hawn MT, Chauhan DP, Luce MC, Marra G, Koi M, Boland CR. Competency in mismatch repair prohibits clonal expansion of cancer cells treated with N-methyl-N'-nitro-N-nitrosoguanidine. J Clin Invest. 1996; 98:199-206.

Castanotto D, Rossi JJ. The promises and pitfalls of RNA-interference-based therapeutics. Nature. 2009; 457:426-433.

Ceccotti S, Aquilina G, Macpherson P, Yamada M, Karran P, Bignami M. Processing of O6-methylguanine by mismatch correction in human cell extracts. Curr Biol. 1996; 6:1528-1531.

Cheng CL, Johnson SP, Keir ST, Quinn JA, Ali-Osman F, Szabo C, Li H, Salzman AL, Dolan ME, Modrich P, Bigner DD, Friedman HS. Poly(ADP-ribose) polymerase-1 inhibition reverses temozolomide resistance in a DNA mismatch repair-deficient malignant glioma xenograft. Mol Cancer Ther. 2005; 4:1364-1368.

Choudhury A, Zhao H, Jalali F, Al Rashid S, Ran J, Supiot S, Kiltie AE, Bristow RG. Targeting homologous recombination using imatinib results in enhanced tumor cell chemosensitivity and radiosensitivity. Mol Cancer Ther. 2009; 8:203-213.

Christmann M, Kaina B. O(6)-methylguanine-DNA methyltransferase (MGMT): impact on cancer risk in response to tobacco smoke. Mutat Res. 2011; doi:10.1016/j.mrfmmm.2011.06.004.

Christmann M, Nagel G, Horn S, Krahn U, Wiewrodt D, Sommer C, Kaina B. MGMT activity, promoter methylation and immunohistochemistry of pretreatment and recurrent malignant gliomas: a comparative study on astrocytoma and glioblastoma. Int J Cancer. 2010; 127:2106-2118.

Christmann M, Verbeek B, Roos WP, Kaina B. O(6)-Methylguanine-DNA methyltransferase (MGMT) in normal tissues and tumors: Enzyme activity, promoter methylation and immunohistochemistry. Biochim Biophys Acta. 2011; 1816:179-190.

Citron M, White A, Decker R, Wasserman P, Li B, Randall T, Guerra D, Belanich M, Yarosh D. O6-methylguanine-DNA methyltransferase in human brain tumors detected by activity assay and monoclonal antibodies. Oncol Res. 1995; 7:49-55.

Clémenson C, Marsolier-Kergoat M. DNA damage checkpoint inactivation: adaptation and recovery. DNA Repair (Amst). 2009; 8:1101-1109.

Coquerelle T, Dosch J, Kaina B. Overexpression of N-methylpurine-DNA glycosylase in Chinese hamster ovary cells renders them more sensitive to the production of chromosomal aberrations by methylating agents--a case of imbalanced DNA repair. Mutat Res. 1995; 336:9-17.

Costello JF, Futscher BW, Kroes RA, Pieper RO. Methylation-related chromatin structure is associated with exclusion of transcription factors from and suppressed expression of the O-6-methylguanine DNA methyltransferase gene in human glioma cell lines. Mol Cell Biol. 1994a; 14:6515-6521.

Costello JF, Futscher BW, Tano K, Graunke DM, Pieper RO. Graded methylation in the promoter and body of the O6-methylguanine DNA methyltransferase (MGMT) gene correlates with MGMT expression in human glioma cells. J Biol Chem. 1994b; 269:17228-17237.

Coulondre C, Miller JH. Genetic studies of the lac repressor. IV. Mutagenic specificity in the lacI gene of Escherichia coli. J Mol Biol. 1977; 117:577-606.

Curtin NJ, Wang L, Yiakouvaki A, Kyle S, Arris CA, Canan-Koch S, Webber SE, Durkacz BW, Calvert HA, Hostomsky Z, Newell DR. Novel poly(ADP-ribose) polymerase-1 inhibitor, AG14361, restores sensitivity to temozolomide in mismatch repair-deficient cells. Clin Cancer Res. 2004; 10:881-889.

Davis ME, Zuckerman JE, Choi CHJ, Seligson D, Tolcher A, Alabi CA, Yen Y, Heidel JD, Ribas A. Evidence of RNAi in humans from systemically administered siRNA via targeted nanoparticles. Nature. 2010; 464:1067-1070.

Day RS3, Ziolkowski CH, Scudiero DA, Meyer SA, Lubiniecki AS, Girardi AJ, Galloway SM, Bynum GD. Defective repair of alkylated DNA by human tumour and SV40-transformed human cell strains. Nature. 1980; 288:724-727.

de Villartay J, Fischer A, Durandy A. The mechanisms of immune diversification and their disorders. Nat Rev Immunol. 2003; 3:962-972.

de Wind N, Dekker M, Berns A, Radman M, te Riele H. Inactivation of the mouse Msh2 gene results in mismatch repair deficiency, methylation tolerance, hyperrecombination, and predisposition to cancer. Cell. 1995; 82:321-330.

Deckbar D, Birraux J, Krempler A, Tchouandong L, Beucher A, Walker S, Stiff T, Jeggo P, Löbrich M. Chromosome breakage after G2 checkpoint release. J Cell Biol. 2007; 176:749-755.

Denny BJ, Wheelhouse RT, Stevens MF, Tsang LL, Slack JA. NMR and molecular modeling investigation of the mechanism of activation of the antitumor drug temozolomide and its interaction with DNA. Biochemistry. 1994; 33:9045-9051.

Dolan ME, Moschel RC, Pegg AE. Depletion of mammalian O6-alkylguanine-DNA alkyltransferase activity by O6-benzylguanine provides a means to evaluate the role of this protein in protection against carcinogenic and therapeutic alkylating agents. Proc Natl Acad Sci U S A. 1990; 87:5368-5372.

Dresemann G. Temozolomide in malignant glioma. Onco Targets Ther. 2010; 3:139-146.

Druker BJ, Talpaz M, Resta DJ, Peng B, Buchdunger E, Ford JM, Lydon NB, Kantarjian H, Capdeville R, Ohno-Jones S, Sawyers CL. Efficacy and safety of a specific inhibitor of the BCR-ABL tyrosine kinase in chronic myeloid leukemia. N Engl J Med. 2001; 344:1031-1037.

Duckett DR, Drummond JT, Murchie AI, Reardon JT, Sancar A, Lilley DM, Modrich P. Human MutSalpha recognizes damaged DNA base pairs containing O6-methylguanine, O4-methylthymine, or the cisplatin-d(GpG) adduct. Proc Natl Acad Sci U S A. 1996; 93:6443-6447.

Dumenco LL, Allay E, Norton K, Gerson SL. The prevention of thymic lymphomas in transgenic mice by human O6-alkylguanine-DNA alkyltransferase. Science. 1993; 259:219-222.

Duncan T, Trewick SC, Koivisto P, Bates PA, Lindahl T, Sedgwick B. Reversal of DNA alkylation damage by two human dioxygenases. Proc Natl Acad Sci U S A. 2002; 99:16660-16665.

Eadie JS, Conrad M, Toorchen D, Topal MD. Mechanism of mutagenesis by O6-methylguanine. Nature. 1984; 308:201-203.

Eker APM, Quayle C, Chaves I, van der Horst GTJ. DNA repair in mammalian cells: Direct DNA damage reversal: elegant solutions for nasty problems. Cell Mol Life Sci. 2009; 66:968-980.

Engelward BP, Dreslin A, Christensen J, Huszar D, Kurahara C, Samson L. Repair-deficient 3-methyladenine DNA glycosylase homozygous mutant mouse cells have increased sensitivity to alkylation-induced chromosome damage and cell killing. EMBO J. 1996; 15:945-952.

Esteller M, Sanchez-Cespedes M, Rosell R, Sidransky D, Baylin SB, Herman JG. Detection of aberrant promoter hypermethylation of tumor suppressor genes in serum DNA from non-small cell lung cancer patients. Cancer Res. 1999; 59:67-70.

Fan S, Meng Q, Auborn K, Carter T, Rosen EM. BRCA1 and BRCA2 as molecular targets for phytochemicals indole-3-carbinol and genistein in breast and prostate cancer cells. Br J Cancer. 2006; 94:407-426.

Farmer H, McCabe N, Lord CJ, Tutt ANJ, Johnson DA, Richardson TB, Santarosa M, Dillon KJ, Hickson I, Knights C, Martin NMB, Jackson SP, Smith GCM, Ashworth A. Targeting the DNA repair defect in BRCA mutant cells as a therapeutic strategy. Nature. 2005; 434:917-921.

Ferlay J, Shin HR, Bray F, Forman D, Mathers C, Parkin DM. GLOBOCAN 2008 v1.2, Cancer Incidence and Mortality Worldwide: IARC CancerBase No. 10 [http://globocan.iarc.fr]. Lyon, France: International Agency for Research on Cancer; 2010. Retrieved in December, 2011.

Fischhaber PL, Gall AS, Duncan JA, Hopkins PB. Direct demonstration in synthetic oligonucleotides that N,N'-bis(2-chloroethyl)-nitrosourea cross links N1 of deoxyguanosine to N3 of deoxycytidine on opposite strands of duplex DNA. Cancer Res. 1999; 59:4363-4368.

Fishel R. Mismatch repair, molecular switches, and signal transduction. Genes Dev. 1998; 12:2096-2101.

Fong PC, Boss DS, Yap TA, Tutt A, Wu P, Mergui-Roelvink M, Mortimer P, Swaisland H, Lau A, O'Connor MJ, Ashworth A, Carmichael J, Kaye SB, Schellens JHM, de Bono JS. Inhibition of poly(ADP-ribose) polymerase in tumors from BRCA mutation carriers. N Engl J Med. 2009; 361:123-134.

Fousteri M, Mullenders LHF. Transcription-coupled nucleotide excision repair in mammalian cells: molecular mechanisms and biological effects. Cell Res. 2008; 18:73-84.

Fox M, Brennand J, Margison GP. Protection of Chinese hamster cells against the cytotoxic and mutagenic effects of alkylating agents by transfection of the Escherichia coli alkyltransferase gene and a truncated derivative. Mutagenesis. 1987; 2:491-496.

Fox M, Margison GP. Expression of an E.coli O6-alkylguanine DNA alkyltransferase gene in Chinese hamster cells protects against N-methyl and N-ethylnitrosourea induced reverse mutation at the hypoxanthine phosphoribosyl transferase locus. Mutagenesis. 1988; 3:409-413.

Freire R, van Vugt MATM, Mamely I, Medema RH. Claspin: timing the cell cycle arrest when the genome is damaged. Cell Cycle. 2006; 5:2831-2834.

Furnari FB, Fenton T, Bachoo RM, Mukasa A, Stommel JM, Stegh A, Hahn WC, Ligon KL, Louis DN, Brennan C, Chin L, DePinho RA, Cavenee WK. Malignant astrocytic glioma: genetics, biology, and paths to treatment. Genes Dev. 2007; 21:2683-2710.

Galloway SM, Greenwood SK, Hill RB, Bradt CI, Bean CL. A role for mismatch repair in production of chromosome aberrations by methylating agents in human cells. Mutat Res. 1995; 346:231-245.

Galluzzi L, Vitale I, Abrams JM, Alnemri ES, Baehrecke EH, Blagosklonny MV, Dawson TM, Dawson VL, El-Deiry WS, Fulda S, Gottlieb E, Green DR, Hengartner MO, Kepp O, Knight RA, Kumar S, Lipton SA, Lu X, Madeo F, Malorni W, Mehlen P, Nuñez G, Peter ME, Piacentini M, Rubinsztein DC, Shi Y, Simon H, Vandenabeele P, White E, Yuan J, Zhivotovsky B, Melino G, Kroemer G. Molecular definitions of cell death subroutines: recommendations of the Nomenclature Committee on Cell Death 2012. Cell Death Differ. 2012; 19:107-120.

Gan GN, Wittschieben JP, Wittschieben BØ, Wood RD. DNA polymerase zeta (pol zeta) in higher eukaryotes. Cell Res. 2008; 18:174-183.

Godthelp BC, Wiegant WW, van Duijn-Goedhart A, Schärer OD, van Buul PPW, Kanaar R, Zdzienicka MZ. Mammalian Rad51C contributes to DNA cross-link resistance, sister chromatid cohesion and genomic stability. Nucleic Acids Res. 2002; 30:2172-2182.

Goldmacher VS, Cuzick RAJ, Thilly WG. Isolation and partial characterization of human cell mutants differing in sensitivity to killing and mutation by methylnitrosourea and N-methyl-N'-nitro-N-nitrosoguanidine. J Biol Chem. 1986; 261:12462-12471.

Gondi CS, Lakka SS, Dinh DH, Olivero WC, Gujrati M, Rao JS. RNAi-mediated inhibition of cathepsin B and uPAR leads to decreased cell invasion, angiogenesis and tumor growth in gliomas. Oncogene. 2004; 23:8486-8496.

Goodman LS, Wintrobe MM, Dameshek W, Goodman MJ, Gilman A, McLennan MT. Nitrogen mustard therapy; use of methyl-bis (beta-chloroethyl) amine hydrochloride and tris (beta-chloroethyl) amine hydrochloride for Hodgkin's disease, lymphosarcoma, leukemia and certain allied and miscellaneous disorders. J Am Med Assoc. 1946; 132:126-132.

Goosen N. Scanning the DNA for damage by the nucleotide excision repair machinery. DNA Repair (Amst). 2010; 9:593-596.

Gribble GW. The diversity of naturally produced organohalogens. Chemosphere. 2003; 52:289-297.

Hammond LA, Eckardt JR, Baker SD, Eckhardt SG, Dugan M, Forral K, Reidenberg P, Statkevich P, Weiss GR, Rinaldi DA, Von Hoff DD, Rowinsky EK. Phase I and pharmacokinetic study of temozolomide on a daily-for-5-days schedule in patients with advanced solid malignancies. J Clin Oncol. 1999; 17:2604-2613.

Hampson R, Humbert O, Macpherson P, Aquilina G, Karran P. Mismatch repair defects and O6-methylguanine-DNA methyltransferase expression in acquired resistance to methylating agents in human cells. J Biol Chem. 1997; 272:28596-28606.

Hegde ML, Hazra TK, Mitra S. Early steps in the DNA base excision/single-strand interruption repair pathway in mammalian cells. Cell Res. 2008; 18:27-47.

Hegi ME, Diserens A, Gorlia T, Hamou M, de Tribolet N, Weller M, Kros JM, Hainfellner JA, Mason W, Mariani L, Bromberg JEC, Hau P, Mirimanoff RO, Cairncross JG, Janzer RC, Stupp R. MGMT gene silencing and benefit from temozolomide in glioblastoma. N Engl J Med. 2005; 352:997-1003.

Herman JG, Graff JR, Myöhänen S, Nelkin BD, Baylin SB. Methylation-specific PCR: a novel PCR assay for methylation status of CpG islands. Proc Natl Acad Sci U S A. 1996; 93:9821-9826.

Heyer W, Ehmsen KT, Liu J. Regulation of homologous recombination in eukaryotes. Annu Rev Genet. 2010; 44:113-139.

Hickman MJ, Samson LD. Role of DNA mismatch repair and p53 in signaling induction of apoptosis by alkylating agents. Proc Natl Acad Sci U S A. 1999; 96:10764-10769.

Hinsdale I. CBTRUS Statistical Report: Primary Brain and Central Nervous System Tumors Diagnosed in the United States in 2004-2007. February 2011.

Horton JK, Watson M, Stefanick DF, Shaughnessy DT, Taylor JA, Wilson SH. XRCC1 and DNA polymerase beta in cellular protection against cytotoxic DNA single-strand breaks. Cell Res. 2008; 18:48-63.

Horton TM, Jenkins G, Pati D, Zhang L, Dolan ME, Ribes-Zamora A, Bertuch AA, Blaney SM, Delaney SL, Hegde M, Berg SL. Poly(ADP-ribose) polymerase inhibitor ABT-888 potentiates the cytotoxic activity of temozolomide in leukemia cells: influence of mismatch repair status and O6-methylguanine-DNA methyltransferase activity. Mol Cancer Ther. 2009; 8:2232-2242.

Hotchkiss RS, Strasser A, McDunn JE, Swanson PE. Cell death. N Engl J Med. 2009; 361:1570-1583.

Hsieh P, Yamane K. DNA mismatch repair: molecular mechanism, cancer, and ageing. Mech Ageing Dev. 2008; 129:391-407.

Hunter C, Smith R, Cahill DP, Stephens P, Stevens C, Teague J, Greenman C, Edkins S, Bignell G, Davies H, O'Meara S, Parker A, Avis T, Barthorpe S, Brackenbury L, Buck G, Butler A, Clements J, Cole J, Dicks E, Forbes S, Gorton M, Gray K, Halliday K, Harrison R, Hills K, Hinton J, Jenkinson A, Jones D, Kosmidou V, Laman R, Lugg R, Menzies A, Perry J, Petty R, Raine K, Richardson D, Shepherd R, Small A, Solomon H, Tofts C, Varian J, West S, Widaa S, Yates A, Easton DF, Riggins G, Roy JE, Levine KK, Mueller W, Batchelor TT, Louis DN, Stratton MR, Futreal PA, Wooster R. A hypermutation phenotype and somatic MSH6 mutations in recurrent human malignant gliomas after alkylator chemotherapy. Cancer Res. 2006; 66:3987-3991.

Hurley LH. DNA and its associated processes as targets for cancer therapy. Nat Rev Cancer. 2002; 2:188-200.

IARC. International Agency for Research in Cancer Monographs on the Evaluation of Carcinogenic Risks to Humans: Smokeless Tobacco and Some Tobacco-specific N-Nitrosamines. 2007; v89.

Jackman J, O'Connor PM. Methods for synchronizing cells at specific stages of the cell cycle. Curr Protoc Cell Biol. 2001; Chapter 8:Unit 8.3.

Jensen RB, Carreira A, Kowalczykowski SC. Purified human BRCA2 stimulates RAD51-mediated recombination. Nature. 2010; 467:678-683.

Kaina B. Mechanisms and consequences of methylating agent-induced SCEs and chromosomal aberrations: a long road traveled and still a far way to go. Cytogenet Genome Res. 2004; 104:77-86.

Kaina B, Aurich O. Dependency of the yield of sister-chromatid exchanges induced by alkylating agents on fixation time. Possible involvement of secondary lesions in sister-chromatid exchange induction. Mutat Res. 1985; 149:451-461.

Kaina B, Fritz G, Mitra S, Coquerelle T. Transfection and expression of human O6-methylguanine-DNA methyltransferase (MGMT) cDNA in Chinese hamster cells: the role of MGMT in protection against the genotoxic effects of alkylating agents. Carcinogenesis. 1991; 12:1857-1867.

Kaina B, Ziouta A, Ochs K, Coquerelle T. Chromosomal instability, reproductive cell death and apoptosis induced by O6-methylguanine in Mex-, Mex+ and methylation-tolerant mismatch repair compromised cells: facts and models. Mutat Res. 1997; 381:227-241.

Kaina B, Mühlhausen U, Piee-Staffa A, Christmann M, Garcia Boy R, Rösch F, Schirrmacher R. Inhibition of O6-methylguanine-DNA methyltransferase by glucose-conjugated inhibitors: comparison with nonconjugated inhibitors and effect on fotemustine and temozolomide-induced cell death. J Pharmacol Exp Ther. 2004; 311:585-593.

Kaina B, Christmann M, Naumann S, Roos WP. MGMT: key node in the battle against genotoxicity, carcinogenicity and apoptosis induced by alkylating agents. DNA Repair (Amst). 2007; 6:1079-1099.

Kaina B, Margison GP, Christmann M. Targeting O^6-methylguanine-DNA methyltransferase with specific inhibitors as a strategy in cancer therapy. Cell Mol Life Sci. 2010; 67:3663-3681.

Karran P, Bignami M. DNA damage tolerance, mismatch repair and genome instability. Bioessays. 1994; 16:833-839.

Kat A, Thilly WG, Fang WH, Longley MJ, Li GM, Modrich P. An alkylation-tolerant, mutator human cell line is deficient in strand-specific mismatch repair. Proc Natl Acad Sci U S A. 1993; 90:6424-6428.

Kerr JF, Wyllie AH, Currie AR. Apoptosis: a basic biological phenomenon with wide-ranging implications in tissue kinetics. Br J Cancer. 1972; 26:239-257.

Ko J, Ciou S, Cheng C, Wang L, Hong J, Jheng M, Ling S, Lin Y. Involvement of Rad51 in cytotoxicity induced by epidermal growth factor receptor inhibitor (gefitinib, IressaR) and chemotherapeutic agents in human lung cancer cells. Carcinogenesis. 2008a; 29:1448-1458.

Ko J, Hong J, Wang L, Cheng C, Ciou S, Lin S, Jheng M, Lin Y. Role of repair protein Rad51 in regulating the response to gefitinib in human non-small cell lung cancer cells. Mol Cancer Ther. 2008b; 7:3632-3641.

Ko J, Ciou S, Jhan J, Cheng C, Su Y, Chuang S, Lin S, Chang C, Lin Y. Roles of MKK1/2-ERK1/2 and phosphoinositide 3-kinase-AKT signaling pathways in erlotinib-induced Rad51 suppression and cytotoxicity in human non-small cell lung cancer cells. Mol Cancer Res. 2009; 7:1378-1389.

Koch D, Hundsberger T, Boor S, Kaina B. Local intracerebral administration of O(6)-benzylguanine combined with systemic chemotherapy with temozolomide of a patient suffering from a recurrent glioblastoma. J Neurooncol. 2007; 82:85-89.

Koi M, Umar A, Chauhan DP, Cherian SP, Carethers JM, Kunkel TA, Boland CR. Human chromosome 3 corrects mismatch repair deficiency and microsatellite instability and reduces N-methyl-N'-nitro-N-nitrosoguanidine tolerance in colon tumor cells with homozygous hMLH1 mutation. Cancer Res. 1994; 54:4308-4312.

Koldehoff M, Steckel NK, Beelen DW, Elmaagacli AH. Therapeutic application of small interfering RNA directed against bcr-abl transcripts to a patient with imatinib-resistant chronic myeloid leukaemia. Clin Exp Med. 2007; 7:47-55.

Krempler A, Deckbar D, Jeggo PA, Löbrich M. An imperfect G2M checkpoint contributes to chromosome instability following irradiation of S and G2 phase cells. Cell Cycle. 2007; 6:1682-1686.

Kroemer G, Galluzzi L, Vandenabeele P, Abrams J, Alnemri ES, Baehrecke EH, Blagosklonny MV, El-Deiry WS, Golstein P, Green DR, Hengartner M, Knight RA, Kumar S, Lipton SA, Malorni W, Nuñez G, Peter ME, Tschopp J, Yuan J, Piacentini M, Zhivotovsky B, Melino G. Classification of cell death: recommendations of the Nomenclature Committee on Cell Death 2009. Cell Death Differ. 2009; 16:3-11.

Kunz C, Saito Y, Schär P. DNA Repair in mammalian cells: Mismatched repair: variations on a theme. Cell Mol Life Sci. 2009; 66:1021-1038.

Laemmli UK. Cleavage of structural proteins during the assembly of the head of bacteriophage T4. Nature. 1970; 227:680-685.

Lamarche BJ, Orazio NI, Weitzman MD. The MRN complex in double-strand break repair and telomere maintenance. FEBS Lett. 2010; 584:3682-3695.

Larson K, Sahm J, Shenkar R, Strauss B. Methylation-induced blocks to in vitro DNA replication. Mutat Res. 1985; 150:77-84.

Lehmann AR, Niimi A, Ogi T, Brown S, Sabbioneda S, Wing JF, Kannouche PL, Green CM. Translesion synthesis: Y-family polymerases and the polymerase switch. DNA Repair (Amst). 2007; 6:891-899.

Leibeling D, Laspe P, Emmert S. Nucleotide excision repair and cancer. J Mol Histol. 2006; 37:225-238.

Li G. Mechanisms and functions of DNA mismatch repair. Cell Res. 2008; 18:85-98.

Li L, Wang H, Yang ES, Arteaga CL, Xia F. Erlotinib attenuates homologous recombinational repair of chromosomal breaks in human breast cancer cells. Cancer Res. 2008; 68:9141-9146.

Li X, Heyer W. Homologous recombination in DNA repair and DNA damage tolerance. Cell Res. 2008; 18:99-113.

Lieber MR. The mechanism of double-strand DNA break repair by the nonhomologous DNA end-joining pathway. Annu Rev Biochem. 2010; 79:181-211.

Lin DP, Wang Y, Scherer SJ, Clark AB, Yang K, Avdievich E, Jin B, Werling U, Parris T, Kurihara N, Umar A, Kucherlapati R, Lipkin M, Kunkel TA, Edelmann W. An Msh2 point mutation uncouples DNA mismatch repair and apoptosis. Cancer Res. 2004; 64:517-522.

Lindahl T, Demple B, Robins P. Suicide inactivation of the E. coli O6-methylguanine-DNA methyltransferase. EMBO J. 1982; 1:1359-1363.

Lips J, Kaina B. DNA double-strand breaks trigger apoptosis in p53-deficient fibroblasts. Carcinogenesis. 2001; 22:579-585.

Liu X, Shi Y, Guan R, Donawho C, Luo Y, Palma J, Zhu G, Johnson EF, Rodriguez LE, Ghoreishi-Haack N, Jarvis K, Hradil VP, Colon-Lopez M, Cox BF, Klinghofer V, Penning T, Rosenberg SH, Frost D, Giranda VL, Luo Y. Potentiation of temozolomide cytotoxicity by poly(ADP)ribose polymerase inhibitor ABT-888 requires a conversion of single-stranded DNA damages to double-stranded DNA breaks. Mol Cancer Res. 2008; 6:1621-1629.

Löbrich M, Jeggo PA. The impact of a negligent G2/M checkpoint on genomic instability and cancer induction. Nat Rev Cancer. 2007; 7:861-869.

Loechler EL, Green CL, Essigmann JM. In vivo mutagenesis by O6-methylguanine built into a unique site in a viral genome. Proc Natl Acad Sci U S A. 1984; 81:6271-6275.

Louis D, Ohgaki H, Wiestler O, Cavenee W. WHO Classification of Tumours of the Central Nervous System, Fourth Edition. IARC (Ed.). WHO Press, 2007a.

Louis DN, Ohgaki H, Wiestler OD, Cavenee WK, Burger PC, Jouvet A, Scheithauer BW, Kleihues P. The 2007 WHO classification of tumours of the central nervous system. Acta Neuropathol. 2007b; 114:97-109.

Loveless A. Possible relevance of O-6 alkylation of deoxyguanosine to the mutagenicity and carcinogenicity of nitrosamines and nitrosamides. Nature. 1969; 223:206-207.

Lupardus PJ, Cimprich KA. Checkpoint adaptation; molecular mechanisms uncovered. Cell. 2004; 117:555-556.

Lyons AB. Analysing cell division in vivo and in vitro using flow cytometric measurement of CFSE dye dilution. J Immunol Methods. 2000; 243:147-154.

Lyons AB, Parish CR. Determination of lymphocyte division by flow cytometry. J Immunol Methods. 1994; 171:131-137.

Mahaney BL, Meek K, Lees-Miller SP. Repair of ionizing radiation-induced DNA double-strand breaks by non-homologous end-joining. Biochem J. 2009; 417:639-650.

Mandel M, Higa A. Calcium-dependent bacteriophage DNA infection. J Mol Biol. 1970; 53:159-162.

Mangerich A, Bürkle A. How to kill tumor cells with inhibitors of poly(ADP-ribosyl)ation. Int J Cancer. 2011; 128:251-265.

Margison GP, Kleihues P. Chemical carcinogenesis in the nervous system. Preferential accumulation of O6-methylguanine in rat brain deoxyribonucleic acid during repetitive administration of N-methyl-N-nitrosourea. Biochem J. 1975; 148:521-525.

Martin SA, Lord CJ, Ashworth A. Therapeutic targeting of the DNA mismatch repair pathway. Clin Cancer Res. 2010; 16:5107-5113.

Martinez SF, Renodon-Cornière A, Nomme J, Eveillard D, Fleury F, Takahashi M, Weigel P. Targeting human Rad51 by specific DNA aptamers induces inhibition of homologous recombination. Biochimie. 2010; 92:1832-1838.

Mazin AV, Mazina OM, Bugreev DV, Rossi MJ. Rad54, the motor of homologous recombination. DNA Repair (Amst). 2010; 9:286-302.

McCulloch SD, Kunkel TA. The fidelity of DNA synthesis by eukaryotic replicative and translesion synthesis polymerases. Cell Res. 2008; 18:148-161.

McElhinney RS, Donnelly DJ, McCormick JE, Kelly J, Watson AJ, Rafferty JA, Elder RH, Middleton MR, Willington MA, McMurry TB, Margison GP. Inactivation of O6-alkylguanine-DNA alkyltransferase. 1. Novel O6-(hetarylmethyl)guanines having basic rings in the side chain. J Med Chem. 1998; 41:5265-5271.

Meikrantz W, Bergom MA, Memisoglu A, Samson L. O6-alkylguanine DNA lesions trigger apoptosis. Carcinogenesis. 1998; 19:369-372.

Middleton MR, Kelly J, Thatcher N, Donnelly DJ, McElhinney RS, McMurry TB, McCormick JE, Margison GP. O(6)-(4-bromothenyl)guanine improves the therapeutic index of temozolomide against A375M melanoma xenografts. Int J Cancer. 2000; 85:248-252.

Mirimanoff R, Gorlia T, Mason W, Van den Bent MJ, Kortmann R, Fisher B, Reni M, Brandes AA, Curschmann J, Villa S, Cairncross G, Allgeier A, Lacombe D, Stupp R. Radiotherapy and temozolomide for newly diagnosed glioblastoma: recursive partitioning analysis of the EORTC 26981/22981-NCIC CE3 phase III randomized trial. J Clin Oncol. 2006; 24:2563-2569.

Mladenov E, Iliakis G. Induction and repair of DNA double strand breaks: the increasing spectrum of non-homologous end joining pathways. Mutat Res. 2011; 711:61-72.

Modrich P. Strand-specific mismatch repair in mammalian cells. J Biol Chem. 1997; 272:24727-24730.

Mojas N, Lopes M, Jiricny J. Mismatch repair-dependent processing of methylation damage gives rise to persistent single-stranded gaps in newly replicated DNA. Genes Dev. 2007; 21:3342-3355.

Moynahan ME, Jasin M. Mitotic homologous recombination maintains genomic stability and suppresses tumorigenesis. Nat Rev Mol Cell Biol. 2010; 11:196-207.

Muniandy PA, Liu J, Majumdar A, Liu S, Seidman MM. DNA interstrand crosslink repair in mammalian cells: step by step. Crit Rev Biochem Mol Biol. 2010; 45:23-49.

Myrnes B, Norstrand K, Giercksky KE, Sjunneskog C, Krokan H. A simplified assay for O6-methylguanine-DNA methyltransferase activity and its application to human neoplastic and non-neoplastic tissues. Carcinogenesis. 1984; 5:1061-1064.

Naumann SC, Roos WP, Jöst E, Belohlavek C, Lennerz V, Schmidt CW, Christmann M, Kaina B. Temozolomide- and fotemustine-induced apoptosis in human malignant melanoma cells: response related to MGMT, MMR, DSBs, and p53. Br J Cancer. 2009; 100:322-333.

Nelson ME, Loktionova NA, Pegg AE, Moschel RC. 2-amino-O4-benzylpteridine derivatives: potent inactivators of O6-alkylguanine-DNA alkyltransferase. J Med Chem. 2004; 47:3887-3891.

Nikolova T, Ensminger M, Löbrich M, Kaina B. Homologous recombination protects mammalian cells from replication-associated DNA double-strand breaks arising in response to methyl methanesulfonate. DNA Repair (Amst). 2010; 9:1050-1063.

Nouspikel T. DNA repair in mammalian cells : Nucleotide excision repair: variations on versatility. Cell Mol Life Sci. 2009; 66:994-1009.

Ochs K, Kaina B. Apoptosis induced by DNA damage O6-methylguanine is Bcl-2 and caspase-9/3 regulated and Fas/caspase-8 independent. Cancer Res. 2000; 60:5815-5824.

Pardo B, Gómez-González B, Aguilera A. DNA repair in mammalian cells: DNA double-strand break repair: how to fix a broken relationship. Cell Mol Life Sci. 2009; 66:1039-1056.

Parthasarathy R, Fridey SM. Conformation of O6-alkylguanosines: molecular mechanism of mutagenesis. Carcinogenesis. 1986; 7:221-227.

Patel M, McCully C, Godwin K, Balis FM. Plasma and cerebrospinal fluid pharmacokinetics of intravenous temozolomide in non-human primates. J Neurooncol. 2003; 61:203-207.

Pecot CV, Calin GA, Coleman RL, Lopez-Berestein G, Sood AK. RNA interference in the clinic: challenges and future directions. Nat Rev Cancer. 2011; 11:59-67.

Pegg AE, Boosalis M, Samson L, Moschel RC, Byers TL, Swenn K, Dolan ME. Mechanism of inactivation of human O6-alkylguanine-DNA alkyltransferase by O6-benzylguanine. Biochemistry. 1993; 32:11998-12006.

Petrocca F, Lieberman J. Promise and challenge of RNA interference-based therapy for cancer. J Clin Oncol. 2011; 29:747-754.

Plant JE, Roberts JJ. A novel mechanism for the inhibition of DNA synthesis following methylation: the effect of N-methyl-N-nitrosourea on HeLa cells. Chem Biol Interact. 1971; 3:337-342.

Preuss I, Thust R, Kaina B. Protective effect of O6-methylguanine-DNA methyltransferase (MGMT) on the cytotoxic and recombinogenic activity of different antineoplastic drugs. Int J Cancer. 1996; 65:506-512.

Quiros S, Roos WP, Kaina B. Processing of O6-methylguanine into DNA double-strand breaks requires two rounds of replication whereas apoptosis is also induced in subsequent cell cycles. Cell Cycle. 2010; 9:168-178.

Quiros S, Roos WP, Kaina B. Rad51 and BRCA2 - New Molecular Targets for Sensitizing Glioma Cells to Alkylating Anticancer Drugs. PLoS ONE. 2011; 6:e27183.

Rajesh P, Rajesh C, Wyatt MD, Pittman DL. RAD51D protects against MLH1-dependent cytotoxic responses to O(6)-methylguanine. DNA Repair (Amst). 2010; 9:458-467.

Ralhan R, Kaur J. Alkylating agents and cancer therapy. Expert Opin Ther Pat. 2007; 17:1061-1075.

Reinhard J, Eichhorn U, Wiessler M, Kaina B. Inactivation of O(6)-methylguanine-DNA methyltransferase by glucose-conjugated inhibitors. Int J Cancer. 2001a; 93:373-379.

Reinhard J, Hull WE, von der Lieth CW, Eichhorn U, Kliem HC, Kaina B, Wiessler M. Monosaccharide-linked inhibitors of O(6)-methylguanine-DNA methyltransferase (MGMT): synthesis, molecular modeling, and structure-activity relationships. J Med Chem. 2001b; 44:4050-4061.

Ringvoll J, Nordstrand LM, Vågbø CB, Talstad V, Reite K, Aas PA, Lauritzen KH, Liabakk NB, Bjørk A, Doughty RW, Falnes PØ, Krokan HE, Klungland A. Repair deficient mice reveal mABH2 as the primary oxidative demethylase for repairing 1meA and 3meC lesions in DNA. EMBO J. 2006; 25:2189-2198.

Robertson AB, Klungland A, Rognes T, Leiros I. DNA repair in mammalian cells: Base excision repair: the long and short of it. Cell Mol Life Sci. 2009; 66:981-993.

Rodier F, Campisi J. Four faces of cellular senescence. J Cell Biol. 2011; 192:547-556.

Rogakou EP, Pilch DR, Orr AH, Ivanova VS, Bonner WM. DNA double-stranded breaks induce histone H2AX phosphorylation on serine 139. J Biol Chem. 1998; 273:5858-5868.

Roos W, Baumgartner M, Kaina B. Apoptosis triggered by DNA damage O6-methylguanine in human lymphocytes requires DNA replication and is mediated by p53 and Fas/CD95/Apo-1. Oncogene. 2004; 23:359-367.

Roos WP, Batista LFZ, Naumann SC, Wick W, Weller M, Menck CFM, Kaina B. Apoptosis in malignant glioma cells triggered by the temozolomide-induced DNA lesion O6-methylguanine. Oncogene. 2007; 26:186-197.

Roos WP, Nikolova T, Quiros S, Naumann SC, Kiedron O, Zdzienicka MZ, Kaina B. Brca2/Xrcc2 dependent HR, but not NHEJ, is required for protection against O(6)-methylguanine triggered apoptosis, DSBs and chromosomal aberrations by a process leading to SCEs. DNA Repair (Amst). 2009; 8:72-86.

Rosato RR, Almenara JA, Maggio SC, Coe S, Atadja P, Dent P, Grant S. Role of histone deacetylase inhibitor-induced reactive oxygen species and DNA damage in LAQ-824/fludarabine antileukemic interactions. Mol Cancer Ther. 2008; 7:3285-3297.

Russell JS, Brady K, Burgan WE, Cerra MA, Oswald KA, Camphausen K, Tofilon PJ. Gleevec-mediated inhibition of Rad51 expression and enhancement of tumor cell radiosensitivity. Cancer Res. 2003; 63:7377-7383.

Rydberg B, Lindahl T. Nonenzymatic methylation of DNA by the intracellular methyl group donor S-adenosyl-L-methionine is a potentially mutagenic reaction. EMBO J. 1982; 1:211-216.

Ryken TC, Frankel B, Julien T, Olson JJ. Surgical management of newly diagnosed glioblastoma in adults: role of cytoreductive surgery. J Neurooncol. 2008; 89:271-286.

San Filippo J, Sung P, Klein H. Mechanism of eukaryotic homologous recombination. Annu Rev Biochem. 2008; 77:229-257.

Sandell LL, Zakian VA. Loss of a yeast telomere: arrest, recovery, and chromosome loss. Cell. 1993; 75:729-739.

Sandhu SK, Yap TA, de Bono JS. Poly(ADP-ribose) polymerase inhibitors in cancer treatment: a clinical perspective. Eur J Cancer. 2010; 46:9-20.

Sassanfar M, Dosanjh MK, Essigmann JM, Samson L. Relative efficiencies of the bacterial, yeast, and human DNA methyltransferases for the repair of O6-methylguanine and O4-methylthymine. Suggestive evidence for O4-methylthymine repair by eukaryotic methyltransferases. J Biol Chem. 1991; 266:2767-2771.

Scott RB. Cancer chemotherapy--the first twenty-five years. Br Med J. 1970; 4:259-265.

Sedgwick B, Bates PA, Paik J, Jacobs SC, Lindahl T. Repair of alkylated DNA: recent advances. DNA Repair (Amst). 2007; 6:429-442.

Shao C, Fu J, Shi H, Mu Y, Chen Z. Activities of DNA-PK and Ku86, but not Ku70, may predict sensitivity to cisplatin in human gliomas. J Neurooncol. 2008; 89:27-35.

Shephard SE, Lutz WK. Nitrosation of dietary precursors. Cancer Surv. 1989; 8:401-421.

Short SC, Giampieri S, Worku M, Alcaide-German M, Sioftanos G, Bourne S, Lio KI, Shaked-Rabi M, Martindale C. Rad51 inhibition is an effective means of targeting DNA repair in glioma models and CD133+ tumor-derived cells. Neuro Oncol. 2011; 13:487-499.

Shuck SC, Short EA, Turchi JJ. Eukaryotic nucleotide excision repair: from understanding mechanisms to influencing biology. Cell Res. 2008; 18:64-72.

Silber JR, Blank A, Bobola MS, Mueller BA, Kolstoe DD, Ojemann GA, Berger MS. Lack of the DNA repair protein O6-methylguanine-DNA methyltransferase in histologically normal brain adjacent to primary human brain tumors. Proc Natl Acad Sci U S A. 1996; 93:6941-6946.

Slamon DJ, Leyland-Jones B, Shak S, Fuchs H, Paton V, Bajamonde A, Fleming T, Eiermann W, Wolter J, Pegram M, Baselga J, Norton L. Use of chemotherapy plus a monoclonal antibody against HER2 for metastatic breast cancer that overexpresses HER2. N Engl J Med. 2001; 344:783-792.

Song E, Lee S, Wang J, Ince N, Ouyang N, Min J, Chen J, Shankar P, Lieberman J. RNA interference targeting Fas protects mice from fulminant hepatitis. Nat Med. 2003; 9:347-351.

Southern PJ, Berg P. Transformation of mammalian cells to antibiotic resistance with a bacterial gene under control of the SV40 early region promoter. J Mol Appl Genet. 1982; 1:327-341.

Spencer SL, Gaudet S, Albeck JG, Burke JM, Sorger PK. Non-genetic origins of cell-to-cell variability in TRAIL-induced apoptosis. Nature. 2009; 459:428-432.

Spencer SL, Sorger PK. Measuring and modeling apoptosis in single cells. Cell. 2011; 144:926-939.

Srivenugopal KS, Yuan XH, Friedman HS, Ali-Osman F. Ubiquitination-dependent proteolysis of O6-methylguanine-DNA methyltransferase in human and murine tumor cells following inactivation with O6-benzylguanine or 1,3-bis(2-chloroethyl)-1-nitrosourea. Biochemistry. 1996; 35:1328-1334.

Stojic L, Mojas N, Cejka P, Di Pietro M, Ferrari S, Marra G, Jiricny J. Mismatch repair-dependent G2 checkpoint induced by low doses of SN1 type methylating agents requires the ATR kinase. Genes Dev. 2004; 18:1331-1344.

Stupp R, Mason WP, van den Bent MJ, Weller M, Fisher B, Taphoorn MJB, Belanger K, Brandes AA, Marosi C, Bogdahn U, Curschmann J, Janzer RC, Ludwin SK, Gorlia T, Allgeier A, Lacombe D, Cairncross JG, Eisenhauer E, Mirimanoff RO, . Radiotherapy plus concomitant and adjuvant temozolomide for glioblastoma. N Engl J Med. 2005; 352:987-996.

Stupp R, Hegi ME, Gilbert MR, Chakravarti A. Chemoradiotherapy in malignant glioma: standard of care and future directions. J Clin Oncol. 2007; 25:4127-4136.

Stupp R, Hegi ME, Mason WP, van den Bent MJ, Taphoorn MJB, Janzer RC, Ludwin SK, Allgeier A, Fisher B, Belanger K, Hau P, Brandes AA, Gijtenbeek J, Marosi C, Vecht CJ, Mokhtari K, Wesseling P, Villa S, Eisenhauer E, Gorlia T, Weller M, Lacombe D, Cairncross JG, Mirimanoff R, . Effects of radiotherapy with concomitant and adjuvant temozolomide versus radiotherapy alone on survival in glioblastoma in a randomised phase III study: 5-year analysis of the EORTC-NCIC trial. Lancet Oncol. 2009; 10:459-466.

Sudo H, Tsuji AB, Sugyo A, Imai T, Saga T, Harada Y. A loss of function screen identifies nine new radiation susceptibility genes. Biochem Biophys Res Commun. 2007; 364:695-701.

Svendsen JM, Harper JW. GEN1/Yen1 and the SLX4 complex: Solutions to the problem of Holliday junction resolution. Genes Dev. 2010; 24:521-536.

Syljuåsen RG. Checkpoint adaptation in human cells. Oncogene. 2007; 26:5833-5839.

Syljuåsen RG, Jensen S, Bartek J, Lukas J. Adaptation to the ionizing radiation-induced G2 checkpoint occurs in human cells and depends on checkpoint kinase 1 and Polo-like kinase 1 kinases. Cancer Res. 2006; 66:10253-10257.

Takeda S, Nakamura K, Taniguchi Y, Paull TT. Ctp1/CtIP and the MRN complex collaborate in the initial steps of homologous recombination. Mol Cell. 2007; 28:351-352.

Toczyski DP, Galgoczy DJ, Hartwell LH. CDC5 and CKII control adaptation to the yeast DNA damage checkpoint. Cell. 1997; 90:1097-1106.

Tominaga Y, Tsuzuki T, Shiraishi A, Kawate H, Sekiguchi M. Alkylation-induced apoptosis of embryonic stem cells in which the gene for DNA-repair, methyltransferase, had been disrupted by gene targeting. Carcinogenesis. 1997; 18:889-896.

Tong WP, Kirk MC, Ludlum DB. Formation of the cross-link 1-[N3-deoxycytidyl),2-[N1-deoxyguanosinyl]ethane in DNA treated with N,N'-bis(2-chloroethyl)-N-nitrosourea. Cancer Res. 1982; 42:3102-3105.

Toorchen D, Lindamood C3, Swenberg JA, Topal MD. O6-Methylguanine-DNA transmethylase converts O6-methylguanine thymine base pairs to guanine thymine base pairs in DNA. Carcinogenesis. 1984; 5:1733-1735.

Tornaletti S. DNA repair in mammalian cells: Transcription-coupled DNA repair: directing your effort where it's most needed. Cell Mol Life Sci. 2009; 66:1010-1020.

Towbin H, Staehelin T, Gordon J. Electrophoretic transfer of proteins from polyacrylamide gels to nitrocellulose sheets: procedure and some applications. Proc Natl Acad Sci U S A. 1979; 76:4350-4354.

Tsang LL, Quarterman CP, Gescher A, Slack JA. Comparison of the cytotoxicity in vitro of temozolomide and dacarbazine, prodrugs of 3-methyl-(triazen-1-yl)imidazole-4-carboxamide. Cancer Chemother Pharmacol. 1991; 27:342-346.

Tutt A, Robson M, Garber JE, Domchek SM, Audeh MW, Weitzel JN, Friedlander M, Arun B, Loman N, Schmutzler RK, Wardley A, Mitchell G, Earl H, Wickens M, Carmichael J. Oral poly(ADP-ribose) polymerase inhibitor olaparib in patients with BRCA1 or BRCA2 mutations and advanced breast cancer: a proof-of-concept trial. Lancet. 2010; 376:235-244.

Umar A, Koi M, Risinger JI, Glaab WE, Tindall KR, Kolodner RD, Boland CR, Barrett JC, Kunkel TA. Correction of hypermutability, N-methyl-N'-nitro-N-nitrosoguanidine resistance, and defective DNA mismatch repair by introducing chromosome 2 into human tumor cells with mutations in MSH2 and MSH6. Cancer Res. 1997; 57:3949-3955.

Villano JL, Seery TE, Bressler LR. Temozolomide in malignant gliomas: current use and future targets. Cancer Chemother Pharmacol. 2009; 64:647-655.

Villano JL, Letarte N, Yu JM, Abdur S, Bressler LR. Hematologic adverse events associated with temozolomide. Cancer Chemother Pharmacol. 2011; doi 10.1007/s00280-011-1679-8.

Walker MD, Alexander EJ, Hunt WE, MacCarty CS, Mahaley MSJ, Mealey JJ, Norrell HA, Owens G, Ransohoff J, Wilson CB, Gehan EA, Strike TA. Evaluation of BCNU and/or radiotherapy in the treatment of anaplastic gliomas. A cooperative clinical trial. J Neurosurg. 1978; 49:333-343.

Wang Y, Qin J. MSH2 and ATR form a signaling module and regulate two branches of the damage response to DNA methylation. Proc Natl Acad Sci U S A. 2003; 100:15387-15392.

Weller M, Stupp R, Reifenberger G, Brandes AA, van den Bent MJ, Wick W, Hegi ME. MGMT promoter methylation in malignant gliomas: ready for personalized medicine?. Nat Rev Neurol. 2010; 6:39-51.

Welsh JW, Ellsworth RK, Kumar R, Fjerstad K, Martinez J, Nagel RB, Eschbacher J, Stea B. Rad51 protein expression and survival in patients with glioblastoma multiforme. Int J Radiat Oncol Biol Phys. 2009; 74:1251-1255.

Weterings E, Chen DJ. The endless tale of non-homologous end-joining. Cell Res. 2008; 18:114-124.

Wiewrodt D, Nagel G, Dreimüller N, Hundsberger T, Perneczky A, Kaina B. MGMT in primary and recurrent human glioblastomas after radiation and chemotherapy and comparison with p53 status and clinical outcome. Int J Cancer. 2008; 122:1391-1399.

Wirtz S, Nagel G, Eshkind L, Neurath MF, Samson LD, Kaina B. Both base excision repair and O6-methylguanine-DNA methyltransferase protect against methylation-induced colon carcinogenesis. Carcinogenesis. 2010; 31:2111-2117.

Wood RD. Mammalian nucleotide excision repair proteins and interstrand crosslink repair. Environ Mol Mutagen. 2010; 51:520-526.

Wood RD, Burki HJ. Repair capability and the cellular age response for killing and mutation induction after UV. Mutat Res. 1982; 95:505-514.

Wyatt MD, Pittman DL. Methylating agents and DNA repair responses: Methylated bases and sources of strand breaks. Chem Res Toxicol. 2006; 19:1580-1594.

Xia C, Zhang Y, Zhang Y, Boado RJ, Pardridge WM. Intravenous siRNA of brain cancer with receptor targeting and avidin-biotin technology. Pharm Res. 2007; 24:2309-2316.

Xu-Welliver M, Pegg AE. Degradation of the alkylated form of the DNA repair protein, O(6)-alkylguanine-DNA alkyltransferase. Carcinogenesis. 2002; 23:823-830.

Yang G, Scherer SJ, Shell SS, Yang K, Kim M, Lipkin M, Kucherlapati R, Kolodner RD, Edelmann W. Dominant effects of an Msh6 missense mutation on DNA repair and cancer susceptibility. Cancer Cell. 2004; 6:139-150.

Yoo HY, Kumagai A, Shevchenko A, Shevchenko A, Dunphy WG. Adaptation of a DNA replication checkpoint response depends upon inactivation of Claspin by the Polo-like kinase. Cell. 2004; 117:575-588.

Yoshioka K, Yoshioka Y, Hsieh P. ATR kinase activation mediated by MutSalpha and MutLalpha in response to cytotoxic O6-methylguanine adducts. Mol Cell. 2006; 22:501-510.

Yuan J, Kroemer G. Alternative cell death mechanisms in development and beyond. Genes Dev. 2010; 24:2592-2602.

Zarbl H, Sukumar S, Arthur AV, Martin-Zanca D, Barbacid M. Direct mutagenesis of Ha-ras-1 oncogenes by N-nitroso-N-methylurea during initiation of mammary carcinogenesis in rats. Nature. 1985; 315:382-385.

Zhang Y, Zhang Y, Bryant J, Charles A, Boado RJ, Pardridge WM. Intravenous RNA interference gene therapy targeting the human epidermal growth factor receptor prolongs survival in intracranial brain cancer. Clin Cancer Res. 2004; 10:3667-3677.

Zharkov DO. Base excision DNA repair. Cell Mol Life Sci. 2008; 65:1544-1565.

Zou L. DNA repair: A protein giant in its entirety. Nature. 2010; 467:667-668.

7. Supplementary information

7.1. Abbreviations and Symbols

Chemical compounds, elements, amino acids and nucleotides are named and abbreviated following the corresponding International Union of Pure and Applied Chemistry (IUPAC) nomenclature, and are omitted from the list below. Amino acids and nucleotides are abbreviated making use of the one letter code.

Symbols for base and derived units of measurement are according to the International System of Units (SI), and are omitted from the list below. Temperature is expressed in Celsius (°C). Other non SI units officially accepted for use with the SI (namely Da, l, M, min, h) are indicated below.

All human proteins are annotated with their official names and symbols. In case of alternative names used by the scientific community far much more widespread than the official name, the abbreviation for the preferred alternative name is utilized, but the official full name and abbreviation are also given below.

Abbreviation	**Full name**
1st	First
2nd	Second
3rd	Third
^{3}H	Tritium
^{32}P	Phosphorus-32
4th	Fourth
5'-dRP	5'-deoxyribose phosphate
[γ-^{32}P]ATP	Adenosine triphosphate radiolabeled with Phosphorus-32 in its gamma phosphate
γH2A.X	Histone H2A.X phosphorylated on S139
$\Delta\psi_m$	Mitochondrial transmembrane potential
a.k.a.	Also known as
ACNU	Nimustine: 3-[(4-amino-2-methylpyrimidin-5-yl)methyl]-1-(2-chloroethyl)-1-nitrosourea hydrochloride
ADP	Adenosine diphosphate
AIF	Apoptosis-inducing factor, mitochondrion-associated, 1 (**AIFM1**). *a.k.a.* Apoptosis-inducing factor (*AIF, preferred name*)

ALKBH2 alkB, alkylation repair homolog 2 (*Escherichia coli*).
a.k.a. Alpha-ketoglutarate-dependent dioxygenase alkB homolog 2 (ABH2)

ALKBH3 alkB, alkylation repair homolog 3 (*E. coli*).
a.k.a. Alpha-ketoglutarate-dependent dioxygenase alkB homolog 3 (ABH3)

AP site Apurinic or apyrimidinic site.
a.k.a. Abasic site

APAF1 Apoptotic peptidase activating factor 1

APC Allophycocyanin

APE DNA-(apurinic or apyrimidinic site) endonuclease (either APEX1, APEX2 or APLF)

APEX1 APEX nuclease (multifunctional DNA repair enzyme) 1.
a.k.a. DNA-(apurinic or apyrimidinic site) lyase.
a.k.a. AP endonuclease 1

APEX2 APEX nuclease (apurinic/apyrimidinic endonuclease) 2.
a.k.a. DNA-(apurinic or apyrimidinic site) lyase 2.
a.k.a. AP endonuclease 2

APLF Aprataxin and PNKP like factor.
a.k.a. Apurinic-apyrimidinic endonuclease APLF

APS Ammonium persulfate

APTX Aprataxin

Artemis DNA cross-link repair 1C (**DCLRE1C**).
a.k.a. Protein Artemis (*Artemis, preferred name*)

ATM Ataxia telangiectasia mutated.
a.k.a. Serine-protein kinase ATM

ATP Adenosine triphosphate

ATR Ataxia telangiectasia and Rad3 related.
a.k.a. Serine/threonine-protein kinase ATR

ATRIP ATR interacting protein

B-NHEJ Backup NHEJ.
a.k.a. Alternative NHEJ (Alt-NHEJ)

BAK1 BCL2-antagonist/killer.
a.k.a. Apoptosis regulator BAK.
a.k.a. BCL2L7

BAX BCL2-associated X protein.
a.k.a. Apoptosis regulator BAX.
a.k.a. BCL2L4

BCL2 B-cell CLL/lymphoma 2.

a.k.a. Apoptosis regulator Bcl-2 (Bcl-2)

BCLXL BCL2-like 1 (**BCL2L1**).

a.k.a. Apoptosis regulator Bcl-XL (*BCLXL, preferred name*)

BCNU Carmustine: 1,3-bis(2-chloroethyl)-1-nitrosourea

BCR-ABL Fusion protein between breakpoint cluster region (bcr) and c-abl oncogene 1, non-receptor tyrosine kinase product of the Philadelphia chromosome [t(9;22)(q34;q11)]

BECN1 Beclin 1, autophagy related.

a.k.a. Beclin-1.

a.k.a. ATG6 autophagy related 6 homolog

BER Base excision repair

BID BH3 interacting domain death agonist

BIR Homologous recombination break-induced repair

BLM Bloom syndrome, RecQ helicase-like

a.k.a. Bloom syndrome protein

BRCA1 Breast cancer 1, early onset.

a.k.a. Breast Cancer type 1 susceptibility protein

BRCA2 Breast cancer 2, early onset.

a.k.a. Breast Cancer type 2 susceptibility protein.

a.k.a. Fanconi anemia, complementation group D1 *(*FANCD1)

BrdU Bromodeoxyuridine

BRIP1 BRCA1 interacting protein C-terminal helicase 1

a.k.a. Fanconi anemia, complementation group J (FANCJ)

BSA Bovine serum albumin

CA Chromosomal aberration

CASP2 Caspase 2, apoptosis-related cysteine peptidase.

a.k.a. Caspase-2

CASP3 Caspase 3, apoptosis-related cysteine peptidase.

a.k.a. Caspase-3

CASP6 Caspase 6, apoptosis-related cysteine peptidase.

a.k.a. Caspase-6

CASP7 Caspase 7, apoptosis-related cysteine peptidase.

a.k.a. Caspase-7

CASP8 Caspase 8, apoptosis-related cysteine peptidase.

a.k.a. Caspase-8

CASP9 Caspase 9, apoptosis-related cysteine peptidase.

	a.k.a. Caspase-9
CASP10	Caspase 10, apoptosis-related cysteine peptidase.
	a.k.a. Caspase-10
CCNU	Lomustine: 1-(2-chloro-ethyl)-3-cyclohexyl-1-nitrosourea
CDK1	Cyclin-dependent kinase 1.
	a.k.a. Cell cycle controller CDC2
CDKN2A	Cyclin-dependent kinase inhibitor 2A (melanoma, p16, inhibits CDK4).
	a.k.a. Cell cycle negative regulator beta.
	a.k.a. P16INK4A
CETN2	Centrin, EF-hand protein, 2.
	a.k.a. centrin-2
CFA	Colony formation assay
CFDA-SE	Carboxyfluorescein diacetate succinimidyl ester
CFSE	Carboxyfluorescein succinimidyl ester
CHK1	CHK1 checkpoint homolog (*Schizosaccharomyces pombe*).
	a.k.a. serine/threonine-protein kinase Chk1
CHK2	CHK2 checkpoint homolog (*S. pombe*).
	a.k.a. serine/threonine-protein kinase Chk2
CisPt	Cisplatin: [5-(2-amino-6-oxo-3H-purin-9-yl)-3-hydroxyoxolan-2-yl][5-(6-aminopurin-9-yl)-2-[[[2-[[[5-(6-aminopurin-9-yl)-2-(hydroxymethyl)oxolan-3-yl]oxy-hydroxyphosphoryl]oxymethyl]-5-(5-methyl-2,4-dioxopyrimidin-1-yl)oxolan-3-yl]oxy-hydroxyphosphoryl]oxymethyl]oxolan-3-yl] hydrogen phosphate; azane; azanide; platinum($^{2+}$)
CNS	Central nervous system
cpm	Counts per minute
CSA	Excision repair cross-complementing rodent repair deficiency, complementation group 8 (**ERCC8**).
	a.k.a. Cockayne syndrome WD repeat protein CSA (*CSA, preferred name*)
CSB	Excision repair cross-complementing rodent repair deficiency, complementation group 6 (**ERCC6**).
	a.k.a. Cockayne syndrome protein CSB (*CSB, preferred name*)
CtIP	Retinoblastoma binding protein 8 (**RBBP8**).
	a.k.a. CTBP-interacting protein (*CtIP, preferred name*)
CYTC	Cytochrome c, somatic (**CYCS**).
	a.k.a. Cytochrome c (*CYTC, preferred name*)
D-loop	Displacement loop

D-NHEJ	DNA-PKcs dependent NHEJ. Canonical NHEJ (NHEJ)
Da	Dalton
DABCO	1,4-diazabicyclo[2.2.2]octane
DAPI	4',6-diamidino-2-phenylindole
DDB1	Damage-specific DNA binding protein 1, 127kDa. *a.k.a.* DNA damage-binding protein 1. *a.k.a.* Xeroderma pigmentosum group E-complementing protein (XPE)
DDB2	Damage-specific DNA binding protein 2, 48kDa. *a.k.a.* DNA damage-binding protein 2
DDR	DNA damage response
dH_2O	Deionized water
DIABLO	Diablo, IAP-binding mitochondrial protein. *a.k.a. S*econd mitochondria-derived activator of caspase (SMAC)
DISC	Death-inducing signaling complex
DMSO	Dimethyl sulfoxide
DNA	Deoxyribonucleic acid
DNA-PKcs	Protein kinase, DNA-activated, catalytic polypeptide (**PRKDC**). *a.k.a.* DNA-dependent protein kinase catalytic subunit (*DNA-PKcs, preferred name*)
ds	Double-stranded
DSBR	Homologous recombination double strand break repair
DSB	DNA double-strand break
DSS1	split hand/foot malformation (ectrodactyly) type 1 (**SHFM1**) *a.k.a.* 26S proteasome complex subunit DSS1 (*DSS1, preferred name*)
DTT	Dithiothreitol: (2S,3S)-1,4-bis(sulfanyl)butane-2,3-diol
e.g.	*exempli gratia*: for the sake of example
EDTA	Ethylenediaminetetraacetic acid
EGFR	Epidermal growth factor receptor
ENDOG	Endonuclease G. *a.k.a.* Endonuclease G, mitochondrial
ERBB2	v-erb-b2 erythroblastic leukemia viral oncogene homolog 2, neuro/glioblastoma derived oncogene homolog (avian). *a.k.a.* Receptor tyrosine-protein kinase erbB-2 (HER-2/neu)
ERCC1	Excision repair cross-complementing rodent repair deficiency, complementation group 1. *a.k.a.* DNA excision repair protein ERCC-1

ERK2 Mitogen-activated protein kinase 1 (**MAPK1**).
a.k.a. Extracellular signal-regulated kinase 2 (*ERK2, preferred name*)

etc. e*t cetera*: and other things, or and so forth

EXO1 Exonuclease 1

FAS Fas (TNF receptor superfamily, member 6).
a.k.a. Tumor necrosis factor receptor superfamily member 6.
a.k.a. CD95.
a.k.a. APO-1 cell surface antigen (APO-1)

FBS Fetal bovine serum

FEN1 Flap structure-specific endonuclease 1.
a.k.a. Flap endonuclease 1

Fig. Figure

FITC Fluorescein isothiocyanate

G_1-phase Gap 1 phase of the cell cycle

G_2-phase Gap 2 phase of the cell cycle

GBM Glioblastoma.
a.k.a. Glioblastoma multiforme

GEN1 Gen homolog 1, endonuclease (Drosophila).
a.k.a. Flap endonuclease GEN homolog 1

GG-NER Global genomic NER

GLB1 Galactosidase, beta 1
a.k.a. β-galactosidase

h Hour

H2A.X H2A histone family, member X (H2AFX).
a.k.a. Histone H2A.x.
a.k.a. H2AX

HEPES 4-(2-hydroxyethyl)-1-piperazineethanesulfonic acid

HMGB1 High mobility group box 1.
a.k.a. High mobility group protein B1
a.k.a. HMGB-1

HMGN1 High mobility group nucleosome binding domain 1.
a.k.a. Non-histone chromosomal protein HMG-14

HR Homologous recombination

HRAS v-Ha-ras Harvey rat sarcoma viral oncogene homolog
a.k.a. GTPase HRas

HTRA2 HtrA serine peptidase 2.

	a.k.a. serine protease HTRA2, mitochondrial
i.e.	*id est*: that is
IR	Ionizing radiation
IRDye	Commercial name referring to infrared dye-labeled secondary antibodies. Not related to IR (above).
Ku70	X-ray repair complementing defective repair in Chinese hamster cells 6 (**XRCC6**). *a.k.a.* 70 kDa subunit of Ku antigen *(Ku70, preferred name*)
Ku80	X-ray repair complementing defective repair in Chinese hamster cells 5 (**XRCC5**). *a.k.a.* 86 kDa subunit of Ku antigen (*Ku80, referred name*)
l	Litre
LC3	Microtubule-associated protein 1 light chain 3 beta (**MAP1LC3B**). *a.k.a.* Microtubule-associated proteins 1A/1B light chain 3B *a.k.a.* ATG8 *a.k.a.* LC3B *a.k.a.* LC3 (*preferred name*)
LIG1	Ligase I, DNA, ATP-dependent. *a.k.a.* DNA ligase 1
LIG3	Ligase III, DNA, ATP-dependent. *a.k.a.* DNA ligase 3
LIG4	Ligase IV, DNA, ATP-dependent. *a.k.a.* DNA ligase 4
LP-BER	Long-patch BER
M	Molar concentration (mol/l)
M-phase	Mitosis phase of the cell cycle
MBD4	Methyl-CpG binding domain protein 4
Me	Methyl
MGMT	O^6-methylguanine-DNA methyltransferase
min	Minute
MLH1	mutL homolog 1, colon cancer, nonpolyposis type 2 (*E. coli*). *a.k.a.* DNA mismatch repair protein Mlh1
MLH3	mutL homolog 3 (*E. coli*). *a.k.a.* DNA mismatch repair protein Mlh3
MMR	DNA mismatch repair
MMS	Methyl methanesulfonate
MNNG	Methylnitronitrosoguanidine: 1-methyl-2-nitro-1-nitrosoguanidine
MNU	1-methyl-1-nitrosourea

MOMP Mitochondrial outer membrane permeabilization

MPG N-methylpurine-DNA glycosylase.

a.k.a. DNA-3-methyladenine glycosylase.

a.k.a. alkyladenine DNA glycosylase (AAG)

MRE11 Meiotic recombination 11 homolog A (*Saccharomyces cerevisiae*)

MRN MRE11/RAD50/NBN complex

MSH2 mutS homolog 2, colon cancer, nonpolyposis type 1 (*E. coli*).

a.k.a. DNA mismatch repair protein Msh2

MSH3 mutS homolog 3 (*E. coli*).

a.k.a. DNA mismatch repair protein Msh3

MSH6 mutS homolog 6 (*E. coli*).

a.k.a. DNA mismatch repair protein Msh6

MutLα MLH1/PMS2 heterodimer

MutSα MSH2/MSH6 heterodimer

MUTYH mutY homolog (*E. coli*).

a.k.a. A/G-specific adenine DNA glycosylase

N1MeA N1-methyladenine

N3MeA N3-methyladenine

N3MeC N3-methylcytosine

N7MeG N7-methylguanine

NBN Nibrin.

a.k.a. Nijmegen breakage syndrome 1 (NBS1)

NEIL1 nei endonuclease VIII-like 1 (*E. coli*).

a.k.a. endonuclease 8-like 1

NEIL2 nei endonuclease VIII-like 2 (*E. coli*).

a.k.a. endonuclease 8-like 2

NEIL3 nei endonuclease VIII-like 3 (*E. coli*).

a.k.a. endonuclease 8-like 3

NER Nucleotide excision repair

NFM Non-fat milk

NHEJ Non-homologous end joining

NTHL1 nth endonuclease III-like 1 (*E. coli*).

a.k.a. endonuclease III-like protein 1

O^6BG O^6-benzylguanine

O^6BTG O^6-(4-bromothenyl)guanine.

a.k.a. Lomeguatrib

	a.k.a. PaTrin-2
O^6ClEtG	O^6-chloroethylguanine
O^6MeG	O^6-methylguanine
OGG1	8-oxoguanine DNA glycosylase.
	a.k.a. N-glycosylase/DNA lyase
P-*NAME* **(#)**	phospho-*protein* (*Position of phosphorylation*)
	e.g.: P-ATR (S428): ATR protein phosphorylated on serine 428
p53	Tumor protein p53
PAGE	Polyacrylamide gel electrophoresis
PALB2	Partner and localizer of BRCA2.
	a.k.a. Fanconi anemia, complementation group N (FANCN)
PARP1	Poly (ADP-ribose) polymerase 1
PBS	Phosphate buffered saline
PCNA	Proliferating cell nuclear antigen
PE	Phycoerythrin
PI	Propidium iodide
PLK1	Polo like kinase.
	a.k.a. Serine/threonine-protein kinase PLK1
PMS1	PMS1 postmeiotic segregation increased 1 (*S. cerevisiae*).
	a.k.a. PMS1 protein homolog 1
PMS2	PMS2 postmeiotic segregation increased 2 (*S. cerevisiae*).
	a.k.a. DNA mismatch repair endonuclease PMS2
PMSF	Phenylmethanesulfonylfluoride
PNKP	Polynucleotide kinase 3'-phosphatase.
	a.k.a. bifunctional polynucleotide phosphatase/kinase
POLB	Polymerase (DNA directed), beta.
	a.k.a. DNA polymerase beta (Pol β)
POLD	Polymerase (DNA directed), delta.
	a.k.a. DNA polymerase delta (Pol δ)
POLE	Polymerase (DNA directed), epsilon.
	a.k.a. DNA polymerase epsilon (Pol ε)
POLH	polymerase (DNA directed), eta.
	a.k.a. DNA polymerase eta (Pol η)
POLI	polymerase (DNA directed) iota.
	a.k.a. DNA polymerase iota (Pol ι)
POLK	Polymerase (DNA directed), kappa.

	a.k.a. DNA polymerase kappa (Pol κ)
POLL	Polymerase (DNA directed), lambda.
	a.k.a. DNA polymerase lambda (Pol λ)
POLM	Polymerase (DNA directed), mu.
	a.k.a. DNA polymerase mu (Pol μ)
POLZ	Polymerase (DNA directed), zeta.
	a.k.a. DNA polymerase zeta (Pol ζ)
rpm	Revolutions per minute
R.T.	Room temperature (do not confuse with *RT = radiotherapy*)
RAD23B	RAD23 homolog B (*S. cerevisiae*).
	a.k.a. UV excision repair protein RAD23 homolog B
RAD50	RAD50 homolog (*S. cerevisiae*).
	a.k.a. DNA repair protein RAD50
RAD51	Rad51 homolog (*S.cerevisiae*).
	a.k.a. DNA repair protein RAD51 homolog 1
RAD51B	Rad51 homolog B (*S. cerevisiae*).
	a.k.a. DNA repair protein RAD51 homolog 2
RAD51C	Rad51 homolog C (*S. cerevisiae*).
	a.k.a. DNA repair protein RAD51 homolog 3
RAD51D	Rad51 homolog D (*S. cerevisiae*).
	a.k.a. DNA repair protein RAD51 homolog 4
RAD52	Rad52 homolog (*S. cerevisiae*).
	a.k.a. DNA repair protein RAD52 homolog
RAD54	RAD54-like (S. cerevisiae) (**RAD54L**)
	a.k.a. DNA repair and recombination protein RAD54 (*RAD54, preferred name*)
REV1	REV1 homolog (S. cerevisiae).
	a.k.a. DNA repair protein REV1
REV3L	REV3-like, catalytic subunit of DNA polymerase zeta (yeast).
	a.k.a. DNA polymerase zeta catalytic subunit.
	a.k.a. REV3
RFC	Replication factor C protein complex
RIP1	Receptor (TNFRSF)-interacting serine-threonine kinase 1 (**RIPK1**).
	a.k.a. Receptor-interacting serine/threonine-protein kinase 1
	a.k.a. Receptor-interacting protein 1 (*RIP1, preferred name*)
RIP3	Receptor-interacting serine-threonine kinase 3 (**RIPK3**).
	a.k.a. Receptor-interacting serine/threonine-protein kinase 3.

	a.k.a. Receptor interacting protein 3 (*RIP3, preferred name*)
RNA	Ribonucleic acid
RNAi	RNA interference
RNase A	Ribonuclease A
ROS	Reactive oxygen species
RPA	Replication protein A1, 70 kDa.
	a.k.a. Replication protein A 70 kDa DNA-binding subunit
RT	Radiotherapy (do not confuse with *R.T. = Room temperature*)
S-phase	Synthesis phase of the cell cycle
SCE	Sister chromatid exchange
SD	Standard deviation
SDS	Sodium dodecyl sulfate
SDSA	Homologous recombination synthesis-dependent strand annealing
shRNA	Short hairpin RNA
siRNA	Small interfering RNA
SLX1	SLX1 structure-specific endonuclease subunit homolog (S. cerevisiae)
SLX4	SLX4 structure-specific endonuclease subunit homolog (S. cerevisiae).
	a.k.a. Fanconi anemia, complementation group P *(*FANCP)
SMC1A	Structural maintenance of chromosomes 1A
SMUG1	Single-strand-selective monofunctional uracil-DNA glycosylase 1
SP-BER	Short-patch or single nucleotide BER
SQSTM1	Sequestosome 1.
	a.k.a. ubiquitin-binding protein p62.
	a.k.a. phosphotyrosine independent ligand for the Lck SH2 domain p62
SSB1	Oligonucleotide/oligosaccharide-binding fold containing 2B (**OBFC2B**).
	a.k.a. Single-stranded DNA-binding protein 1 (*SSB1, preferred name*)
ss	Single-stranded
SSA	Single-strand annealing
SSBs	DNA single-strand breaks
Supp.	Supplementary
tBID	Truncated BID
TBS	Tris buffered saline
TC-NER	Transcription coupled NER
TDG	Thymine-DNA glycosylase.
	a.k.a. G/T mismatch-specific thymine DNA glycosylase
TDP1	Tyrosyl-DNA phosphodiesterase 1

TEMED Tetramethylethylenediamine

TCEA1 Transcription elongation factor A (SII), 1.
a.k.a. TFIIS

TLS Translesion DNA synthesis

TMZ Temozolomide: 8-carbamoyl-3-methylimidazo(5,1-d)-1,2,3,5-tetrazin-4(3H)-one

TNFR1 Tumor necrosis factor receptor superfamily, member 1A (**TNFRSF1A**).
a.k.a. CD120a.
a.k.a. Tumor necrosis factor receptor type 1 (*TNFR1, preferred name*)

TOP3A Topoisomerase (DNA) III alpha.
a.k.a. DNA topoisomerase 3-alpha
a.k.a. TOPOIIIα

TP53BP1 Tumor protein p53 binding protein 1.
a.k.a. p53-binding protein 1 (53BP1)

TRAILR1 Tumor necrosis factor receptor superfamily, member 10a (**TNFRSF10A**).
a.k.a. Death receptor 4 (DR4).
a.k.a. TRAIL receptor 1 (*TRAILR1, preferred name*)

Tris Tris(hydroxymethyl)aminomethane

UNG Uracil-DNA glycosylase

UV Ultraviolet light

WB Western blot

WHO World Health Organization

WRN Werner syndrome, RecQ helicase-like.
a.k.a. Werner syndrome ATP-dependent helicase

XAB2 XPA binding protein 2.
a.k.a. Pre-mRNA-splicing factor SYF1

XLF Nonhomologous end-joining factor 1 (**NHEJ1**).
a.k.a. Protein cernunnos.
a.k.a. XRCC4-like factor (*XLF, preferred name*)

XPA Xeroderma pigmentosum, complementation group A.
a.k.a. DNA repair protein complementing XP-A cells

XPB Excision repair cross-complementing rodent repair deficiency, complementation group 3 (xeroderma pigmentosum group B complementing) (**ERCC3**).
a.k.a. TFIIH basal transcription factor complex helicase XPB subunit.
a.k.a. DNA repair protein complementing XP-B cells *(XPB, preferred name*)

XPC Xeroderma pigmentosum, complementation group C.
a.k.a. DNA repair protein complementing XP-C cells

XPD Excision repair cross-complementing rodent repair deficiency, complementation group 2 (**ERCC2**).

a.k.a. TFIIH basal transcription factor complex helicase XPD subunit.

a.k.a. DNA repair protein complementing XP-D cells *(XPD, preferred name*)

XPF Excision repair cross-complementing rodent repair deficiency, complementation group 4 (**ERCC4**).

a.k.a. DNA repair endonuclease XPF *(XPF, preferred name*)

XPG Excision repair cross-complementing rodent repair deficiency, complementation group 5 (**ERCC5**).

a.k.a. DNA repair protein complementing XP-G cells *(XPG, preferred name*)

XRCC1 X-ray repair complementing defective repair in Chinese hamster cells 1.

a.k.a. DNA repair protein XRCC1

XRCC2 X-ray repair complementing defective repair in Chinese hamster cells 2.

a.k.a. DNA repair protein XRCC2

XRCC3 X-ray repair complementing defective repair in Chinese hamster cells 3.

a.k.a. DNA repair protein XRCC3

XRCC4 X-ray repair complementing defective repair in Chinese hamster cells 4

a.k.a. DNA repair protein XRCC4

7.2. Supplementary Tables

Table Supplementary 1. RPMI media without divalent cations.

Components	**Concentration**
Amino acids	**(mM)**
Glycine	0.133
L-Arginine	1.150
L-Asparagine	0.379
L-Aspartic acid	0.150
L-Cystine	0.083
L-Glutamic Acid	0.136
L-Glutamine	2.050
L-Histidine	0.097
L-Hydroxyproline	0.153
L-Isoleucine	0.382
L-Leucine	0.382
L-Lysine hydrochloride	0.219
L-Methionine	0.101
L-Phenylalanine	0.091
L-Proline	0.174
L-Serine	0.286
L-Threonine	0.168
L-Tryptophan	0.025
L-Tyrosine	0.110
L-Valine	0.171
Vitamins	**(µM)**
Biotin	0.820
Choline chloride	21.400
D-Calcium pantothenate	0.524
Folic Acid	2.270
i-Inositol	194.000
Niacinamide	8.200
Para-Aminobenzoic Acid	7.300
Pyridoxine hydrochloride	4.850
Riboflavin	0.532
Thiamine hydrochloride	2.970
Vitamin B12	0.004
Inorganic salts and other components	**(mM)**
Calcium nitrate ($Ca(NO_3)_2$ $4H_2O$)	0.424
Magnesium Sulfate ($MgSO_4$ $7H_2O$)	0.407
Potassium Chloride (KCl)	5.330
Sodium Bicarbonate ($NaHCO_3$)	23.810
Sodium Chloride (NaCl)	103.450
Sodium Phosphate dibasic (Na_2HPO_4)	5.630
D-Glucose	11.11

Table Supplementary 2. Sister chromatid exchanges (SCE), chromosomal aberrations (CA), apoptosis and survival in CHO-9 cells after MNNG treatment. Data compiled from Kaina et al., 1991; Kaina et al., 1997; Ochs & Kaina, 2000; Roos et al., 2009.

End point	Low dose	High Dose
SCE / cell	Untreated: < 5 0.5 μM MNNG: 35 1 μM MNNG: 55 (Kaina *et al.*, 1991)	No data
CA / cell	Untreated: 0 1 μM MNNG: <1 (Kaina *et al.*, 1997; Roos *et al.*, 2009)	Untreated: 0 10 μM MNNG: 4 (Kaina *et al.*, 1997; Roos *et al.*, 2009)
Sub-G_1 fraction	Untreated and 1 μM MNNG: < 5% at 72 h after treatment (Ochs & Kaina, 2000)	10 μM MNNG: > 15% at 72 h after treatment (Ochs & Kaina, 2000)
Survival	0.5 μM MNNG: 100%, 1 μM MNNG: 40% (Kaina *et al.*, 1991)	10 μM MNNG: < 0.1% (Kaina *et al.*, 1991)

7.3. Supplementary Figures

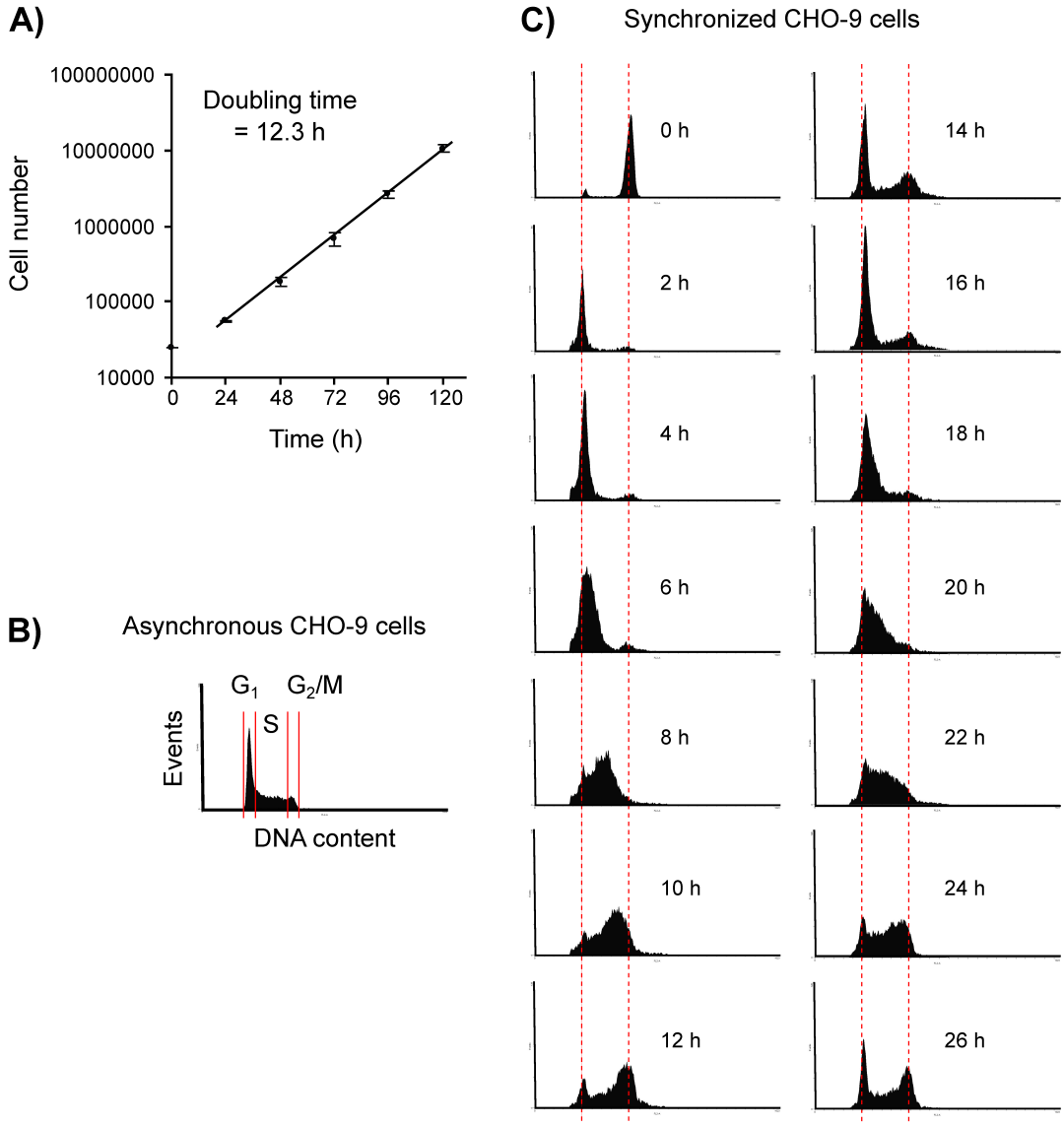

Figure Supplementary 1. Synchronization of CHO-9 cells by colcemid arrest and mitotic shake off. (A) Growth curve for CHO-9 cells cultured in RPMI medium supplemented with 5% FBS (B) DNA content histogram for exponentially growing asynchronous CHO-9 cells as assessed by flow cytometry. Cell cycle phases are indicated. (C) Cell cycle progression of CHO-9 cells synchronized by colcemid arrest and mitotic shake off (see Section 2.2.2.2 for synchronization protocol). DNA content histograms (as in B) are depicted as a function of time after shake off and release from colcemid arrest. Striped red lines were drawn in the middle of G_1- and G_2/M-phases as points of comparison for progression of the cell population.

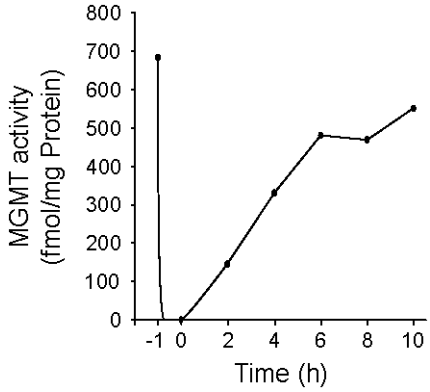

Figure Supplementary 2. Reactivation of MGMT expression in CHO-9-MGMT cells following release from the MGMT inhibitor O^6BG.
MGMT activity was inhibited in CHO-9-MGMT cells with 10 μM O^6BG (time -1). After 1 h inhibition, cell monolayers were rinsed twice with compete medium and medium without inhibitor was re-added to the culture flasks (time 0). MGMT activity was measured at the indicated time points after release from inhibition by quantifying the transfer of ^{3}H-methyl group from ^{3}H-methylated DNA substrate to the protein fraction in total cell extracts.

NOTE: It is worth mentioning that GBM patients with tumor MGMT activity above 30 fmol/mg protein show a significantly worst therapeutic response that patients expressing MGMT below this threshold (Wiewrodt *et al.*, 2008), and that for our cell system a 100% protection after MNNG treatment is achieved with MGMT activity of 210 fmol/mg protein (Kaina *et al.*, 1991). A systematic determination of protection with lower MGMT levels as to determine a precise threshold has not been performed for this cell line. Nevertheless, it is safe to say that for this experiment MGMT activity higher than 210 fmol/mg protein, and hence protection for this dose, was achieved within 3 h after release from the MGMT inhibitor O^6BG. Level of 30 fmol/mg protein were achieved within 1 h. It is also worth mentioning that repair of 50% of the O^6MeG lesions from dsDNA by the enzyme occurs within 0.5-1 s (Lindahl *et al.*, 1982), thereby suggesting complete repair within seconds once MGMT expression achieves the threshold.

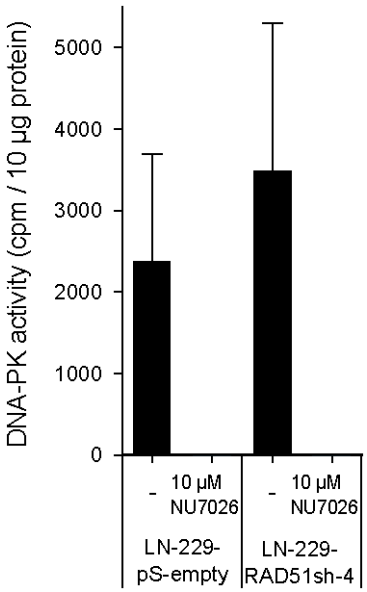

Figure Supplementary 3. Inhibition of DNA-PK activity with NU7026. DNA-PK activity was determined in cell extracts in the presence and absence of 10 µM NU7026. DNA-PK activity was determined by quantifying the incorporation of ^{32}P from [γ-^{32}P]ATP to a DNA-PK peptide substrate, and is shown as the mean ± SD of three independent experiments.

7.4. Publications

Publications listed below correspond to those based on research carried on at the Institute for Toxicology at the Medical Center of the Johannes Gutenberg University during my time as doctoral student.

The data from the publications marked with an asterisk (*) is presented in this thesis.

Research papers

Damrot J, Helbig L, Roos WP, **Barrantes SQ**, Kaina B, Fritz G. DNA replication arrest in response to genotoxic stress provokes early activation of stress-activated protein kinases (SAPK/JNK). J Mol Biol. 2009; 385:1409-1421.

Roos WP, Nikolova T, **Quiros S**, Naumann SC, Kiedron O, Zdzienicka MZ, Kaina B. Brca2/Xrcc2 dependent HR, but not NHEJ, is required for protection against O^6-methylguanine triggered apoptosis, DSB and chromosomal aberrations by a process leading to SCEs. DNA Repair (Amst). 2009; 8:72-86.

* **Quiros S**, Roos WP, Kaina B. Processing of O^6-methylguanine into DNA double-strand breaks requires two rounds of replication whereas apoptosis is also induced in subsequent cell cycles. Cell Cycle. 2010; 9:168-178.

Commented in:
Margison G. O^6-methylguanine in DNA: bad penny? Cell Cycle. 2010; 9:441-442.

* **Quiros S**, Roos WP, Kaina B. Rad51 and BRCA2 - New molecular targets for sensitizing glioma cells to alkylating anticancer drugs. PLoS One. 2011; 6:e27183.

Berdelle N, Nikolova T, **Quiros S**, Efferth T, Kaina B. Artesunate induces oxidative DNA damage, sustained DNA double-strand breaks and the ATM/ATR damage response in cancer cells. Mol Cancer Ther. 2011; 10:2224-2233.

Published abstract

Roos WP, Nikolova T, **Quiros S**, Naumann SC, Kiedron O, Zdzienicka MZ, Kaina B. Homologous recombination protects against O^6-methylguanine-triggered apoptosis, DNA double-strand break formation and chromosomal aberrations, but not against sister chromatid exchange formation. NAUNYN-SCHMIEDEBERGS ARCHIVES OF PHARMACOLOGY 2008; 377:German Soc Expt & Clin Pharmacol & Toxicol-80.

Roos WP, Nikolova T, **Quiros S**, Naumann SC, Kiedron O, Zdzienicka MZ, Kaina B. The role of Brca2 and Xrcc2 dependent homologous recombination in the protection of cells against genotoxicity caused by O^6-methylguanine. NAUNYN-SCHMIEDEBERGS ARCHIVES OF PHARMACOLOGY 2009; 379:Deutsch Gesell Experiment & Klinis Pharmakol & Toxikol-76.

Quiros S, Roos WP, Kaina B. Processing of O^6-methylguanine adducts to a toxic lesion requires at least two rounds of DNA replication, but cell death can also be induced at subsequent cell cycles. NAUNYN-SCHMIEDEBERGS ARCHIVES OF PHARMACOLOGY 2009; 379:Deutsch Gesell Experiment & Klinis Pharmakol & Toxikol-76.

Quiros S, Roos WP, Kaina B. Cell death by apoptosis executed several cell cycles after DNA damage induction. NAUNYN-SCHMIEDEBERGS ARCHIVES OF PHARMACOLOGY 2010; 381:Deutsch Gesell Expt & Klin Pharmakol & Toxikol-70.

Berdelle N, **Quiros S**, Efferth T, Nikolova T, Christmann M, Kaina B. The influence of the TCM drug artesunate on the sensitivity of tumor cell lines and his cytotoxic an genotoxic activity. NAUNYN-SCHMIEDEBERGS ARCHIVES OF PHARMACOLOGY 2011; 383:German Soc Expt & Clin Pharmacol & Toxicol-101.

7.5. Congresses attended

2nd International Conference on MGMT: O^6-Methylguanine-DNA Methyltransferase: From Basics to Clinical Applications
Mainz, Germany. June 13-16, 2007.

10. Jahrestagung der Gesellschaft für Biologische Strahlenforschung (GBS)
Mainz, Germany. October 10-12, 2007.

49. Jahrestagung der Deutschen Gesellschaft für Experimentelle und Klinische Pharmakologie und Toxikologie (DGPT)
Mainz, Germany. March 11-13, 2008.

Advances in Cell Death Research - from Basic Principles to New Therapeutic Concepts
Günzburg, Germany. July 16-20, 2008.

10th Biennial Meeting of the German Society for Research on DNA Repair (DGDR)
Berlin, Germany. September 2-5, 2008.
Poster: Cell cycle analysis of O^6-methylguanine triggered apoptosis.

50. Jahrestagung der Deutschen Gesellschaft für Experimentelle und Klinische Pharmakologie und Toxikologie (DGPT)
Mainz, Germany. March 10-12, 2009.
Poster: Processing of O^6-methylguanine to a toxic lesion requires at least two rounds of DNA replication, but cell death can also be induced at subsequent cell cycles.

51. Jahrestagung der Deutschen Gesellschaft für Experimentelle und Klinische Pharmakologie und Toxikologie (DGPT)
Mainz, Germany. March 23-25, 2010.
Oral presentation: Cell death by apoptosis can be executed several cell cycles after DNA damage induction.

Symposium der DFG-Forschergruppe 527 „Suszeptibilitätsfaktoren der Tumorgenese“: DNA Repair in Cancer Protection.
Mainz, Germany. May 21, 2010
Oral presentation: Methylating anticancer drugs activate the damage response and trigger apoptosis several cell cycles after damage induction.

25. GUM - Tagung
Potsdam, Germany. October 12-15, 2010.
Oral presentation: S_N1-methylating genotoxicants activate the DNA-damage response and trigger cell death several cell cycles after damage induction.

16th International AEK Cancer Congress
Düsseldorf, Germany. March 16-18, 2011
Poster: Genotoxic anticancer drugs trigger cell death several cell cycles after DNA damage induction.

7.6. *Curriculum Vitae*

Personal Information

Name	**Steve Quirós Barrantes** (Quiros, S)
Date / Place of Birth	January 14, 1980 / San José, Costa Rica
Nationality	Costa Rican
Passport	110600117
Mailing address	Frauenlobstr. 29a. D-55118 Mainz. Germany
e-mail	squirosb@gmail.com

Education

Secondary Education
Lyceum Dr. Castro Madriz. San José, Costa Rica. November, 1997
Graduated with Honors

Higher Education
- Academic degrees awarded
Licentiate (**Lic.**) Microbiology and Clinical Chemistry
University of Costa Rica. San José, Costa Rica. August, 2003
Graduated with Honors

Magister Scientae (**M.Sc.**) Microbiology
University of Costa Rica. San José, Costa Rica. September, 2006
Graduated with Honors

- Professional degrees awarded
Doctor (**Dr.**) Microbiology and Clinical Chemistry
University of Costa Rica. San José, Costa Rica. August, 2003

Work and research experience

Dr. Microbiology and Clinical Chemistry
Health and Social Security System of Costa Rica
2003-2004

Research Associate / Instructor
Clodomiro Picado Institute and Clinical Analysis Department
Faculty of Microbiology. University of Costa Rica
2003-2006

Doctorate student
Institute of Toxicology
University Medical Center of the Johannes Gutenberg University, Mainz, Germany
2007 to 2011

Publications

Santamaría C, Larios S, **Quirós S**, Pizarro-Cerda J, Gorvel JP, Lomente B, Moreno E. Bactericidal and antiendotoxic properties of short cationic peptides derived from the snake venom Lys49 phospholipase A_2. Antimicrob Agents Chemother. 2005; 49:1340-1345.

Quirós S, Alape-Girón A, Angulo Y, Lomonte B. Isolation, characterization and molecular cloning of AnMIP, a new alpha-type phospholipase A_2 myotoxin inhibitor from the plasma of the snake *Atropoides nummifer* (Viperidae: Crotalinae). Comp Biochem Physiol B Biochem Mol Biol. 2007; 146:60-68.

Damrot J, Helbig L, Roos WP, **Barrantes SQ**, Kaina B, Fritz G. DNA replication arrest in response to genotoxic stress provokes early activation of stress-activated protein kinases (SAPK/JNK). J Mol Biol. 2009; 385:1409-1421.

Roos WP, Nikolova T, **Quiros S**, Naumann SC, Kiedron O, Zdzienicka MZ, Kaina B. Brca2/Xrcc2 dependent HR, but not NHEJ, is required for protection against O^6-methylguanine triggered apoptosis, DSBs and chromosomal aberrations by a process leading to SCEs. DNA Repair (Amst). 2009; 8:72-86.

Quiros S, Roos WP, Kaina B. Processing of O^6-methylguanine into DNA double-strand breaks requires two rounds of replication whereas apoptosis is also induced in subsequent cell cycles. Cell Cycle. 2010; 9:168-178.

Quiros S, Roos WP, Kaina B. Rad51 and BRCA2 - New molecular targets for sensitizing glioma cells to alkylating anticancer drugs. PLoS One. 2011; 6:e27183.

Berdelle N, Nikolova T, **Quiros S**, Efferth T, Kaina B. Artesunate induces oxidative DNA damage, sustained DNA double-strand breaks and the ATM/ATR damage response in cancer cells. Mol Cancer Ther. 2011; 10:2224-2233.

Recognitions

First of the class in the Lic. courses of the Faculty of Microbiology and Clinical Chemistry. University of Costa Rica. Academic year 2002

Graduated with Honors, Lic. in Microbiology and Clinical Chemistry
University of Costa Rica, 2003

First of the class in the M.Sc. courses of the M.Sc.'s programs of the Health Sciences Area. University of Costa Rica. Academic year 2004

Graduated with Honors, M.Sc. in Microbiology
University of Costa Rica, 2006

Founding awarded

Scholarship for further academic study and training in Germany
Founded by the German Academic Exchange Service (DAAD)
April 2007 to September 2010